CRITICAL CORROSION PIT DEPTH FOR FATIGUE CRACK INITIATION IN 2024-T3, 6061-T6 AND 7075-T6 ALUMINUM ALLOYS

By

WILLIAM G. KING, JR.

Bachelor of Science in Mechanical Engineering

Auburn University

Auburn, Alabama

1983

Submitted to the Faculty of the
Graduate College of the
Oklahoma State University
in partial fulfillment of
the requirements for
the Degree of
MASTER OF SCIENCE
December, 2006

CRITICAL CORROSION PIT DEPTH FOR FATIGUE

CRACK INITIATION IN 2024-T3, 6061-T6 AND

7075-T6 ALUMINUM ALLOYS

Thesis Approved:

Dr. C.E. Price
Thesis Adviser

Dr. J.K. Good

Dr. P.M. Moretti

Dr. A. Gordon Emslie
Dean of the Graduate College

ACKNOWLEDGMENTS

I would like to thank my family, wife Charlotte and children, for their patience and understanding during the pursuit of this graduate degree. Also, thanks to the faculty and staff of the Department of Mechanical and Aerospace Engineering at Oklahoma State University for a truly enjoyable experience; especially to my Advisor Dr. C.E. Price who was not only enjoyable to work with but a great source of knowledge both inside and outside of the classroom.

TABLE OF CONTENTS

LIST OF TABLES

Table Page

LIST OF FIGURES

Figure Page

CHAPTER 1

INTRODUCTION

As civil and military aircraft fleets continue to age, the demand for aircraft to continue flying beyond their original design lives is an increased concern. This raises a number of problems, including the ability of the aircraft's structure to maintain damage tolerance. Corrosion and fatigue damage can occur simultaneously and the resulting combined effect can have a much greater impact than each one on its own. Multi-site damage (MSD) is the simultaneous presence of fatigue and/or corrosion at multiple locations, and can jeopardize the structural integrity of an aircraft [1, 2]. Thus the topic of aging aircraft is an ongoing concern to authorities. Many instances of failures have been reported due to metal fatigue, maybe triggered by corrosion. Some varied catastrophic examples include – the top of the cabin lost in flight on Aloha Airline Flight 243 (Boeing 737, 1988) [3], Fire Fighting Aircraft fatal mishap due to catastrophic wing separation (Lockheed C-130, 2002) [4] and about a year ago the Sea Plane off Miami fatal crash also due to catastrophic wing separation (Grumman G-73, 2005) [5].

The Aloha airline incident, shown in Figure 1, is a classically cited mishap that resulted in explosive decompression and in-flight loss of approximately 18 feet of the top section of cabin fuselage. The incident centered on the failure of lap joints due to the

cold bonding technique, corrosion and fatigue cracking and has since served as a rally point for supporters of the possibility MSD and widespread fatigue damage (WFD) which arguably can lead to catastrophic structural failures and basically represented the beginning of the Federal Aviation Administration's (FAA) entry into the aging aircraft program [6]. The fairly recent incident of wing separation of Figure 2, captured on video tape during the 2002 California fire fighting season and the seaplane wing separation witnessed by many near Miami graphically reinforced to the general public the potential catastrophic impact of fatigue failures on flight safety [7].

Even relatively benign examples such as that of a U.S. Coast Guard helicopter fuel pylon failure (which supports a tank containing several hundred pounds of fuel), as shown in Figure 3, reveals how quickly a small corrosion pit can compel a substantial fatigue crack to grow. In this incident the crack was discovered before anything extraordinary happened due to the crack progression being temporarily arrested by a stiffener within the forging; however the catastrophic implications are obvious [8].

Many U.S. Air Force (USAF) planes are decade's old and continued service is planed for many years to come; for example: B-52, KC-135, C-5 and T-38. To further emphasize the point of aging aircraft, the KC-135 celebrated its 50th anniversary of operational service in September 2006 and current plans are to keep it in service out to the year 2040 but reportedly that will only be possible with an aggressive corrosion control program [9]. The implications are the U.S. commercial aviation fleet includes many aging aircraft as well. As of the year 2002, the average age of the United States commercial fleet is reportedly over 10 years old with several of the major airlines coming in with ranges of 20-27 years [10].

Figure 1 – Aloha Airlines Flight 243, Boeing 737, explosive decompression failure; approximately 18 feet length of cabin lost in flight. Aircraft was safely landed; miraculously only one fatality resulted (28 Apr 1988). [11]

The recognized detriment that corrosion inflicts on aircraft assets is omnipresent as the fleets become older. Historically, about 25% of all cracking failures incidents are attributable to corrosion fatigue [12]. U.S. government studies conducted in 1996 and 2001 estimated the direct corrosion-related costs for all systems and infrastructure at about $10 billion and $20 billion, respectively [13]. In 1995 the annual cost of corrosion for all aircraft systems in the U.S. was estimated to be $13 billion including that for the military to be nearly $3 billion [14, 15]. At the 2002 Aging Aircraft Conference, it was reported the Air Force expenditures for corrosion maintenance was $720 million in 1990, nearly $800 million in 1997 and over $1 billion in 2002 [16]. It is noteworthy that about 50% of the $800 million spent on corrosion by the Air Force in the quoted 1997 figure was related to older transport aircraft. A more up to date opinion was put forward at the

9th Joint Aging Aircraft Conference in 2006; that the Air Force has greatly under-estimated the cost of corrosion to the extent that it is sometimes incorrectly portrayed as being a minor operational problem; the evidence suggests that the cost is actually about $6–8 billion per year [17].

The U.S. Air Force recognized the economic and safety concerns of fatigue and formed the Aircraft Structural Integrity Program (ASIP) back in 1958 and adopted a safe life approach to structural safety based on laboratory fatigue testing. However this was not effective because it did not account for the presence of pitting corrosion which substantially impacted the safe life by nucleating cracks much earlier than anticipated. ASIP was modified it to its current state in 1975 by adapting to damage tolerance principles [18].

Figure 2 – Catastrophic wing separation of U.S. Forest Service C-130 fire fighting aircraft, Walker, CA (2002) [7]

Also, the USAF recognized the special concerns of aging aircraft several years ago and began holding annual conferences and sponsoring in-house and external research and in recent years has partnered with all of the Department of Defense (DoD), Federal

FAA and the National Aeronautic and Space Administration (NASA) for Joint Aging aircraft conferences and symposiums; the 10th annual which is scheduled to be in Palm Springs, CA in April 2007 [19].

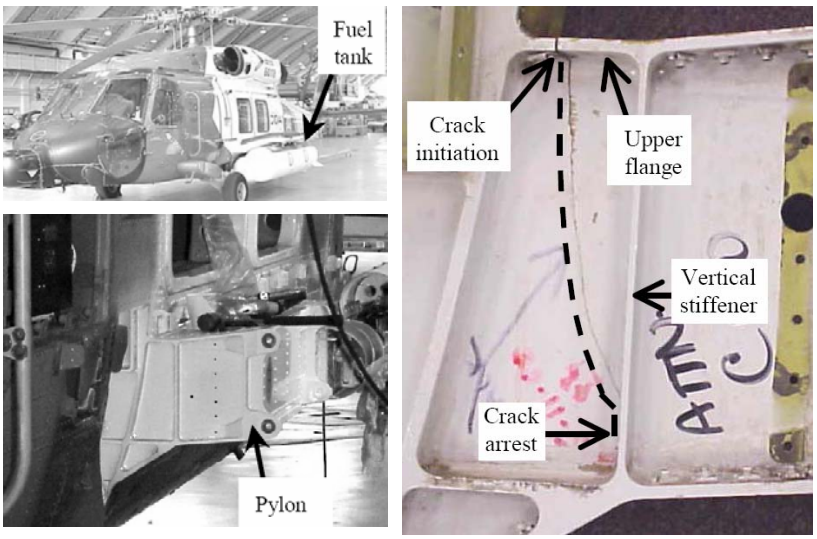

Figure 3 – U.S. Coast Guard HH-60J rescue helicopter fuel tank pylon fatigue crack. The crack initiated at a corrosion pit and progressed 8 inches before being discovered (right photo). Material was a 7075 (temper not given) aluminum forging [8].

The design of aircraft is based on a fatigue life that may allow a transport aircraft to theoretically be in service for several decades. The original design was not necessarily based on corrosion resistance but with increasing age, corrosion has now become a more significant problem. These aging aircraft are largely made of aluminum that is well served by an inherent protective oxide layer at the surface. However, the chloride ion can locally disrupt the oxide scale and lead to pitting corrosion that can provide a source for fatigue cracking and/or lead to corrosion fatigue. It is very difficult to detect corrosion when it is not visible externally. Furthermore, it is difficult to determine whether any corrosion is but cosmetic or dangerous. As aircraft age inspections become increasingly

more problematic due to inaccessible areas, multiple failure modes, and unique structure; many of these inspections will be even more difficult if required inspection intervals are forced to occur at times other than depot maintenance [6, 20].

Prior corrosion has a large effect on fatigue life and decreases the lives significantly at all stress levels. This is because, at any given stress level, the life of specimens with pre-existing damage will always be lower than those without such damage and it is more detrimental than continuous corrosion at high stresses and relatively short lives. At the high stress levels that result in low fatigue lives, sufficient corrosion damage may not develop in the available time in the environment prior to fatigue failure. The concurrent effect of a corrosive environment and fatigue loading is synergistic at lower stress levels and relatively longer fatigue lives because corrosion damage continues to accumulate with time. Thus, in the presence of a corrosive environment, the fatigue life will continue to decrease more rapidly with increasing stress compared with the lives in the absence of a corrosive environment. The nature of corrosion fatigue interactions has broad implications on the life assessment of military aircraft, which typically fly fewer hours than commercial aircraft and accumulate fatigue damage at a slower rate but corrosion damage at a higher rate [21].

The principal need is to quantify the structural performance of critical areas of aircraft with the assumed presence of prior corrosion in the representative environment that is present during service. Because corrosive environments such as salt water are typically absent during flight, many of the corrosion fatigue investigations have concentrated on the testing and modeling of the fatigue behavior of materials and components with prior corrosion but in-flight service in a benign environment. However,

the need also exists for understanding and accounting for the effects of the corrosive environments during flight service. Cases have been reported of the presence of corrosive environments during growth of fatigue cracks in aircraft during flight service and a major concern is the continued aging of aircraft beyond a 20 year design life [22].

The effect of corrosion, and the degradation it inflicts upon materials is multifaceted and not readily deterministic as a function of time. Aircraft manufacturers select materials and processes that hopefully impede the effect of corrosion and users of the aircraft attempt to bar the destructive nature of corrosion as a regular part of their inspection program [23].

Two aluminum alloys widely used in many of these aging aircraft are 2024-T3 and 7075-T6. Replacement parts, often sheet, are usually done to the same specification as the original. Of late, laser cutting has proved efficient in being able to make parts of complex geometry and close tolerance specifications. However, laser cutting is a melting process and as such must alter the edge condition. The question arose as to whether laser cutting was detrimental concerning fatigue crack initiation. This led to a series of studies (unpublished) at Oklahoma State University (OSU) where the fatigue behavior of sheet specimen, laser cut, machined, and machined and polished were compared [24 - 27].

As well as 7075-T6 and 2024-T3, a third common aluminum alloy, 6061-T6, was studied at Oklahoma State University. In all instances, the fatigue cracks began at the prepared edges; never on the surface, away from the edge. It was observed that usually laser-cut specimens did generate fatigue cracks earlier, with a corresponding reduction in fatigue life. On this basis, laser cutting could be considered detrimental. However, in "practice" it is known that fatigue cracks begin at inclusions or, in a corrosive

environment, at pits associated with inclusions. Therefore, the notion arose that, since all aircraft are exposed to saltwater environments, any "harm" caused by laser cutting would be inconsequential compared to that caused by corrosion. Preliminary studies quickly established that very little corrosion was needed to cause fatigue cracks to initiate at the tensile surface of fatigued sheet specimens, at multiple locations across the width, instead of at the laser-cut edges. This was made obvious by the occurrences of ratchet marks on the fracture surface.

This thesis is a fuller study of fatigue cracking in sheet specimens of 2024-T3, 6061-T6 and 7075-T6 as a result of corrosion. The testing was done in one-way bending. Questions asked specifically were how much corrosion was needed to cause damage and subsequent premature failure of cyclically loaded specimens (as witnessed by visual crack initiation at inclusion/pits), occurrence away from the specimen's edge, and possibly how pre-corrosion compared to concomitant corrosion (or both). The concepts of this study benefited much from recent (2004-2005) studies by Jones and Hoeppner [28,29] on the effects of pre-corrosion on 7075-T6 and 2024-T3 under cyclic loading and also a thesis paper by Jones [30] on alloy microstructural effects under concomitant corrosion-fatigue conditions in 7075-T6. These papers all focused on defining critical pitting criteria for yielding fatigue crack nucleation

CHAPTER 2

REVIEW OF LITERATURE

2.1 – Characteristics of Alloys in Study

A detailed source on knowledge of aluminum alloys prior to 1983 is the ASM book edited by Hatch [31]. This text identified numerous intermediate phases found in aluminum rich alloys that are difficult to eliminate impurities; many contain iron and silicon. The compositions of the three alloys of present interest follow in Table 1. Note the significant Si and Fe contents and the presence of other tramp elements. Many of these intermediate phases show up as coarse inclusions in the microstructure. These are formed in the temperature range between liquidus and solidus. While 7075-T6, for example, has a lower fracture toughness than 2024-T3, when 7xxx series and 2xxx series

are compared at the same strength level, the 7xxx alloys are actually tougher [32]. This is due to a smaller quantity of inclusions and a reduced precipitate size. One study shows that toughness increases with a decreasing size of Al_2CuMg particles and the minimalization of Al_2Mg_2Cr inclusions [31].

Table 1 – Alloy composition (Kaiser Aluminum Co.)

Alloy		Si	Fe	Cu	Mn	Mg	Cr	Zn	Ti	V	Zr	Other
2024-T3	Min	0.00	0.00	3.80	0.30	1.20	0.00	0.00	0.00	0.00	0.00	0.05 (max ea)
	Max	0.50	0.50	4.90	0.90	1.80	0.10	0.25	0.15	0.05	0.05	0.15 (max tot)
	Actual [a]	0.10	0.25	4.48	0.58	1.35	0.02	0.12	0.02	0.01	0.01	0.02
6061-T6	Min	0.40	0.00	0.15	0.00	0.80	0.04	0.00	0.00	0.00	0.00	0.05 (max ea)
	Max	0.80	0.70	0.40	0.15	1.20	0.35	0.25	0.15	0.05	0.05	0.15 (max tot)
	Actual [b]	0.73	0.62	0.29	0.08	1.03	0.23	0.18	0.03	0.01	0.00	0.04
7075-T6	Min	0.00	0.00	1.20	0.00	2.10	0.18	5.10	0.00	0.00	0.00	0.05 (max ea)
	Max	0.40	0.50	2.00	0.30	2.90	0.28	6.10	0.20	0.00	0.00	0.15 (max tot)
	Actual [c]	0.08	0.18	1.49	0.08	2.52	0.20	5.95	0.03	0.01	0.00	0.05
	a - Kaiser certified test report, Lot: 320279A3											
	b - Kaiser certified test report, Lot: 305775A9											
	c - Kaiser certified test report, Lot: 241742											
	Note: darkened cells represent primary alloying elements											

Reduced iron and silicon contents do not necessarily improve the fatigue properties but may when crack growth resistance dominates. The dispersoid type doesn't seem to matter [33, 34].

From Hatch [31], it is reported that pitting of aluminum in fresh waters follows a cube root curve. This was found to apply also to 6061-T6 sheet in seawater for a 5-year

study. If corrosion occurs in Al-Mg alloys like 6061-T6 it takes the form of pitting; it seems that extreme value pitting statistics apply to this alloy [35],

$$d_1 = kt_1^{1/3}$$

where d_1 is maximum pit depth in time, t_1. Aluminum magnesium alloys, 6xxx series, are the most resistant to seawater and a pit depth of 1.27 mm is highly unusual even after a decade of immersion. From Hatch [31], it is learned that 2xxx and 7xxx series alloys are much worse and should not be used in seawater.

While stress corrosion cracking in aluminum alloys is intergranular, corrosion fatigue is transgranular. The corrosion fatigue strength is 'low' and, seemingly, not much affected by the heat treatment condition, 'T', in 2xxx, 6xxx or 7xxx series alloys. Even by late 1970's the explanation was the creation of premature cracking at pits due to the associated stress concentration factor [36 - 38].

Three types of second-phase particles are known to influence fracture and fatigue behavior of high-strength aluminum alloys; constituent particles, dispersoid particles and strengthening precipitates; see Table 2 below. Typical constituents are $CuFeAl_7$, $CuAl_2$, and $FeAl_6$ ranging 2-50 μm in size. Dispersoid and strengthening particles are much smaller (<0.01 μm) in size [31].

Table 2 – Alloy typical constituents [31]

Alloy	Soluble	Insoluble
2024-T3	Al_2CuMg	
6061-T6	Mg_2Si	Fe_3SiAl_{12}, Cr_3SiAl_{12}
7075-T6	Al_2CuMg	Mg_2Si

A wrought aluminum alloy, 2024 can be precipitation heat treated to strength levels comparable to the highest among commercially available alloys and was traditionally widely used in the aircraft industry. A limiting factor in usage is the relatively inferior corrosion resistance due the significant copper content [39]. The fatigue strength of this is notably affected by moist corrosive environment. Figure 4 clearly shows the reduction in fatigue life of the pristine material is about 5 times less than that exposed to salt spray [39]. Typical uses of 2024-T3 are as mentioned, aircraft fittings, but also gears and shafts, bolts, clock parts, computer parts, couplings, fuse parts, hydraulic valve bodies, missile parts, munitions, nuts, pistons, rectifier parts, worm gears, fastening devices, veterinary and orthopedic equipment, structures [40].

Excellent features of 6061 are its corrosion resistance which is among the best of the heat treatable alloys and high plane strain fracture toughness. Its typical uses are heavy duty structures requiring corrosion resistance such as truck bodies, marine structures and pipelines. It readily forms protective oxide layer at the surface further enhancing corrosion resistance; however exposure to alkalis can break down the film and increase susceptibility greatly. The fatigue propagation rates are increased by the presence of moisture [39]. This alloy is commonly used in aircraft fittings, camera lens mounts, couplings, marine fittings, electrical fittings, hinge pins, magneto parts, hydraulic pistons, appliance fittings, valves, bike frames and miscellaneous hardware [40].

The high static strength is a trademark characteristic of 7075 in the T6 temper, however a correspondingly high fatigue resistance is not echoed. General fatigue strength is comparable to 2024 which has a lower static strength. The T6 condition is very susceptible to stress corrosion cracking, primarily in the short transverse direction

[39]. Some of the applications of 7075-T6 besides aerospace and defense applications is gears and shafts, fuse parts, missile parts, regulating valves, keys, bike frames and all terrain vehicle sprockets [40].

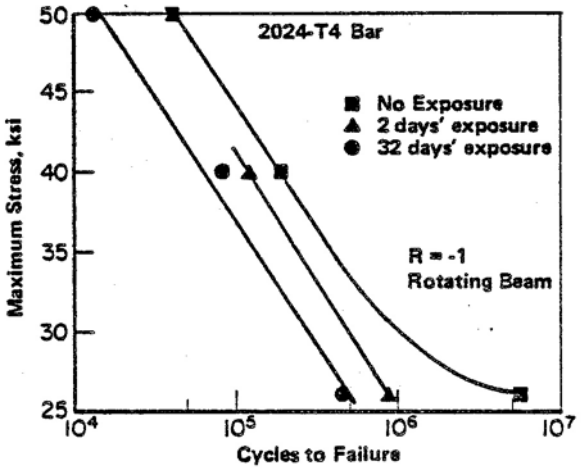

Figure 4 – Pre-corroded 2024 in salt spray [39]

2.2 – Review of Literature

About the time the Air Force stood up ASIP, the National Advisory Committee for Aeronautics commissioned research at the Langley Aeronautical Laboratory on the atmospheric effects of corrosion. The target of these early studies were the on the influence corrosion on in-service aircraft. Leybold, et al [41] in 1958 investigated the effects on 2024-T3 and 7075-T6 in the moist salt spray environment near Langley, Virginia on the Atlantic coastline; an environment common to the operation of military aircraft. The study was conducted on cantilevered 1.3 mm thickness sheet metal

specimens cycled at about 6.7 Hz for a 10 minute period each day. Parallel specimens in a controlled indoor environment sheltered from the outdoor salt spray specimens were run to contrast the ones in the corrosive environment. In an attempt to be consistent with aircraft environment, the vibratory loading was chosen at 83 MPa, equating to an estimated loading of 1g, common to transport aircraft. This loading is about 1/3 the average stress level used in the current study but the idea of bending stress instead of straight tension loading is conformal. As could be imagined, the outdoor exposure shortened the fatigue life of the 2024-T3 and 7075-T6 specimens by a factor of 3 as compared to the indoor uncorroded specimens. In related testing in moist environments in 1973, Hanh and Simon [42] indicated the alloys 2024-T3 and 7075-T6 can show a 20-fold increase in crack propagation rate in moist, NaCl corrosive environments at constant stress intensity (ΔK) levels as compared to dry conditions.

These tests are indicative of the overall effects that corrosive environments can inflict over time to the aging aircraft that is being required to operate for decades in exactly these types of situations. The following are several pertinent modern studies attempting to better understand the mechanism and affects of corrosion pitting in order to better develop engineering models for predictive maintenance and enhanced safety.

2.2.1 – 2024-T3 Literature

Krzysztof [42] reported 2024-T3 fatigue cracks nucleate in the early stages of cyclic life in HCl corrosive environments along copper depleted regions near second phase precipitates and grain boundaries, creating regions of higher stress concentration that results in localized plastic deformation. Tests were performed in reverse bending.

He went on to observe that fatigue cracks start at the surface as intergranular cracks, propagate for a few grains then change to transgranular.

Chen et al [44] studied fatigue crack initiation in 1.6 mm thick sheet exposed to a 0.5M NaCl solution and subjected to tension-tension loading. Center-pin loaded dog-bone type specimens with a 5.08 mm hole in the center of the waist section were used in the tests. Both pre-corroded and corroded-during tests were run. The corrosion pits were modeled as a semi-elliptical surface crack. A notable observation was the pit size increase and associated stress intensity factor increased at cyclic frequencies less than 5 Hz. It was reasoned that this transition from pit growth to fatigue crack growth was due to a pitting-cracking rate competition. This competition of rates involved both stress intensity factors and crack/pitting times. The equivalent stress intensity factor for a corrosion pit has to reach the threshold stress intensity factor (ΔK_{th}) for fatigue crack growth, and the time-based corrosion fatigue crack growth rate must exceed the pit growth rate. Also of note was that pitting was found to be associated with constituent particles in the hole and pit growth often involved coalescence of individual particle-nucleated pits. A study by Bray et al [45] noted prior corrosion pitting reduced the fatigue strength of the aluminum alloys 2024-T3 and 2524-T3 at 10^5 cycles by approximately 40% as compared to pristine samples.

Chandrasekaran et al [46] accomplished a study on fatigue crack initiation in 2024-T3 aluminum, pre-corroded in 5% NaCl solution and accelerated by a 3-5VDC charge. Pitting range was from 2–15 μm deep. The specimen material used in the test was stated to be 1.6 mm thick new sheet material and from a discarded fuselage panel from an E-8C JSTARS aircraft. The specimens were of conventional narrow waist

geometry; however a 5 mm hole was placed in the center of the waist to simulate a fastener hole. Cyclic tensile loading was at 10Hz and 138-207 MPa with R=0.1 stress ratio. They noted shallower pit depths required more cycles in order to form the first detectable fatigue cracks. The crack formation occurred solely at the 5 mm hole in the un-corroded specimens and at both the hole and large pits on the corroded ones. The length of the smallest detected initial fatigue crack was used in the AFGROW program, the Air Force developed fatigue crack growth software that uses classical stress intensity factor solutions form linear elastic fracture mechanics, to correlate actual failure data to predict. The results were conservative on the pristine and JSTARS specimens however it over-predicted the fatigue life on the new corroded sheet material. It is reasoned the error associated with measuring the first detectable crack is related to the values of AFGROW not correlating well with actual data.

A wavelet method to accurately model 2024-T3 pit geometry in 2-D and 3-D images was investigated by Frantziskonis et al [47]. Modeling approaches typically assume definable shapes of pit geometries such as elliptical, hemispheric, etc. in order to simplify the model. The authors contend, for the pitting and crack nucleation modeling tools to technically progress, a more realistic geometry definition is a must. The specimens were corroded during cyclic loading by application of a 0.1 M NaCl solution and polarized at about 500 mV. In parallel fashion, Simon et al defined parameters of existing pits in 2024-T3 such as pit depth, surface roughness and total pit volume in order to correlate with a stress intensity factor. Pits were characterized using white light interference microscopy and scanning electron microscope. Calculation of the stress

intensity factors was not accomplished as per of the scope of their paper but the goal is by measuring pit parameters, insight to the fatigue behavior could be inferred.

Wang et al [48] attempted to define an analytical model for pit nucleation and growth using 2024-T3. They stated corrosion fatigue generally starts with pitting/crack formation and ends with the propagation of the crack initiated at the base of the pits; thus, pitting directly triggers earlier fatigue crack initiation. For structures under cyclic loading and exposed to a corrosive environment, the processes of corrosion and fatigue often occur synergistically. Corrosion fatigue cracks initiate from the most active pits on which tunneling corrosion exists, and they do not necessarily nucleate at the largest pit. To initiate a stable crack, there should be a critical pit size at a given load level for pit–crack transition. The factors contributing to the development of pitting damage as chloride concentration, electrochemical potential, pH, temperature, alloy microstructure composition, and time and that pit size "a" varied with the cube root of time: $a_{pit} = Bt^{1/3}$; where B is a constant depending on the corrosive conditions and microstructure. They went on to state that a critical pit size is required for a fatigue crack to initiate and involves two parameters; the number of cycles to crack initiation and the crack initiation size. In modeling the pit and crack formation, the pit defect is assumed to hemispherical in shape and so the stress intensity factor is given by: $\Delta K = (2.2/\pi)\, K_t\, \Delta\sigma\, (\pi a)^{1/2}$; where K_t is the geometry stress concentration factor such as a fastener hole and the corresponding crack length or pit radius at which the crack is initiated is: $a_i = \pi(\Delta K_{th}/2.2\, K_t\, \Delta\sigma)^{1/2}$; where K_{th} is the threshold value for crack initiation.

A life prediction technique by measuring corrosion and analyzing using FASTRAN II software was studied by Gruenberg et al [1] at NASA Langley. The tests

were performed on 1.6 mm sheet thickness 2024-T3 aluminum pre-corroded for 6, 24 and 72 hours in a NaCl:H_2O_2 solution per ASTM G110. Conventional dog-bone specimen geometries were used in a tension fatigue test, at 10 Hz at amplitudes of 138, 180 and 220 MPa. The effects of 3 variables were examined; corrosion level, metallurgical plane and applied stress. Results showed that an increase in corrosion exposure decreased the fatigue life. At the higher applied stress levels, the differences in fatigue lives from the low corrosion level to the high corrosion level became less pronounced. At a given corrosion level, increasing the stress decreased the fatigue life. At higher stresses the three corrosion levels showed similar lives. Experimental results showed that the L configurations exhibited longer lives than the LT configurations. Notably, the lower the stress level the less the fatigue lives were dependent upon specimen orientation. Input values for the FASTRAN II program came from post failure measurements equating actual corrosion pit nucleation dimensions to those best fitting an approximate elliptical width and radius; on average, the authors claimed to achieve a good correlation of the predicted values vs. actual.

Quantitative fractographic analysis and fracture mechanics modeling to address multiple crack initiation in pre-corroded 2024-T3 aluminum was conducted by van der Walde et al [49] in an effort to model multiple crack effects. Sheet specimens of 1.6 mm thickness that were pre-corroded and subsequently fatigue failed from prior experiments were analyzed. It was found that over half of the specimens had two or more crack-nucleating pits. The number of nucleating pits per specimen was found to directly correlate with stress level and corrosion exposure duration. From the fatigue modeling efforts it is concluded that increased accuracy can be achieved by incorporating multiple

crack effects, particularly at higher stress levels where consistently unconservative life predictions are common. Additionally the plastic zone link-up method, which assumes cracks propagate as elliptical flaws and link-up when their associated plastic zones come in contact, is a simplified means of accounting for the interaction of adjacent flaws.

Kermanidis et al [50] investigated the corrosion of sheet in 1.6 mm thickness that had been pre-corroded with a solution composed of NaCl, KNO_3, HNO_3 and distilled water. Results showed the coexistence of pitting and intergranular corrosion, which facilitated the onset of fatigue cracks thereby reducing the fatigue life of the material appreciably. The endurance limits (at $5(10)^6$ cycles) for the pre-corroded vs. uncorroded specimens were determined to be 95 MPa and 175 MPa respectively. This equates s to a fatigue life reduction by about a factor of 1.8.

Jones and Hoeppner [29] investigated the fatigue of pre-corroded sheet in a 15/1 ratio of 3.5% NaCl solution of hydrogen peroxide for 15 min and 25 min. Two thicknesses of sheet were used; 1.60 mm and 4.06 mm (0.063 and 0.160 inches). The specimens were polished and masked off so that corrosion would take place only in a 1.5 mm^2 window, then pre-corroded to two different average depths; 20 μm and greater than 30 μm (as determined by evaluation with a metallurgical microscope). The loading was tensile-tensile and a frequency of 10 Hz and 201 MPa amplitude. Jones and Hoeppner define a critical pit as "the pit from which the crack ultimately causing failure originated and propagated to fracture" [29]. This notion seems somewhat illogical; specimens pitting in only one region to fairly significant depths are bound to initiate cracks. It would seem a critical pit would be one of a threshold value or the minimum depth required to initiate a fatigue crack. Their conclusion was, pit area more so than depth

affected crack initiation in the 1.6 mm material; while pit depth seemed to influence initiation in the thicker 4.06 mm specimens. Since the corroded area was only 1.5 mm by design it would seem difficult to determine area affects over such a small region.

Ishihara et al [51] accomplished tension-compression (on 5 mm thick rolled plate) and cantilever-type rotating-bending fatigue tests (12 mm dia with 5.6 mm dia waist) in 3% NaCl solution. The tests were conducted in corrosion-during fashion by dropping the solution onto the specimen at a constant flow rate. The pits were measured using the focused focal point method at 400x magnification. The average value of the stress concentration factor for pit to crack initiation was determined to be $K_{p\rightarrow c} = 0.25$ MPa($m^{½}$). Overall they determined the corrosion pit growth rate is affected not only by time but also by stress amplitude and cyclic frequency, however the effect of frequency is largely insignificant. The pit depth "a" was defined using the stress amplitude (σ, MPa) and time (t, hours): $a = 2.34 \times (1.014^{\sigma}) \times (t^{B})$; and B is an experimentally determined constant. According to the authors, most of the fatigue life at very low-stress ranges is occupied with the corrosion pit growth period so an accurate description of the corrosion pit growth law is a requisite in evaluating the corrosion fatigue life.

Edge conditions come in to play in fatigue initiation as well as pitting or stress concentration factors. Tyagi [27] fatigue tested laser cut specimens, of sheet in 1.6 mm thicknesses, in one-way bending. Her results indicated the fatigue life of laser cut specimens to be greatly reduced as compared to machine cut ones. The basic reason for this observation lies in the thermally effected zone produced in laser cutting and the associated edge softening. The laser affected zone was determined to be 1.8 mm wide on average. In a parallel study on 2024-T3, Jakkamreddy [26] explored the effects of edge

condition on fatigue life. One-way bending was used to test the fatigue failure values of 1.6 mm thickness sheet. Various edge conditions were tested at a range of deflection or stress values. The edge conditions were as-received machined, machined and polished and as-received laser cut and de-burred laser cut. Results indicated the polished specimens had an approximate 15% longer fatigue life than the as-received machine specimens but the as-received laser cut was about 110% worse fatigue life compared to as-received machined. The de-burred laser cut specimens showed fatigue life improvement to near the as-received machine finish specimens.

2.2.2 – 6061-T6 Literature

The lack of comparable studies performed on 6061-T6 became obvious in researching this study. The assumption is studies on 2024-T3 and 7075-T6 are common alloys used on older aircraft and the emphasis on aging aircraft over the last decade has focused the balance of attention. Also, 6061-T6 is not commonly used in structural applications on these aircraft. However a couple of studies are appropriate.

Minoda and Yoshida [52] tested 6061-T6 coupons cut from a 6 mm extrusion. The coupons were submerged in a corrosive solution composed of 3% NaCl and 1% HCl for 24, 96 and 240 hours. Results indicated a relatively rapid corrosion rate in the first time segment but the rate was noted to slow greatly after that; indicating conditions were different on the surface than inside the extrusion. The precipitant Mg_2Si was determined to be equally distributed on the surface as well as the center. Further investigation revealed "precipitant–free" zones (PFZ) exist on the surface but not in the center. The aluminum matrix and Mg_2Si particles are both higher (more noble) on the galvanic scale

compared to the PFZ's, which ultimately results in dissolution of the PFZ's due to the electrode potential difference.

Another fatigue study performed by Jagathrakshakan [25] on 1.6 mm thick 6061-T6 sheet in one-way bending was applicable. He noted the top surface was 33% higher in fatigue life from the bottom sheet surface; likely due to the molten metal layer formed during laser cutting creating stress concentrations and possibly a softening effect within the heat affected zone. Also noted was the fatigue life lowered with increasing thermal energy of the laser cutting process; specimens cut at 70% laser power showed a 60% increase in fatigue life over those cut at the 100% laser power setting. Additionally he found that under the same loading conditions, machined specimens experienced fatigue lives 10 times that of laser cut.

2.2.3 - 7075-T6 Literature

In a seawater environment, Holroyd and Hardie [53] investigated fatigue crack velocity of 7000 series aluminum. They found throughout the spectrum of frequencies tested (0.1-70 Hz), the presence of seawater produces a pronounced enhancement of crack propagation rates compared with rates in dry air. Furthermore, the overall frequency dependence of the crack velocities was found to be proportional to the square root of the cycle period; $1/^{0.5}$.

Nakai et al [54] explored crack initiation in 7075-T651 using a scanning atomic force microscope (AFM). This technique allows the investigator to view surface morphology at an atomic scale of resolution in 3-dimesions. Tests were conducted in both push-pull tension and plane bending while concurrently exposing the specimens to a

3% NaCl aqueous solution. The stress amplitude was 100 MPa at a 30 Hz cyclic frequency. Results determined that cracks initiated within corrosion pits; not at the deepest point but at a grain boundary within the pit. The quality and detail of pitting and crack morphology is outstanding in this study using the AFM; the ability to investigate the actual crack initiation is very much useful in determining the minimum amount of pitting damage required to initiate fatigue cracking as is pursued in this study. The researchers noted the commencement of fatigue crack initiation at about 2 μm pit depth.

Sankaran et al [55] performed a study using 7075-T6 in order to validate the use of crack growth modeling using AFGROW. Sheet specimens of 2 mm thickness were pre-corroded in accordance with the ASTM G85 fog-spray technique. The intervals were at increasing exposure times beginning at 24 hours and doubling each period to a maximum 1,536 hours. It was observed that corrosion pitting tended to elongate in the rolled direction indicating preferential pitting in the grain direction. Cyclic loading was at 15 Hz with stress amplitude was 414 MPa and a stress ratio of 0.02. The results claim good correlation between predicted crack growth using AFGROW and the actual lives recorded in testing. The general effect of corrosion pitting resulted in a reduction in fatigue life over pristine specimen by a factor of 6-8. However it is unclear how accounting for large fields of pits all acting possible synergistically were measured and input into the software calculation. The authors address this to a degree in recommending probabilistic studies in defining crack initiation from many pits of different sizes. The ASTM corrosion pitting method appears to be fairly effective in establishing pits of varying degrees however specialized equipment set up and the

significant time required to obtain results makes it much less practical for use in studies like this one that necessitate results quickly.

Huang and Frankel [56] investigated growth kinetics for localized corrosion in both 2024-T3 and 7075-T6 using the foil penetration technique with thicknesses in the 0.1 to 1.0 mm range in three orientations; longitudinal (L), long-transverse (LT) and short–transverse (ST). The noted attack was sharp intergranular for the 2024-T3 and a mixed mode for 7075-T6 of intergranular that opened up into pit cavities along the length of the intergranular attack. When exposed to the low polarizing potential (-725 mV) the 7075-T6 pitted at a much higher rate than the 2024-T3. Overall, the corrosion rates in the LT direction were slower than in the L direction and faster than that observed in the ST direction for the alloys tested. Though not specifically related to fatigue, the corrosion mechanisms in this paper are beneficial in understanding the corrosion fatigue process.

Tugle [57] presented an Air Force Research Laboratory study involving pre-corroded 0.79 mm sheet specimens, exposed to conditions all over the world for 3, 6, 9 and 12 months. An interesting observation was noted; specimens exposed at the same location had essentially the same fatigue life regardless of exposure time. The test only went out to 12 months so it is unknown if this trend would continue over longer periods. Consequently it was determined the development of a corrosion pit caused a significant reduction in fatigue life but fatigue life does not continue to decrease proportionately with continuing corrosion. The study recommended that when analyzing structures for fatigue failures an assumed pit depth of 76 μm to 178 μm should be used since corrosion cannot be completely prevented and the structure cannot be completely inspected due to economic and operational constraints; which is very similar logic to an assumed initial

manufacturing flaw, 127 μm (0.005 inch) radius corner crack, employed in USAF damage tolerant design practices [58].

Wang et al [59] conducted pitting experiments on 3.0 mm sheet at very high numbers of tension cycles and noted fatigue properties are significantly affected by the pre-existing corrosion pits; especially crack initiation in the exceedingly long life range > 10^6 cycles. Furthermore, extensively developed corrosion pitting due to longer exposures accelerates crack initiation and promotes multiple-site damage. Fatigue crack growth rates increased slightly with increasing surface corrosion pitting because surface pre-existing pits might act as stress concentrators. The total number of cycles to failure of pre-corroded 7075-T6 comprises the cycles to form a crack from a critical pit and the remaining cycles are what is needed to propagate the crack to failure. While Sankaran et al [55] noted a reduction in fatigue life of about a factor of 10^1 due to prior pitting, Wang et al demonstrated the magnitude of this life reduction factor could reach 10^2, at stress levels associated with N_f values of $10^6 – 10^9$ cycles.

DuQuesnay et al [2] studied the effects of pre-corrosion on extruded channel material 6.35 mm thick. Specimens were corroded in EXCO solution (prepared accordance with ASTM G 34) at times ranging from as little as 6 hours up to 21 days, then tension-compression cycled at 25 Hz with amplitudes of (+) 315 MPa to (-) 207 MPa, which corresponded to a loading profile derived from a C-130 aircraft. The authors were unclear as to why the loading was designed to go into a compressive state other than the fact that this occurs in actual aircraft service, however, fatigue cracking occurs only in tension loading so the compressive component only seems to slow down the test. The maximum pit depth was determined by measuring the thickness of the material then

sanding and polishing in order to remove surface material until the deepest pit was removed. Pit depth leading to crack initiation was obtained by post failure examination under 50x magnification and identifying the fatigue beach marks then tracing back to the pit origin. Values for the pit depth "a" and surface length "2c" were measured and analyzed using AFGROW crack growth software, which showed good correlation to actual fatigue lives.

Shafiq and Argarwala [60] tested pre-cracked (per ATSM E399) specimens in a 1% NaCl solution and reported even a mildly aggressive salt environment has a detrimental effect on the lifetime of metal aircraft structures irrespective of frequency or stress level; that a structure designed under infinite life methods under faultless conditions will never achieve that level of performance in even a slightly corrosive service environment.

Following on the work of Shafiq and Argarwala [60], Quispitupa, et al [61] performed tests on compact tension specimens by pre-cracking before fatigue testing in accordance with ASTM E399. The specimens were exposed to 1% NaCl solution at 1 Hz in order to observe chemical/mechanical processes occurring simultaneously at the crack tip. They observed by reducing the cyclic frequency results in a decrease in pH at the crack tip due to in increase in dissolution time, supporting the general results of the study noting an enhancement of the corrosion fatigue crack growth rate in the presence of the 1% NaCl corrosive solution.

Jones [30], studied 1.6 and 4.06 mm thicknesses subjected to concomitant fatigue in 3.5% NaCl under cyclic tensile loading amplitude of 17.5 ksi at 10 Hz with a stress ratio of 0.1. She concluded smaller grains within a material thickness result in a higher

quantity of grains available to interfere with fatigue crack transition and growth thereby extending the life. She observed that fatigue cracks in a concomitant fatigue environment grow only when the fatigue propagation rate exceed the corrosion pit growth rate. It was also noted constituent particles within the alloy competed with corrosion pits as crack nucleation sites and that concomitant corrosion fatigue significantly reduced the life over pristine specimens. In her study she reported an average critical pit depth required for crack initiation was about 20 μm for the 1.6 mm thickness. The accuracy of this value seems suspect in that the inspection frequency ranged from 4 to 9 hours; it would seem substantial changes could occur within such a lengthy timeframe and introduce some error to the critical pit determination.

In a related study last year, but under pre-corroded conditions instead, Jones and Hoeppner [28] sought to identify the critical pit criteria in 1.6 and 4.06 mm sheet thicknesses under cyclic tensile loading but with amplitude of 207 MPa. The pre-corrosion was done using a 3.5% NaCl solution at a 15/1 ratio of hydrogen peroxide (30% lab grade) in order to produce two initial discontinuity states measured to be average pitting depths of 20 and >30 μm. They noted the corrosion pits were crack origins in all specimens and large pit surface areas contributed to crack development in a low number of cycles leading to premature failure as compared to pristine specimens. Their observations regarding the lack of evidence supporting a strong relationship between critical pit depth and cycles to fracture lead them to conclude there were other factors at work in determining when and where a crack will form; a such as material thickness, pit geometry (shape, depth and area) and proximity to other pits. Overall they

remarked that in 7075-T6 aluminum alloy, pitting is a major factor affecting the nucleation of fatigue cracks.

In an OSU in-house study by Dashputra [24] on 1.6 mm thick sheet, he reported greatly reduced fatigue lives compared to machine cut specimens due to the thermally affected zone, determined to be approximately 1.6 mm in width, in the laser cutting fabrication process.

Microstructural constituent particles within alloys have also been determined to have considerable influence on their performance. Pao et al [62] observed pre-corroded 7075-T7351 specimens submersed in a 3.5% NaCl solution failed 2-3 times sooner that un-corroded counterparts and reduced the fatigue crack initiation threshold by 50%. The test was performed on 63.5 mm rolled plate cycled at 15 Hz and a stress ratio of 0.1 using blunt notch, wedge opening type loading. The alloy was determined to have constituent particles of $Al_{23}CuFe_4$, Al_2CuMg, and other Si-inclusive particles. The corrosion pits tended to be elongated in the rolled grain direction and the corrosive solution tended to attack the region around and near these constituents and all of the fatigue cracks initiated at the pre-existing corrosion pits. Similar findings were reported by Pao et al [63] in another paper fatigue testing 7075-T6 specimens pre-corroded in an aerated 0.6 M NaCl solution. The alloy was examined by scanning electron microscope and found to contain cathodic constituent particles of $Al_{23}CuFe_4$ which tended to collect parallel to the rolled direction. Significant pit coalescence was observed. Results indicate that the presence of corrosion pits can significantly shorten the fatigue crack initiation life and decrease the threshold K_{th} of the alloy by as much as 50%. Post initiation analyses further confirmed that, when corrosion pits were present, fatigue cracks always initiated from these pits. In

the absence of pits, fatigue cracks initiated from large inclusions. In this fashion Birbilis et al [64] noted the constituents Al_7Cu_2Fe and Mg_2Si are capable of influencing rapid early corrosion of 7075-T651 and that Al_7Cu_2Fe represents a particularly dangerous situation with respect to corrosion, since Al_7Cu_2Fe particles can generate damage beyond their dimensions with overlapping "spheres of influence", which leads to larger pits.

2.3 – Key Points of Literature Review

In summarizing the literature review several aspects keep repeating in the various works; some informative points follow:

Salt environments have a detrimental effect on aircraft structures, irrespective of loading frequency or stress level

To initiate a stable crack, there should be a critical pit size at a given load level for pit–crack transition

Typically when pits were present, cracks initiated from these pits

Cracks initiated within a corrosion pit at a grain boundary within the pit, which was not necessarily the deepest point

Corrosion and/or pitting damage significantly reduces the fatigue life of these aluminum alloys; the degree of values can range, under specific conditions, from 3 to as much as 100 times less than the un-corroded test specimens.

The stress concentration threshold required for fatigue crack propagation can be reduced by as much as 50%.

Electrolytic environments such as NaCl serves as a nucleus for corrosion pitting

The chloride breakdown of the protective oxide layer leaves the alloy susceptible to corrosion pitting but also the presence of constituents within the aluminum matrix creates an anode-cathode relationship leading to a galvanic reaction.

For structures under cyclic loading and exposed to a corrosive environment, the processes of corrosion and fatigue often occur synergistically

Longer exposure to a corrosive environment does not necessarily result in a direct lowering of fatigue life

When corrosion pits were present, fatigue cracks always initiated from these pits; in the absence of pits, fatigue cracks initiated from large inclusions

Pristine, un-corroded, laser cut specimens have a significantly lower fatigue life compared to machine cut specimens

At higher stress levels, the differences in fatigue lives from low corrosion to high corrosion are less pronounced

CHAPTER 3

METHODOLOGY

3.1 – Overview

The primary objective of this study is to determine the minimum amount of corrosion pitting necessary to initiate cracks at pits in sheet aluminum alloys, subject to cyclic loading in an as received manufacture's finish. In previous works all fatigue cracking of specimens, whether machined or laser cut, subject to this type of one-way bending without any corrosion began at the edges [24 – 27].

The corrosive medium chosen to institute pitting damage to the specimens was salt water which has an average sodium chloride (NaCl) concentration of 35 parts per

thousand [65]. It was chosen so as to closely represent a typical ocean water service environment experienced by aircraft and other surface craft. The salt water solution was obtained by mixing 3.5% by weight un-iodized table salt in room temperature distilled water. In the present study, because of time and equipment limitations, a 30% laboratory grade hydrogen peroxide has been used as a corrosion accelerator, similar to the ASTM G110 specification [66]. Fatigue displacements have been chosen to yield failures in 10,000 to 10,000,000 cycles.

Preliminary experiments were conducted in order to ascertain the appropriate mixture ratios of 3.5% salt water solution to hydrogen peroxide. In experiments performed by Jones, et al, salt water to hydrogen peroxide ratios of 15:1 for both 2024-T3 and 7075-T6 [28, 29].

3.2 – Solution Ratio Corrosion Rate Determination

Preliminary experiments were done to identify the degree of corrosion with different solution concentrations. As received coupons of 2024-T3, 7075-T6 and 6061-T6 of 1.6 mm sheet thickness, measuring approximately 10 mm x 10 mm were submerged and laid flat in laboratory Petri dishes containing the room temperature corrosive solution. Varying ratios 3.5% salt water solution to 30% lab grade hydrogen peroxide was used in conjunction with typically 30 min and 60 min exposure times. The coupons were cleaned with soap and water then acetone to thoroughly remove all corrosive solution and to arrest any corrosion underway. They were then evaluated microscopically for degree of corrosive pitting damage. This information would then be used to set the production solution in the formal experiments. The goal in this effort was

to adjust the pitting corrosion rate to values that would produce pits within about a 60 minutes; this was in order to affect the life of fatigue tests that may only last approximately the same amount of time.

3.3 – Fatigue Procedure

The thrust of these experiments was to observe the effects of corrosion pitting on the fatigue lives of sheet alloys. The specimen surface finish and edge conditions used in testing were in an "as-received" condition which would be akin to the application in an actual operational environment. The specimens had no obvious burs, gouges or other noteworthy defects that may influence the experimental outcome. Specimens of only one

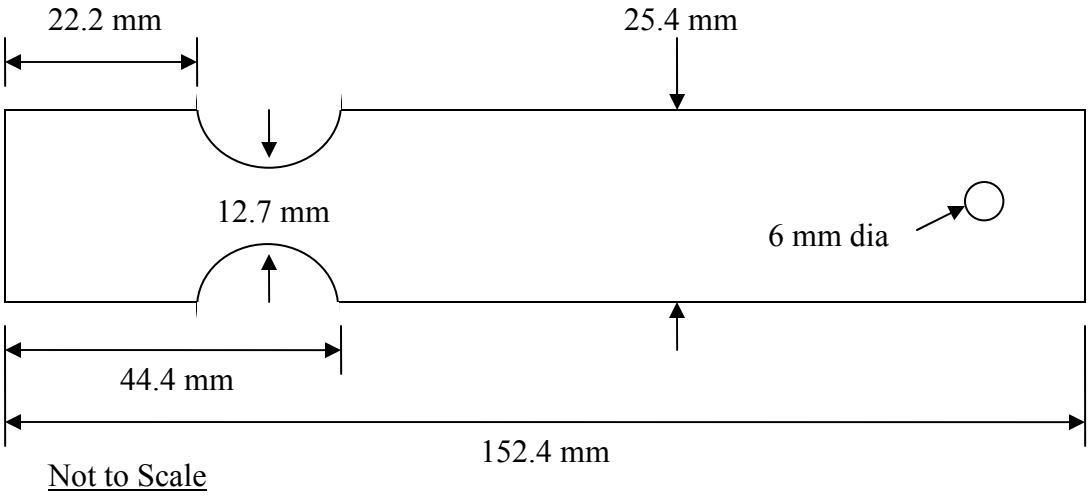

Figure 5 – Fatigue Specimen Illustration

thickness were used in the experiments, 1.600 mm (0.063 inch), and were machined in the geometry illustrated in Figure 5. This thickness is a standard gauge used widely in

aircraft manufacture. This is the geometry used in prior "in-house" studies and was chosen to localize the cracking zone for convenient observation.

Fatigue testing to failure was accomplished on a fatigue machine set up for one-way bending as illustrated in Figure 6. In original laser cut studies it was shown that the bottom or lower side edge exhibited worse fatigue performance thus it was oriented in testing to make that the tensile surface. The amount of end deflection corresponds to tension force values at the top surface of the specimen; see Table 3. The specimens were set up as shown in Figures 7 -10. The clamped end was secured approximately 3 mm above the waist or necked area. The deflected end was then secured to the pivot rod by cap screw/nut/washers.

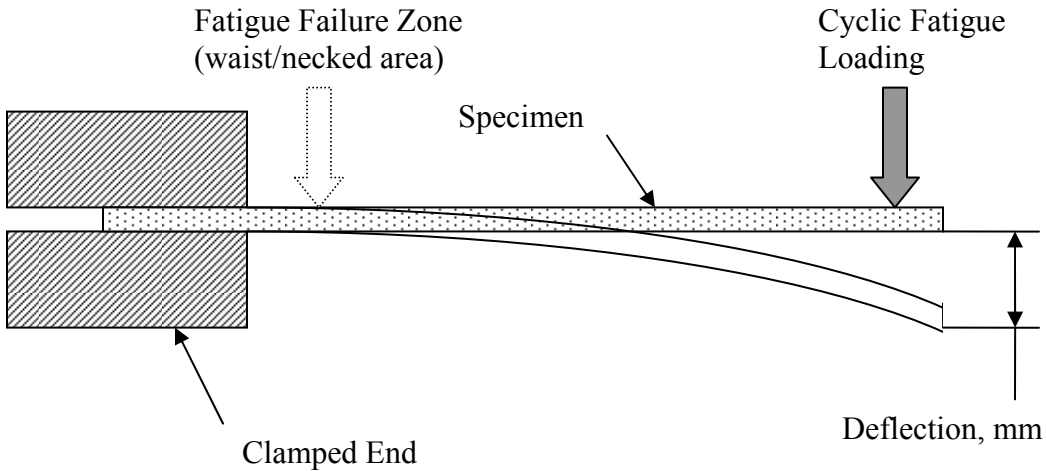

Figure 6 – Fatigue Specimen Cyclic Loading Illustration for One-Way Bending

Care was taken in establishing the null point in the deflection set in order to achieve an accurate one-way bending mode; not properly doing this could result in two-way bending and other errors that would marginalize the experimental results. A caliper was used to measure the minimum or uppermost deflection of the pivot rod at each dial setting of the eccentric, using the machine base plate as reference – the eccentric shaft was rotated until the top-dead-center point was reached while holding the caliper in place; the maximum reading on the dial facing was recorded. This measurement was then used in turn to set the vertical height of the clamping block.

Table 3 - Deflection to Stress at Specimen Top Surface [26]

Deflection, mm	Tensile Stress, MPa	Tensile Stress, ksi
8	125.5	18.2
10	157.2	22.8
11	172.4	25.0
12	188.2	27.3
13	204.1	29.6
14	220.0	31.9
15	235.1	34.1
16	251.0	36.4
17	266.8	38.7
18	282.7	41.0
20	313.7	45.5

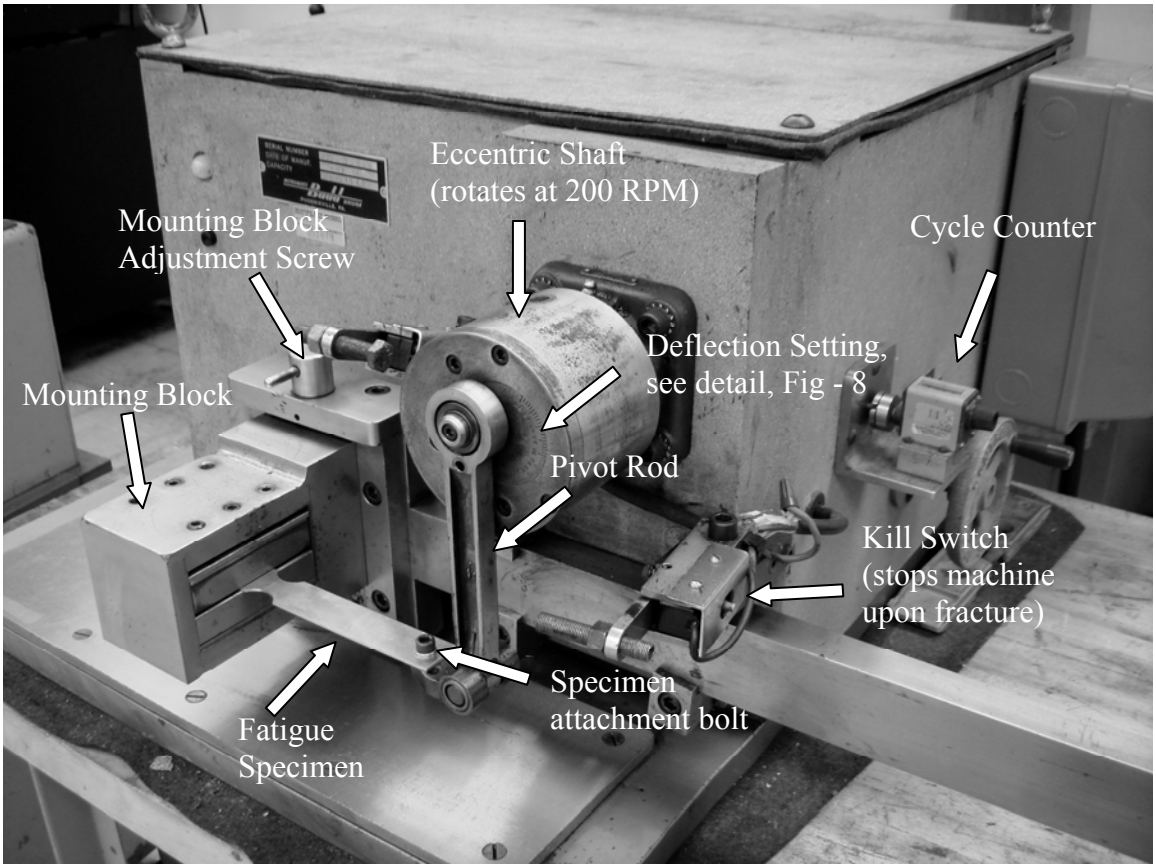

Figure 7 – Fatigue machine set-up (Budd Instruments). The eccentric shaft rotates at 2,000 RPM (33 Hz) and imparts a vertical deflection to the end of the mounted specimen via the pivot arm. The fixed end of the specimen is secured in the mounting block. To ensure on-way bending, the specimen must be calibrated for each deflection by finding the upper most (null) point of the eccentric shaft and adjusting the mounting block to the same value.

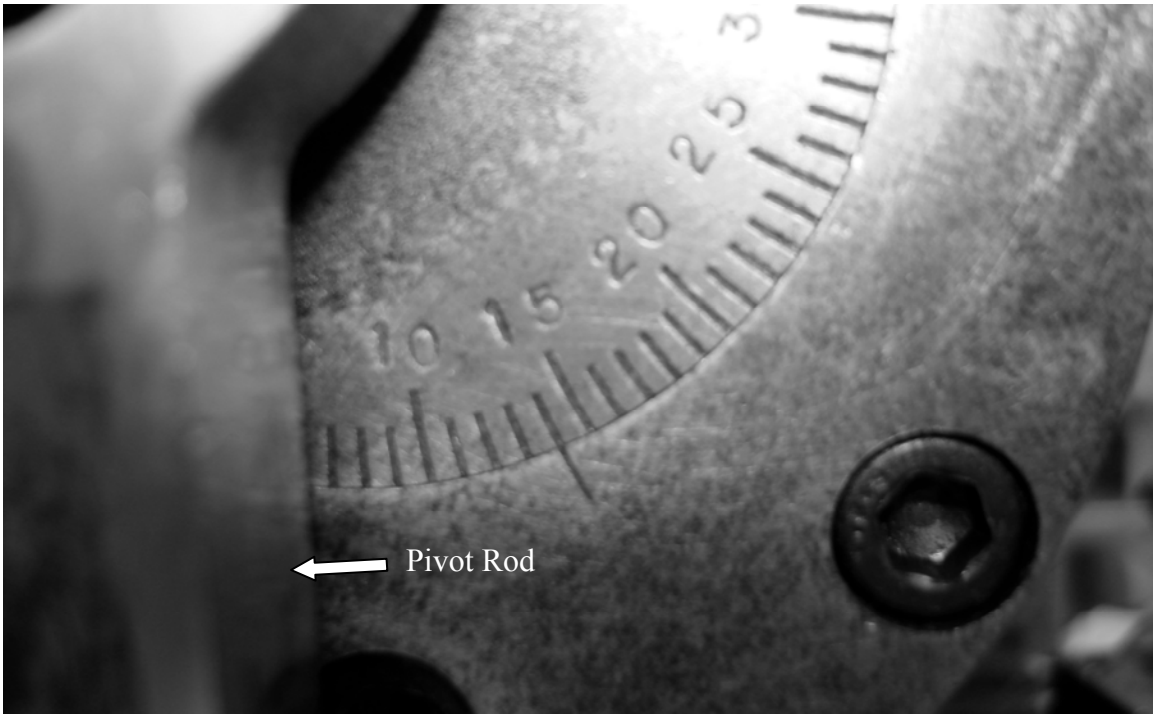

Figure 8 – Detail of eccentric shaft deflection setting. The end deflection is set using this eccentric; this particular setting is for 14 mm.

With the null position accurately set up the one-way bending fatigue testing could now be conducted with ensured integrity – note: this point in the experimental set-up is critical in order to achieve accurate results. Wide differences in some pristine specimen failure values were notes in previous work due to possibly improper set-up but could have been attributed to the general wide variation in lives typically associated with fatigue. The final step was to ensure alignment of the pivot rod end and the clamped end of the specimen in order to prevent any out of plane loading which would result in possibly something other than pure bending/tension. Alignment of the clamped and pivot ends was achieved by measuring the lateral distance of each end to the machine fixture bar and adjusting the specimen prior final clamping so they each measurement was approximately the same; a distance of 86 mm was typical. The fatigue machine rotates at an approximate constant 2000 rpm (33 Hz) until specimen failure. Once failure

separation occurs the freed pivot arm with fractured portion of the specimen attached centrifugally exits the defined orbit configuration, initially constrained by an intact specimen, and contacts a “kill switch” which promptly shuts down the drive motor concluding the test and defining the number of cycles to failure (N_f) recorded by the cycle counter (reading x 100).

Figure 9 – Finding the upper most/null point of travel of the eccentric pivot rod. This measured value will be used to set the mounting block height to ensure the fixed end and mounted end of the specimen are level; a necessary condition for one-way bending.

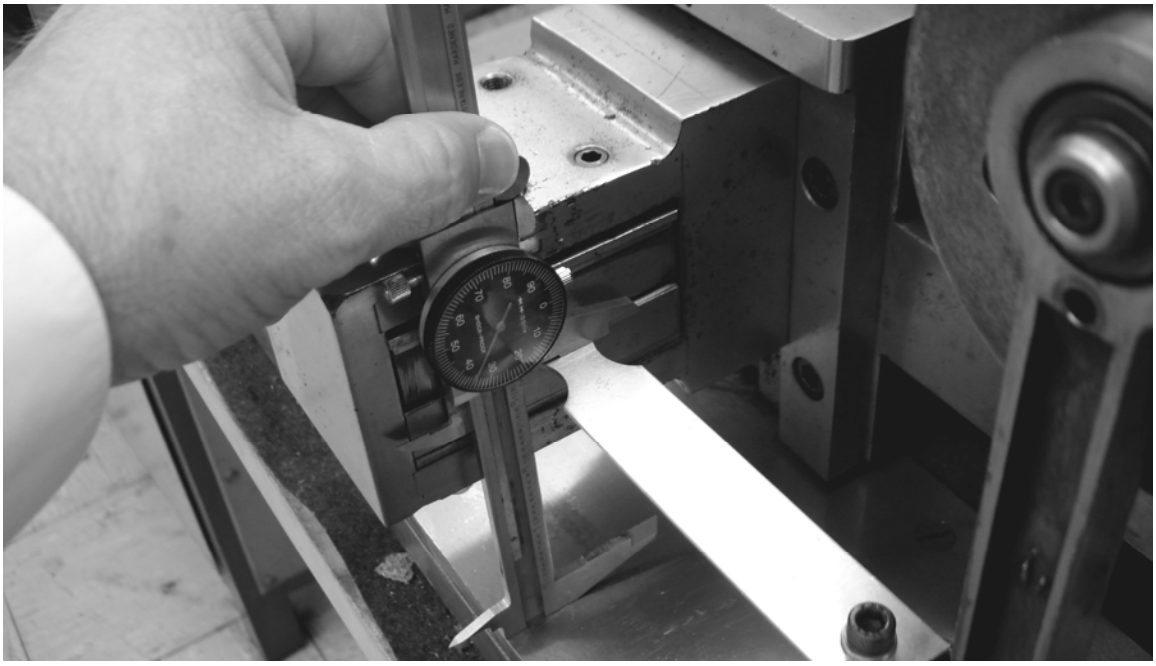

Figure 10 – Setting the mounting block. The null value found in Figure-x is used to set the mounting block height.

3.4 - Corroding During Cyclic Loading

Cotton fiber was used to hold the corrosive solution in place on the specimen, whether during pre-corrosion or corrode-during testing; Figure 11. The fiber was wrapped around the waist, fully encapsulating the fatigue zone. A hypodermic syringe (Figure 12) was then used to inject approximately 3 ml of solution into typically about 0.5 grams weight of cotton fiber, fully saturating so that all surfaces within the fatigue zone were wet with the corrosive solution; the wicking action of the cotton fiber maintained an even, consistent exposure to all surfaces and achieved the desired quasi-uniform corrosion distribution. One possible problem in conducting fatigue testing while also subjecting the specimen to corrosion is the possibility of evaporation of the corrosive solution. Several barriers were investigated to prevent evaporation but the most versatile and effective was an ordinary latex rubber finger cot (Figure 13). The cot was cut at one

end and slipped over the specimen to just below the clamp line then rolled down; encapsulating the cotton fiber.

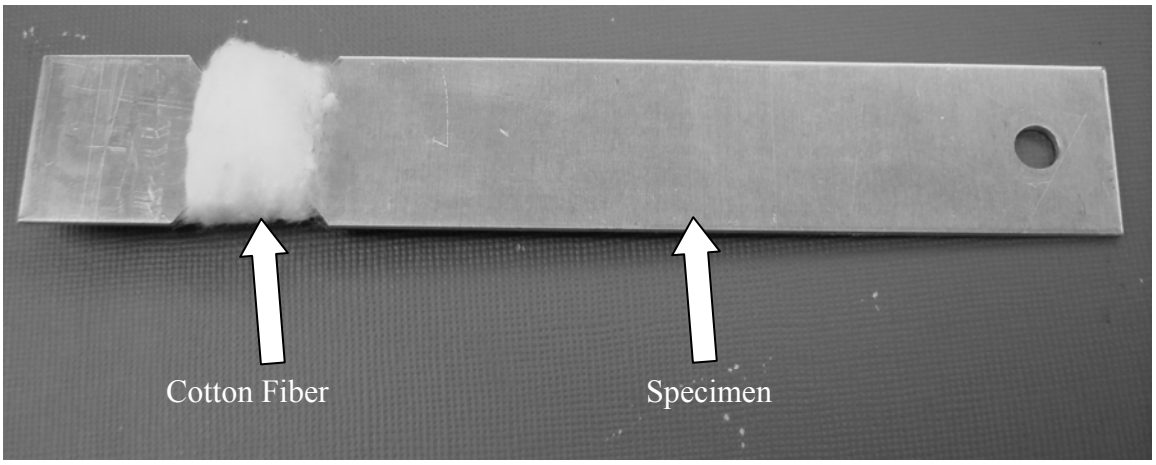

Figure 11 – Specimen with cotton fiber. The cotton fiber wrapped around the specimen waist area and is saturated with the corroding solution.

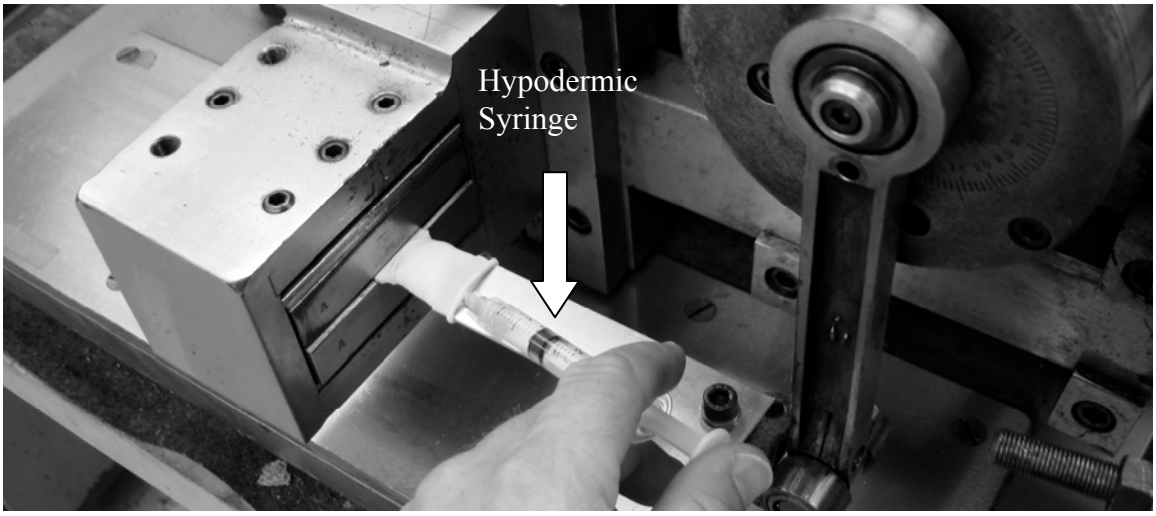

Figure 12 – Injecting the corroding solution in-place with syringe. The specimen is placed in position to cycle to failure; the solution is injected underneath the finger cot just before cyclic loading begins. The solution fully saturated the cotton fiber exposing all sides of the specimen within the waist area/fatigue zone to the corrosive solution.

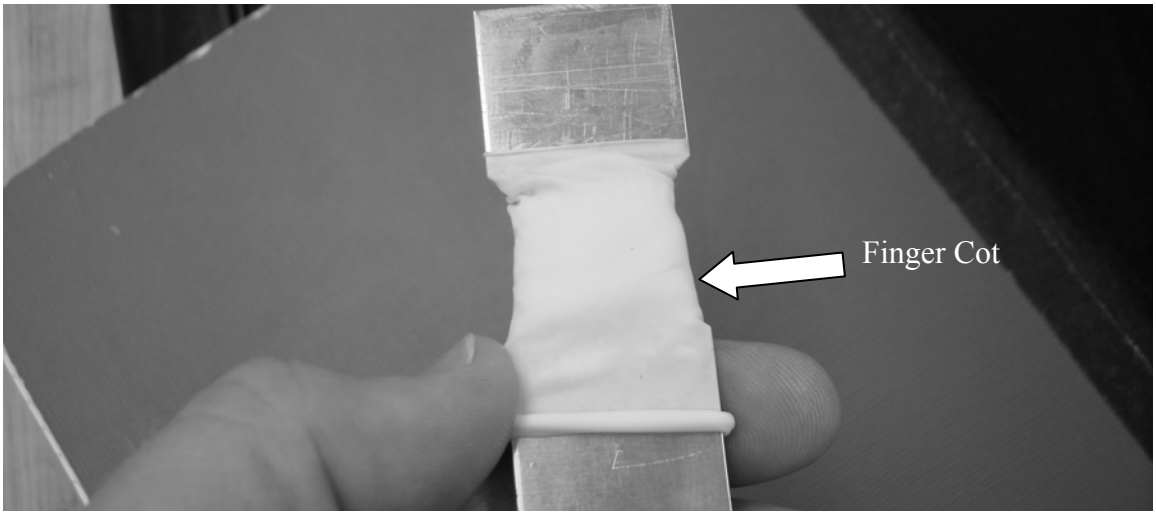

Figure 13 – A finger cot is positioned over the cotton to prevent/minimize evaporation and aid in holding the solution in place during any cyclic loading**.**

Fabricated, specimens with no preexisting corrosion were run to failure in order to establish baseline fatigue lives at various deflection/stress levels. Preliminary pre-corroded specimens were run in order to determine the effectiveness and influence of the corrosion on the fatigue lives and to deduce if the approximately 60 minute target life would be achieved with theses combinations of solution ratio, pre-corrosion time, and the cyclic loading stress level or deflection.

3.5 - Microscopic Examination

Fractured specimens were examined with the Nikon Epihot 200 metallurgical microscope and noteworthy fracture elements photo-documented. Particular attention was given to the degree of pitting and any subsequent crack originations and propagations near the primary fracture surface indicating the possibility of multiple crack origins. Pit depth being directly related to the thrust of these experiments was closely scrutinized and endeavored to quantify approximately the average pit depth and note any

pits of maximum size. A technique utilizing the metallurgical microscope was used to measure pit depth – by drawing from the ASTM Standard G-46 for evaluating pitting corrosion, an optical means for measurement is accomplished using the focal adjustment precise movement [67].

According to the manufacturer's specifications, the fine focus knob moves the microscope object lens cluster up or down vertically a distance of 1 micrometer (μm) for every increment on the fine focus knob. By focusing on the bottom of the pit and then the top of the pit and noting the difference fine focus knob increments a direct correlation to pit depth can be obtained with reasonable accuracy.

A quick validation of this was accomplished using a piece of tape measure with a micrometer to be approximately 58.4 μm thick. The tape was then placed on a piece of flat stock aluminum sheet and viewed under the metallurgical microscope; focusing on the top of the tape and then the aluminum sheet stock and noting the difference in fine focus knob increments. The correlation in measurements to manufacturer specifications closely agreed as seen in Table 4; the average measured value was 62.5 μm which is within 10% of the measured 58.4 μm value.

Table 4 - Measurement and validation of microscope focus knob increments

Magnification	Fine Focus Knob Increments
50x	60
100x	64
200x	69
500x	57
AVERAGE	62.5

3.6 - Hardness Measurements

In order to affirm the material of each specimen group corresponded to correct material specifications, hardness measurements were conducted using a Clark model CR-3e hardness tester (Figure 14). If these measurements corresponded reasonably to the published values for each material, then the identity was judged to be accurate and further testing could proceed with confidence. The averages of a minimum of 3 measured values of in hardness, in the Rockwell-B (HRB) scale, are given in Table 5. The values correspond reasonably well to the published values of each alloy and so it was concluded the identity of each specimen was accurate for testing purposes.

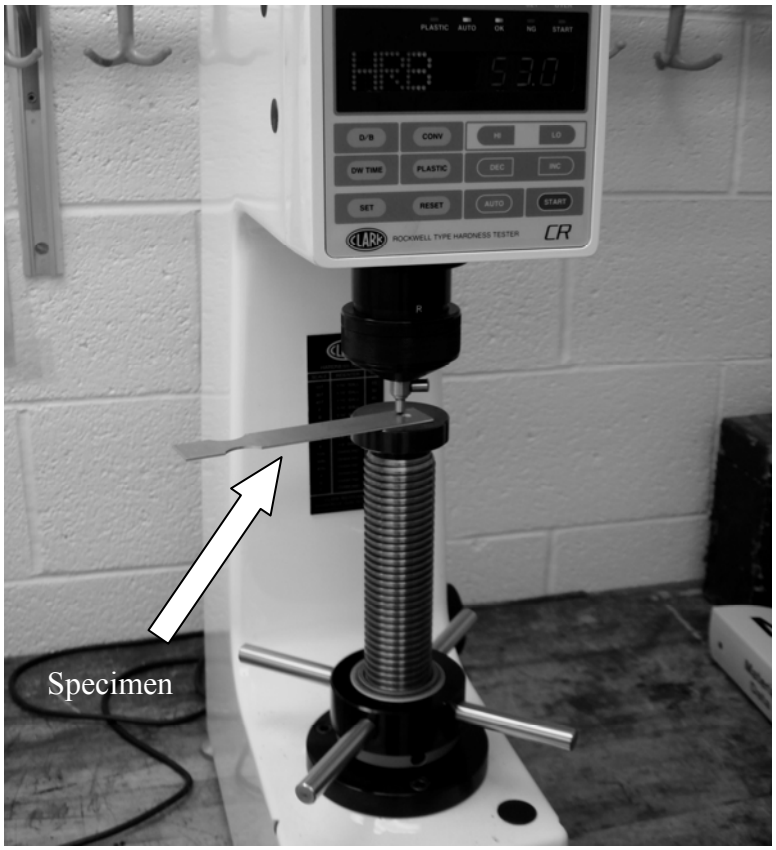

Figure 14 – Hardness Tester, Clark Model CR-3e.
Specimens were spot checked for hardness values.

Table 5 - Measured Values of Specimen Material Hardness

Measured Average Hardness (HRB)	Reference Hardness (HRB) [40]	Difference	Alloy/Condition
74.7	75	0.40%	2024-T3 machined
74.5	75	0.67%	2024-T3 laser cut
93.3	87	6.75%	7075-T6 machined
56.9	60	5.45%	6061-T6 machined

3.7 – Microstructure

For microstructure examination, sections from all 3 surface directions (top, end and side) representing all 3 grain directions were prepared by conventional mounting sectioned pieces of each alloy material in phenolic resin blocks, sanding to 600 grit finish and then rotary wheel polishing with a 5μm alumina slurry. The surfaces of the polished specimens were etched using 0.5% HF solution for all alloys to reveal any inclusions near the surface. Additional etching to contrast the grain boundaries was done with Keller's reagent (solution of 2 ml HF, 3 ml HCl, 5 ml HNO_3 and 190 ml water) for the 2024-T3 and 7075-T6 specimens. A solution of 5 ml HF, 10 ml H_2SO_4 and 85 ml water was applied to the already 0.5% HF etched surface of the 6061-T6 specimens in attempt to contrast the grain boundaries. Results were viewed on the Nikon Epihot 200 metallurgical microscope and photo documented using the Hitachi optical camera and Clemex version 2.2b image software. A complete listing of all supplies and equipment used in the study is given in Table 6.

Table 6 - List of Supplies and Equipment

Item	Model Number/Source
Salt, table	Great-Value, Wal-Mart, Bentonville, AR
Distilled water, sodium free	Central Arkansas Water, Little Rock, AR
Hydrogen peroxide, 30% reagent grade	H323-500, Fisher Scientific
Cotton fiber	Cotton Balls, US Cotton, LLC, Rio Rancho, NM
Hypodermic syringe, 3cc and Needle 22 ga x 0.75 inch	Monoject
Latex Finger Cots	Flents #F414-436, Apothecary Products, Inc.
Acetone (nail polish remover)	Equate, Vi-Jon Laboratories, Inc, St. Louis, MO
Liquid hand soap	Equate, Vi-Jon Laboratories, Inc
Fatigue machine	Model: VSP-150, Budd Instruments, Phoenixville, PA
Inverted metallurgical microscope Optical camera Image software	Model: Epihot 200, Nikon Model: KP-M1U, Hitachi Denshi, Ltd. Model: Clemex Vision, version 2.2b, Clemex Technologies, Inc.
Stereo zoom microscope Optical camera Image software	Model: SZX9, Olympus Model 3.2.0: Diagnostics Instruments, Inc. SPOT version 3.4, Diagnostics Instruments, Inc
Caliper, dial, 6 inch	unk
Phenolic Resin	Buehler
Specimen Mounting Press	Buehler
Alumina, 5 micron	Buehler
Hardness tester	Model: CR-3e, Clark Instruments

CHAPTER 4

FINDINGS

4.1 – Microstructure: Inclusions and Grain Structure

4.2 – Laser Cut and Machine Cut Specimens

4.3 – Fatigue of Pristine Laser Cut and Machine Cut Specimens

4.4 – Corrosion Coupons

4.5 – Corrosion Rates For Top and Bottom Sides of Sheet

4.6 – Initial Fatigue Data

4.7 – Metallography of Initial Fatigue Specimens

4.8 – Corrosion-During Cyclic Loading

4.9 – Fatigue Data with Only NaCl Solution

4.10 – Metallography of Pitted Specimens by Pre-Corrosion

4.11 – Pitting For Fatigue Crack Initiation by Pre-Corrosion

4.12 – Metallography of Pitted Specimens by Pre-Corrosion

4.13 – Pit Depth Measurement

4.1 – Microstructure: Inclusions and Grain Structure

The microstructure of the 3 alloys tested is shown in Figures 15 – 28; depicting constituents, inclusions and grain structure. The captions of Figures in this Section as well as the remaining Sections are detailed and should enable the reader to follow the main points of the study. The microstructural views represented are from each flat sheet surface (top and bottom), an edge parallel to the sheet rolled direction (RD) and an edge perpendicular to the RD.

A 0.5% HF solution was used to highlight the inclusions in each alloy; revealing a moderate amount of "debris" in the makeup of the sheet alloys tested. Most alloys had a noted increase in inclusions from the top flat sheet side to the bottom (opposite) flat side. The relative top and bottom sides were determined by the presence of the as-received machine shop layout dye/ink markings; these markings were also used in mounting the specimens in the fatigue testing machine so that the same "side" was always used as the top tension surface.

To enhance grain structure the 2024 and 7075 alloys were etched with Keller's reagent (2 ml HF, 3 ml HCl, 5 ml HNO_3 and 85 ml water) and the 6061 sheet was etched with a 5 ml HF, 10 ml H_2SO_4 and 85 ml water solution. The presentation of the grain via etching in the 6061 alloy proved fairly difficult at the T6 temper; a marginally acceptable grain etch was completed for the flat sheet side but nothing approaching adequate was accomplished on the edges. The edge grain both parallel and perpendicular to the sheet rolled direction were examined; grains were generally elongated toward the rolled direction and ranged in thickness in both the 2024 and 7075 alloys from about 5 – 25 μm and averaged approximately 10 μm.

The etching revealed constituents and other inclusions present in the alloys in Figures 15 - 18. A slight subjective difference can be seen from one surface to another if scrutinized closely. For instance in Figure 15(a) and 15(b) the top and bottom surface of the 2024-T3 coupons vary in density of constituents. The 6061 and 7075 coupons varied also but most notably in the edge cross-sections; the edge parallel to the RD seemed to have more constituents/inclusions than the perpendicular face.

The grain structure details, shown in Figures 19 - 28, show both grain geometries and size and as well as the distribution of inclusions amongst the grains.

The grains on the top and bottom surfaces of the sheet are more rounded than those of the cross-section (parallel and perpendicular to the RD); which have a much more pronounced length in the RD as compared to the thickness or height. On average the grain thickness for the 2024-T3 and 7075-T6 alloys ranges about 5-25 μm; the top and bottom sheet surface had many thin grains intersecting, some as thin as 5 μm or less. The 6061-T6 proved to be not readily etchable as compared to the other alloys tested; a fair etch was accomplished on the top and bottom flat sheet sides revealing dim grain structure (Figure 25) but delineation of the grains on the edges could not be obtained at the T6 temper. The grain structure didn't differ much from one flat side to the opposite so only one typical view of the flat side is shown.

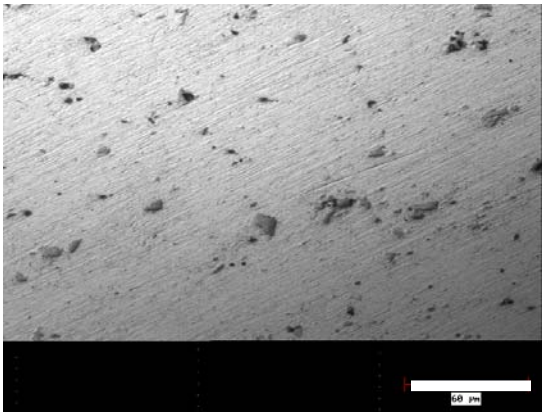

(a) Flat sheet surface (top surface)

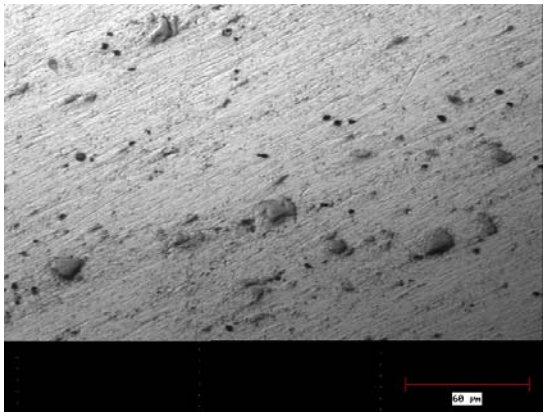

(b) Flat sheet (bottom surface)

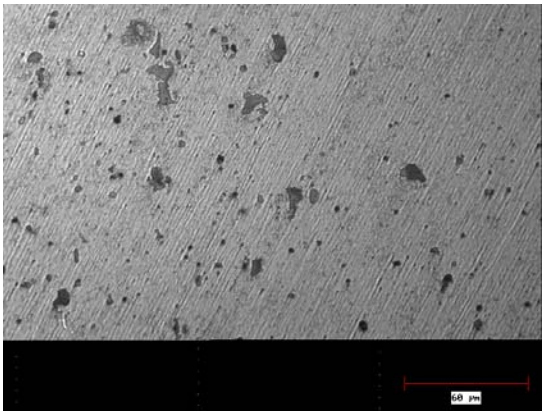

(c) Edge parallel to rolled direction (RD)

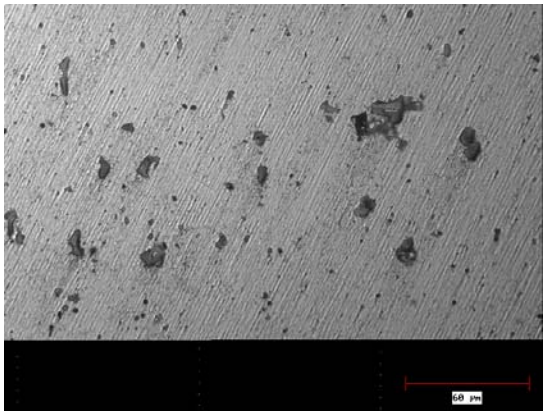

(d) Edge Perpendicular to RD

Figure 15 – 2024-T3 inclusions; (500x). Etched with 0.5% solution of hydrofluoric acid. Views (a) and (b) are from each side of the flat sheet surface (top and bottom); (c) is the sheet edge parallel to the rolled direction (RD) and (d) is from the sheet edge perpendicular to the RD. A slight increase in inclusion density is noted in (b) as compared to (a). The diagonal lines are from specimen polishing, not rolled direction. (photos MS-005/-006/-037/-040)

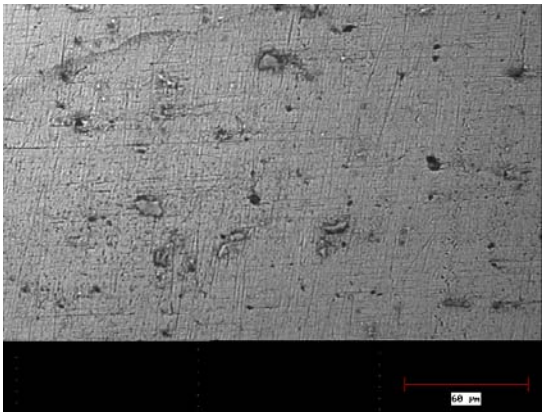

(a) Flat sheet surface (top side)

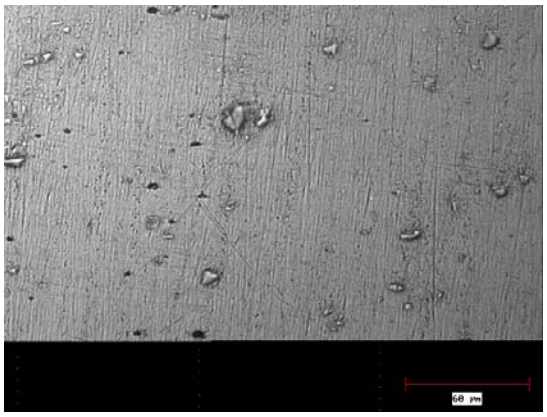

(b) Flat sheet (bottom side)

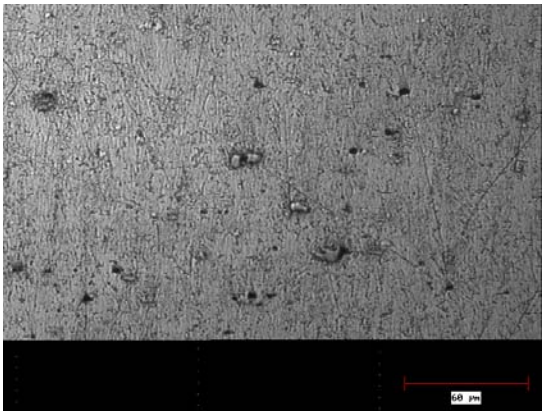

(c) Edge parallel to rolled direction (RD)

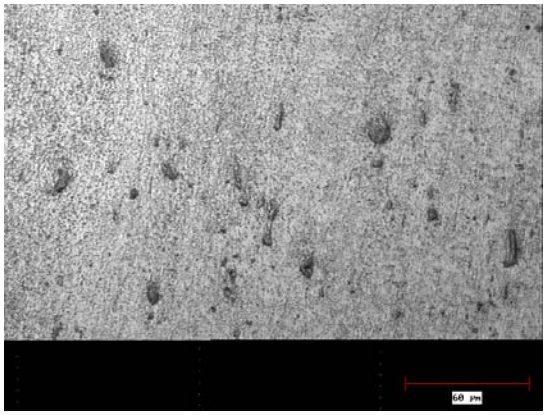

(d) Edge Perpendicular to RD

Figure 16 – 2024-T3 (laser cut series) inclusions; (500x). Etched with 0.5% solution of hydrofluoric acid. Views (a) and (b) are from each side of the flat sheet surface (top and bottom); (c) is the sheet edge parallel to the rolled direction (RD) and (d) is from the sheet edge perpendicular to the RD. (photos MS-005/-006)

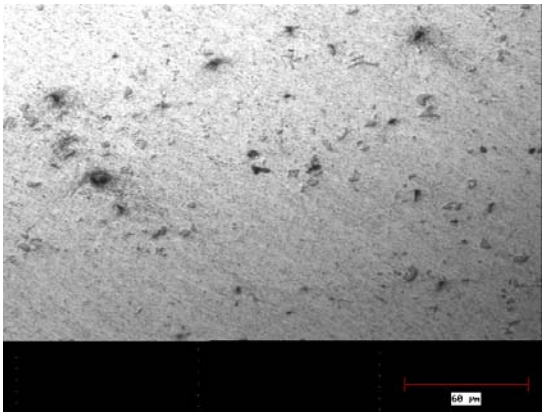

(a) Flat sheet surface (top surface)

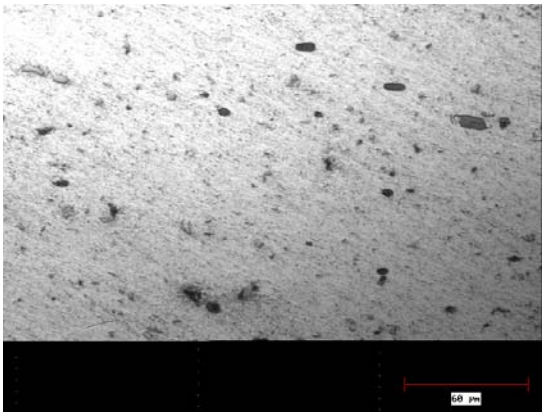

(b) Flat sheet (bottom surface)

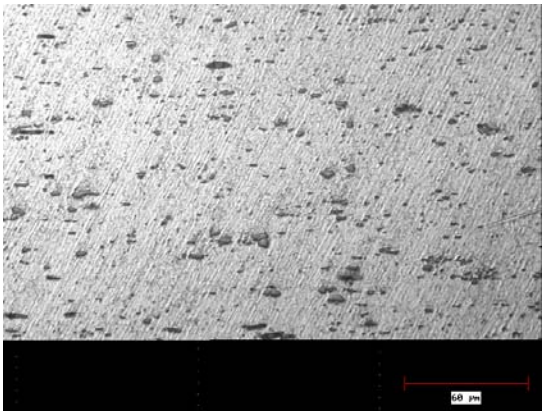

(c) Edge parallel to rolled direction (RD)

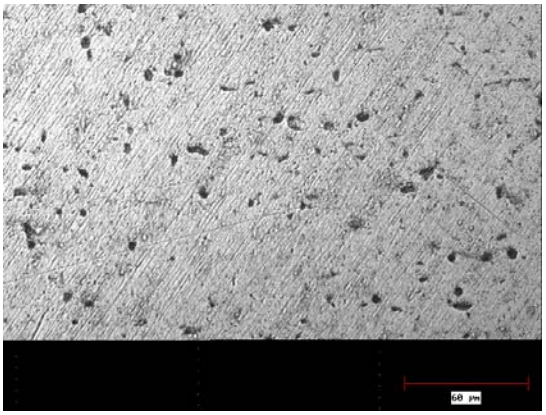

(d) Edge Perpendicular to RD

Figure 17 – 6061-T6 inclusions; 500x. etched with 0.5% solution of hydrofluoric. Views (a) and (b) are from each side of the flat sheet surface (top and bottom); (c) is the sheet edge parallel to the rolled direction (RD) and (d) is from the sheet edge perpendicular to the RD. Inclusion densities are similar in (a) and (b) but much more notable in the edge parallel to the RD (c) as opposed to perpendicular (d). (photos MS-001/-002/-030/-032)

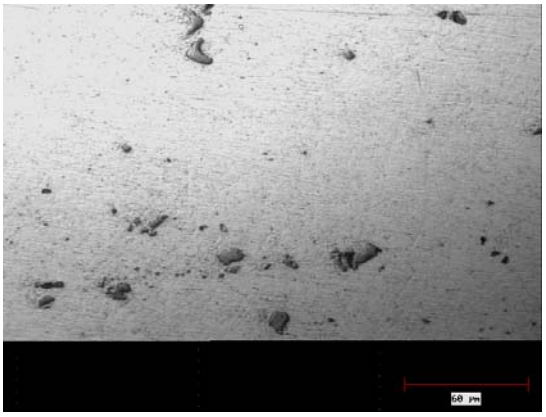

(a) Flat sheet surface (top)

(b) Flat sheet (bottom)

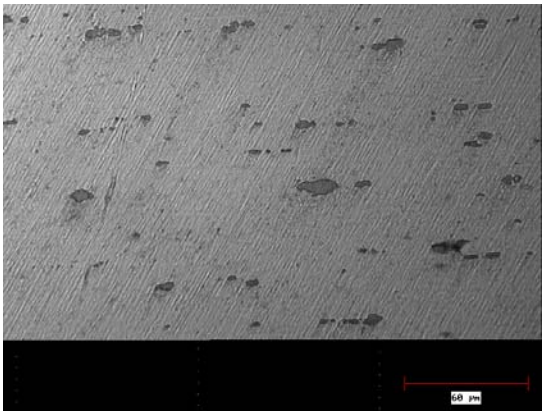

(c) Edge parallel to rolled direction (RD)

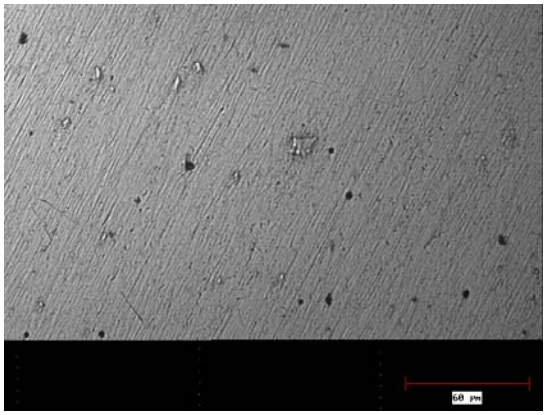

(d) Edge Perpendicular to RD

Figure 18 – 7075-T6 inclusions; each side of flat sheet surface (500x). Etched with 0.5% solution of hydrofluoric acid. Views (a) and (b) are from each side of the flat sheet surface; (c) is the sheet edge parallel to the rolled direction (RD) and (d) is from the sheet edge perpendicular to the RD. Inclusions are more notable in (c) as compared to (d). (photos MS-003/-004)

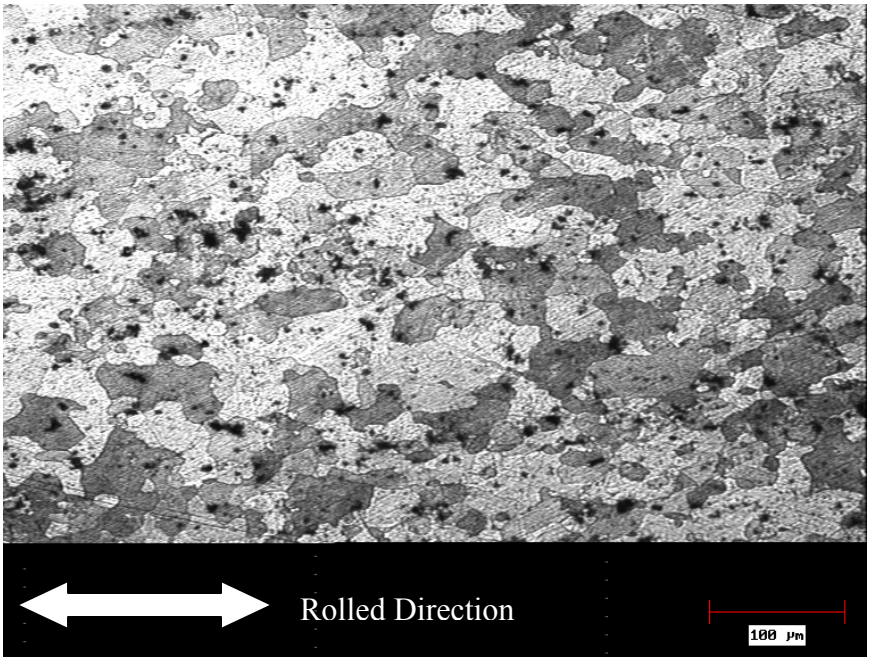

(a) 200x

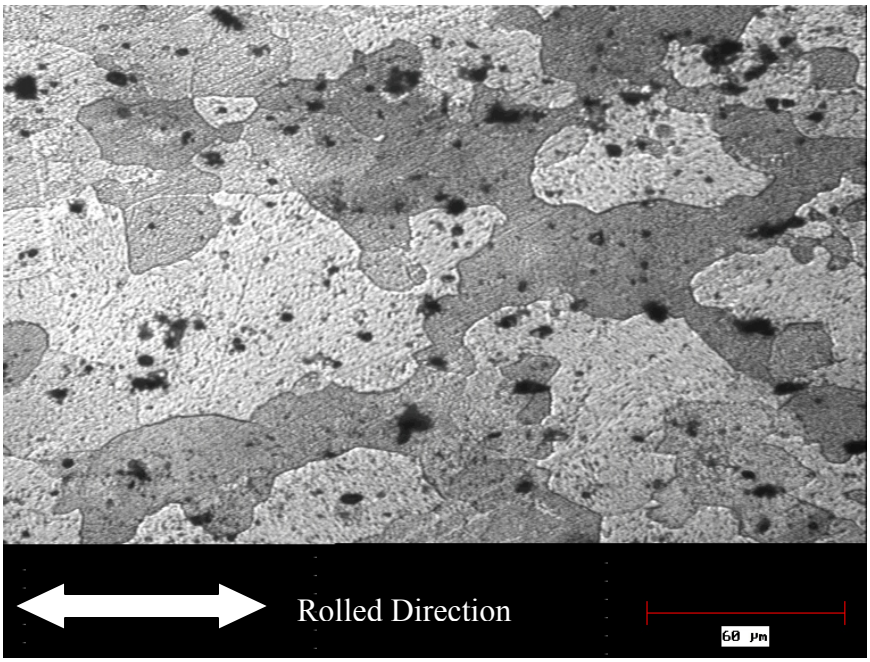

(b) 500x

Figure 19 – 2024-T3 grain structure from flat side sheet surface. Etched with 0.5% HF solution followed by Keller's reagent (2 ml HF, 3 ml HCl, 5 ml HNO_3 and 85 ml water). Also note the significant inclusions (black specks). (photos MS-013and -014)

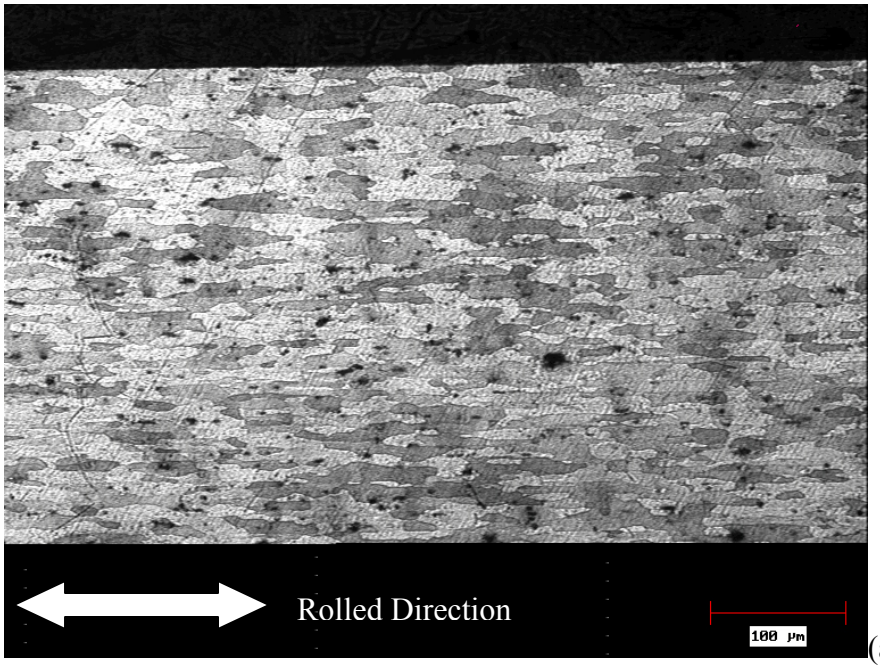

(a) 200x

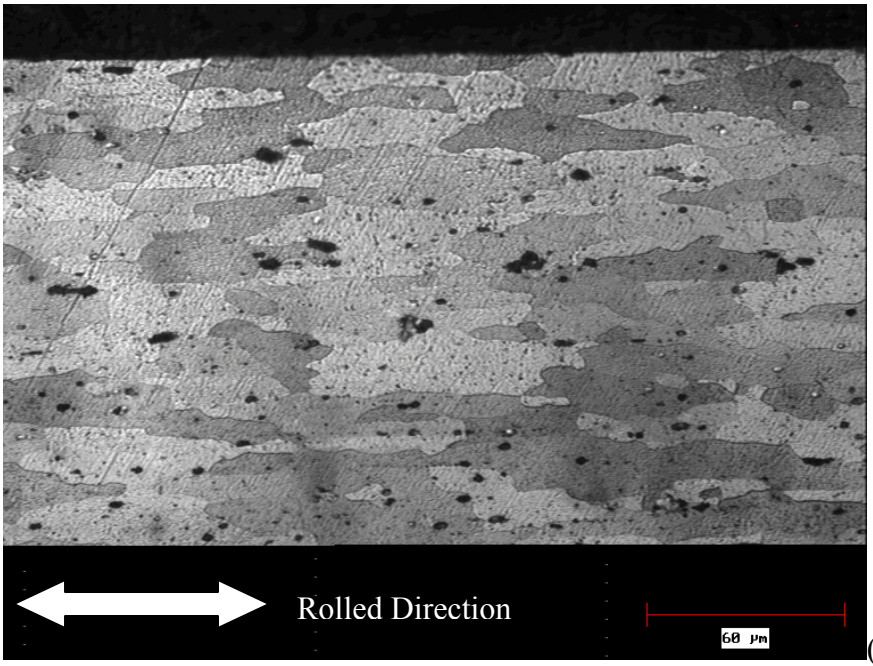

(b) 500x

Figure 20 – 2024 grain structure, edge parallel to the rolled direction. Specimens were etched with 0.5% HF followed by Keller's reagent. The upper edge of the specimen is the free surface, which some fairly thin grains are noted to intersect. The grain size thickness ranges from about 5-25 µm and average about 10 µm. (photo MS-045/-046)

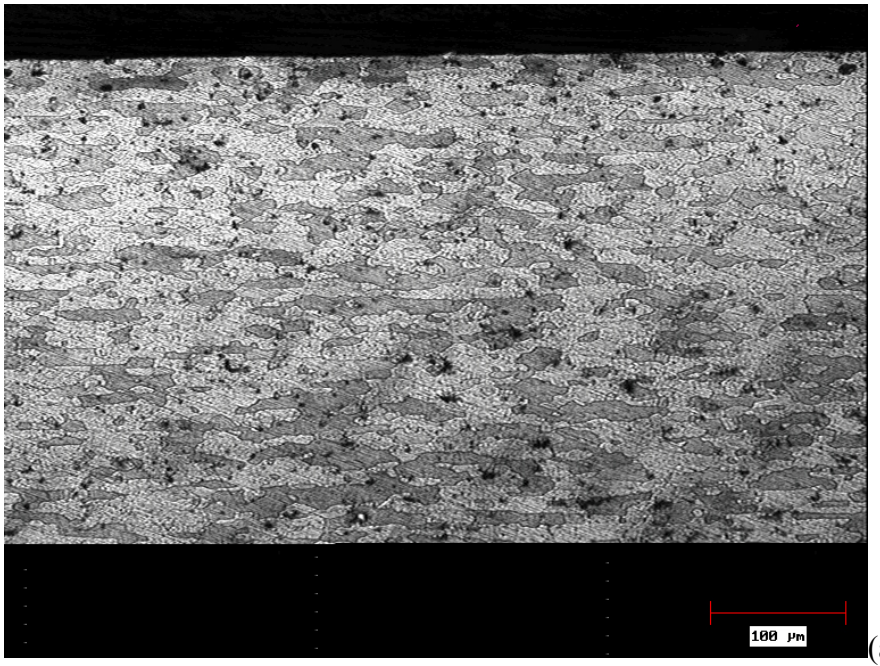

(a) 200x

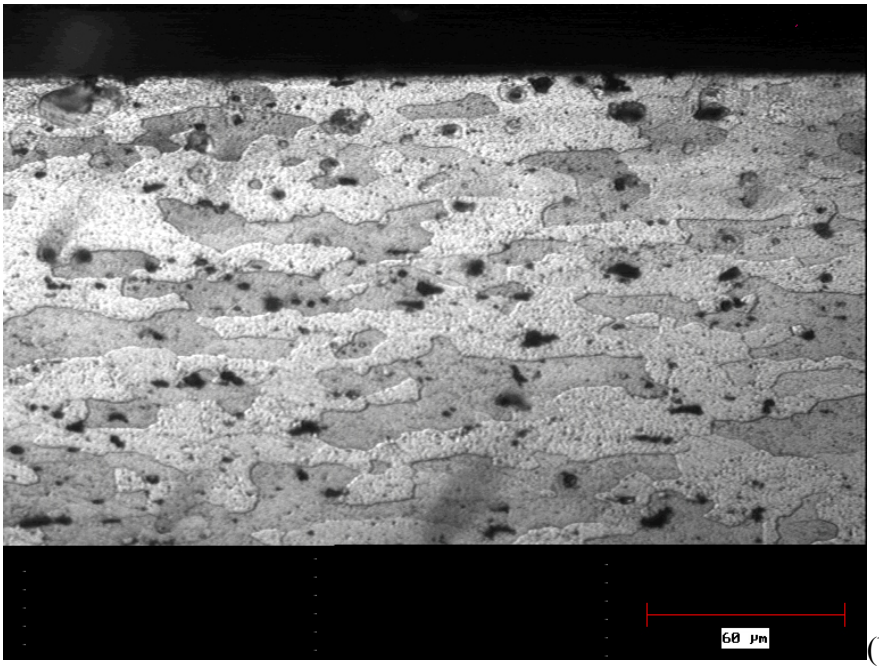

(b) 500x

Figure 21 – 2024 grain structure, edge perpendicular to the rolled direction. Specimens were etched with 0.5% HF followed by Keller's reagent. The upper edge of the specimen is the free surface, which some fairly thin grains are noted to intersect. The grain size thickness ranges from about 5-25 µm and average about 10 µm. Notable inclusions observed (black specks). (photo MS-047/-048)

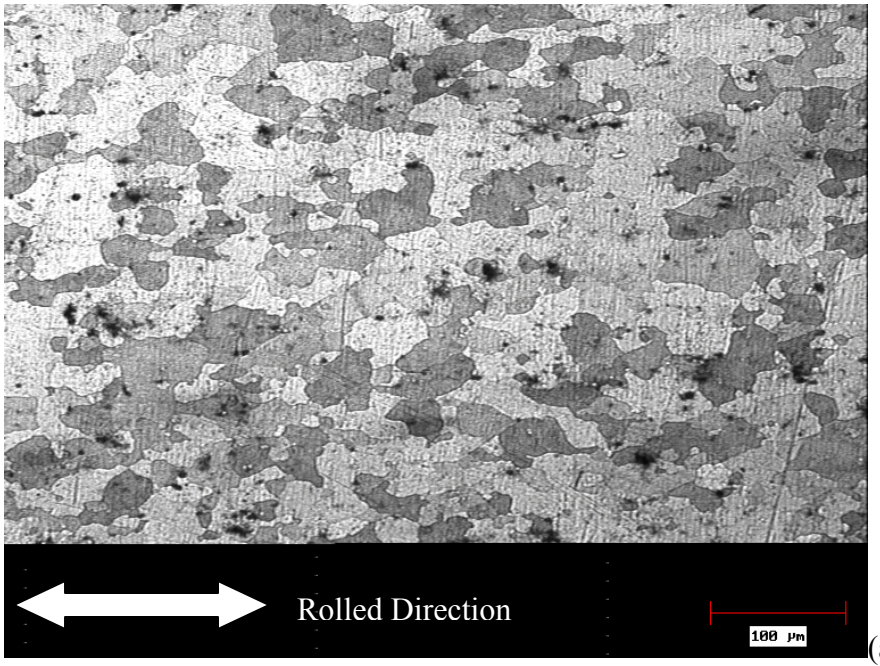

(a) 200x

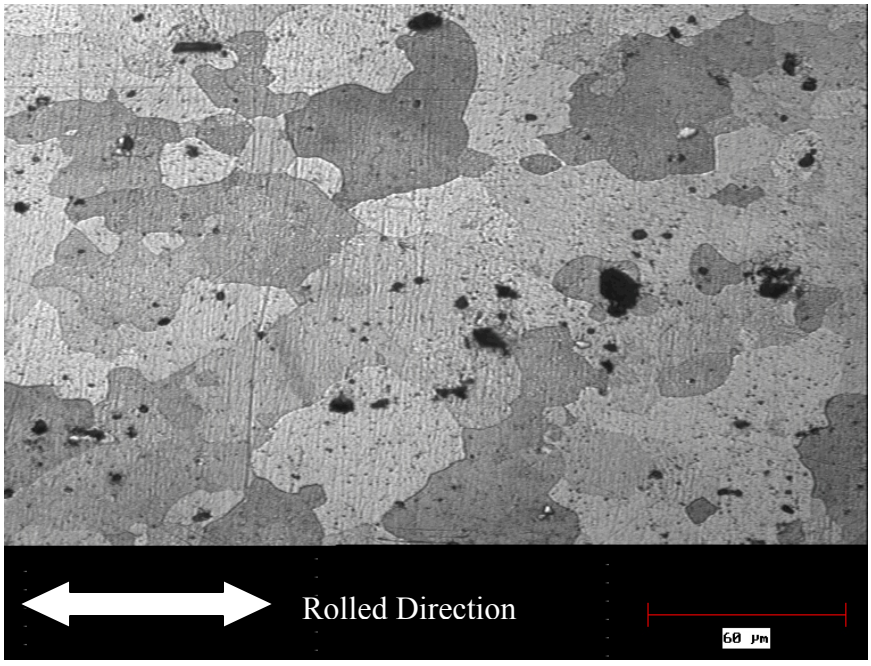

(b) 500x

Figure 22 – 2024-T3 (laser cut) grain structure from flat side sheet surface. Specimens were etched with 0.5% HF followed by Keller's reagent. (photos MS-028 and -027)

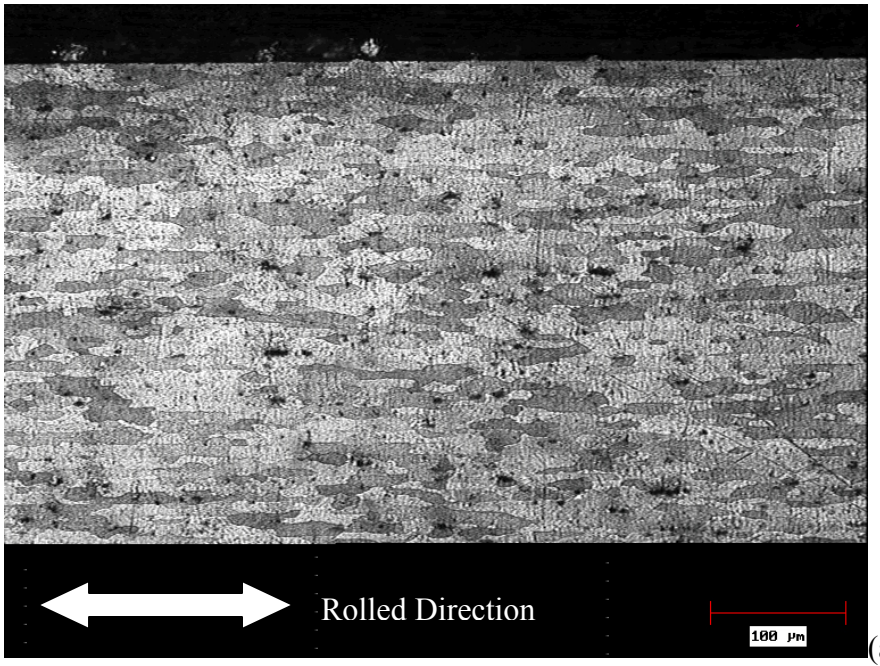

(a) 200x

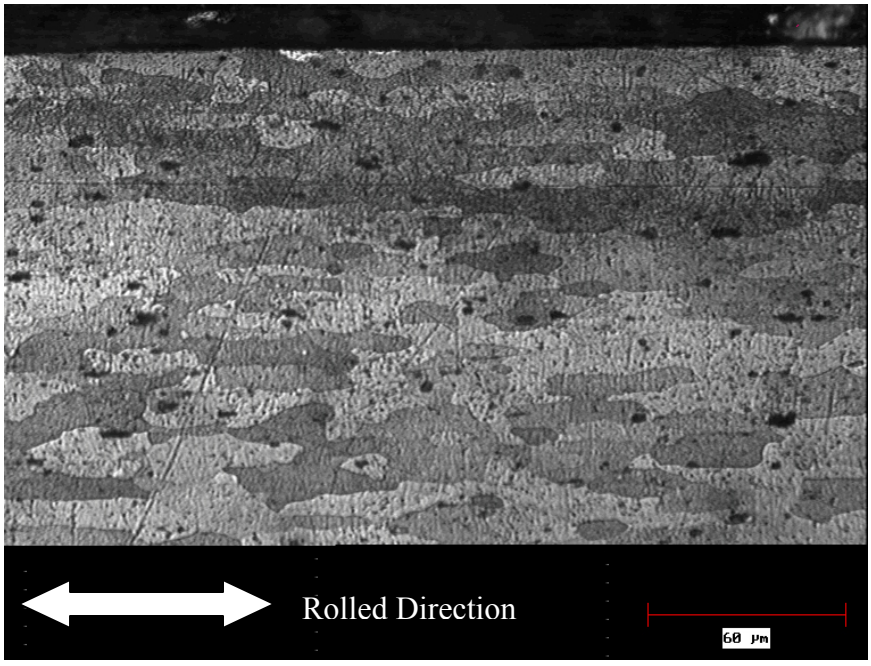

(b) 500x

Figure 23 – 2024 (laser cut) grain structure, edge parallel to the rolled direction. Specimens were etched with 0.5% HF followed by Keller's reagent. The upper edge of the specimen is the free surface, which some fairly thin grains are noted to intersect. The grain size thickness ranges from about 5-25 µm and average about 10 µm. (photos MS-049/-050)

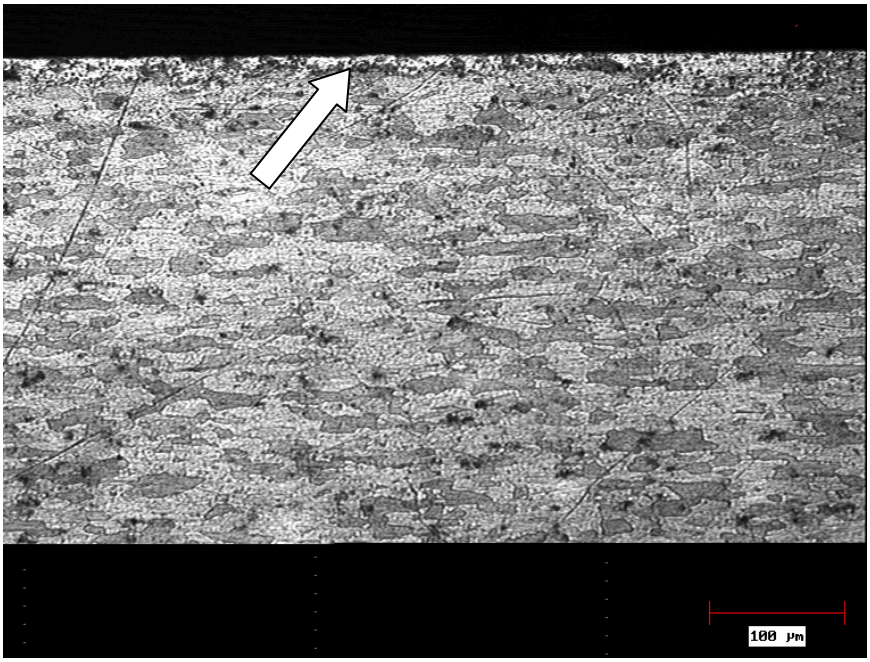

(a) 200x

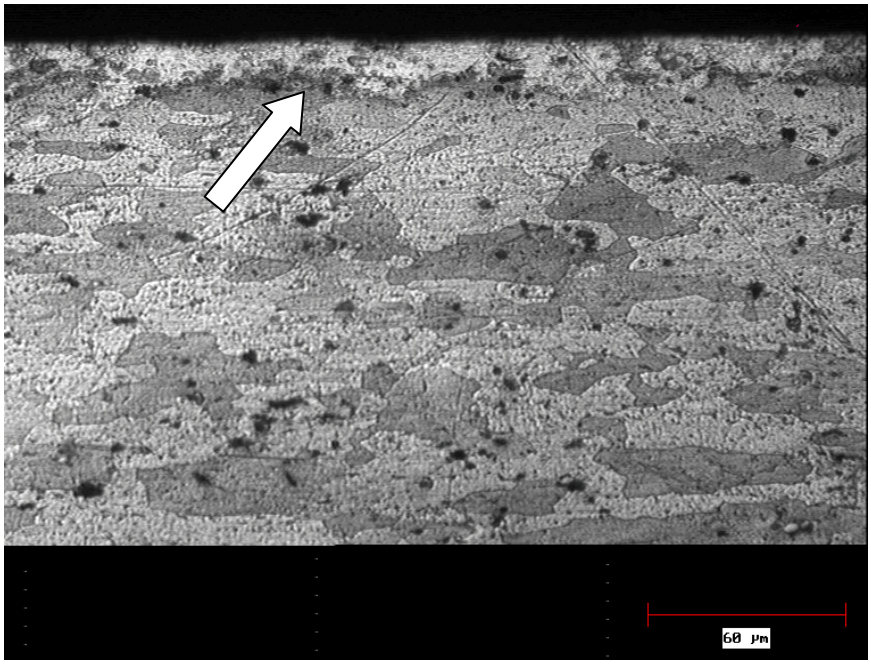

(b) 500x

Figure 24 – 2024 (laser cut) grain structure, edge perpendicular to the rolled direction. Specimens were etched with 0.5% HF followed by Keller's reagent. The upper edge of the specimen is the free surface, which some fairly thin grains are noted to intersect. The grain size thickness ranges from about 5-25 µm and average about 10 µm. The solid band across the top is a result of melting within the laser cutting heat affected zone. (photos MS-051/-052)

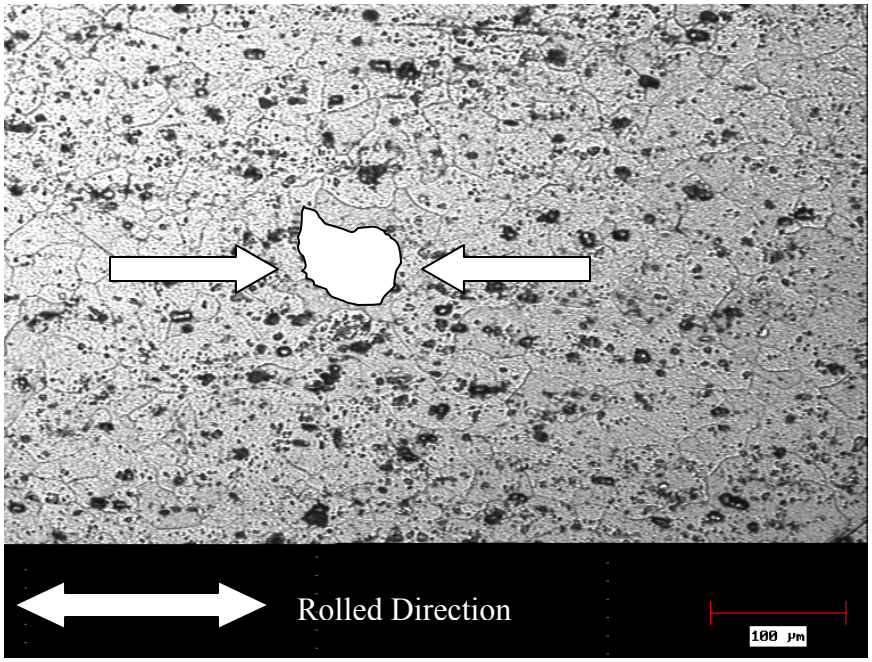

(a) 200x

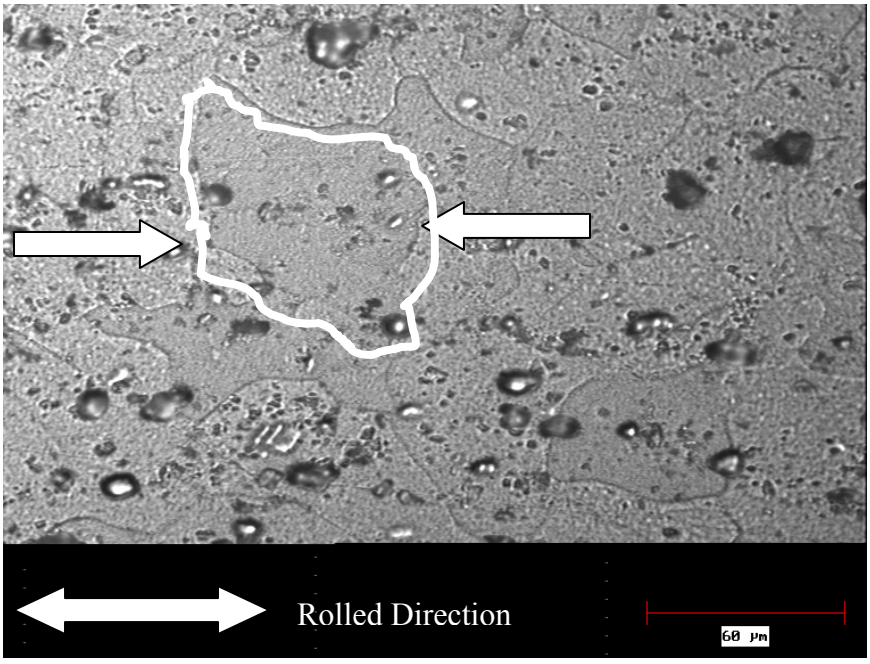

(b) 500x

Figure 25 – 6061 grain structure on flat sheet surface. Specimens etched with 0.5% HF then again separately with 5% HF and 10% H_2SO_4 solution. A typical grain is shown between arrows in both photos; in (a) and (b) a grain is filled-in and outlined for illustration. Significant inclusions noted. (photos MS-058 and MS-057)

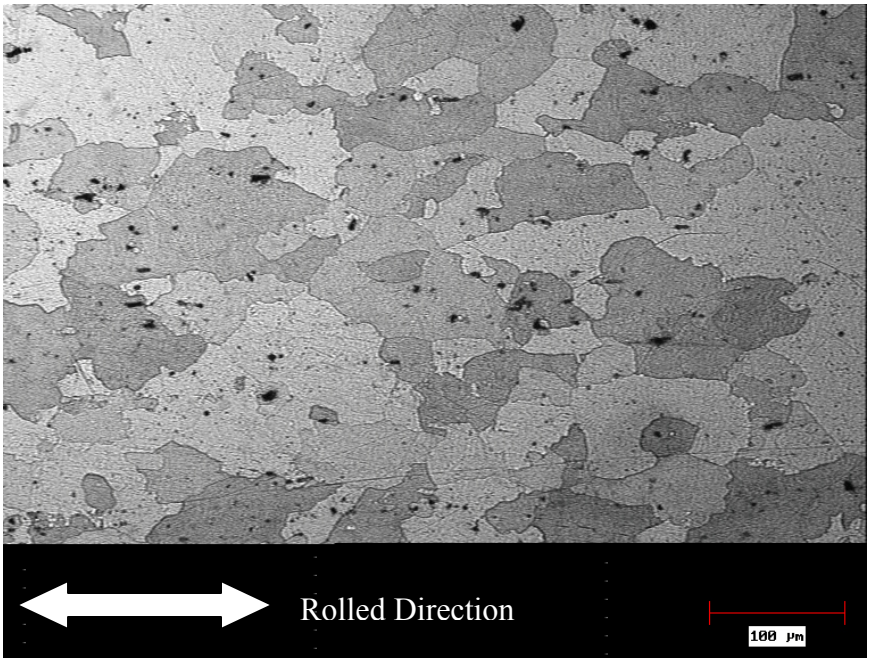

(a) 200x

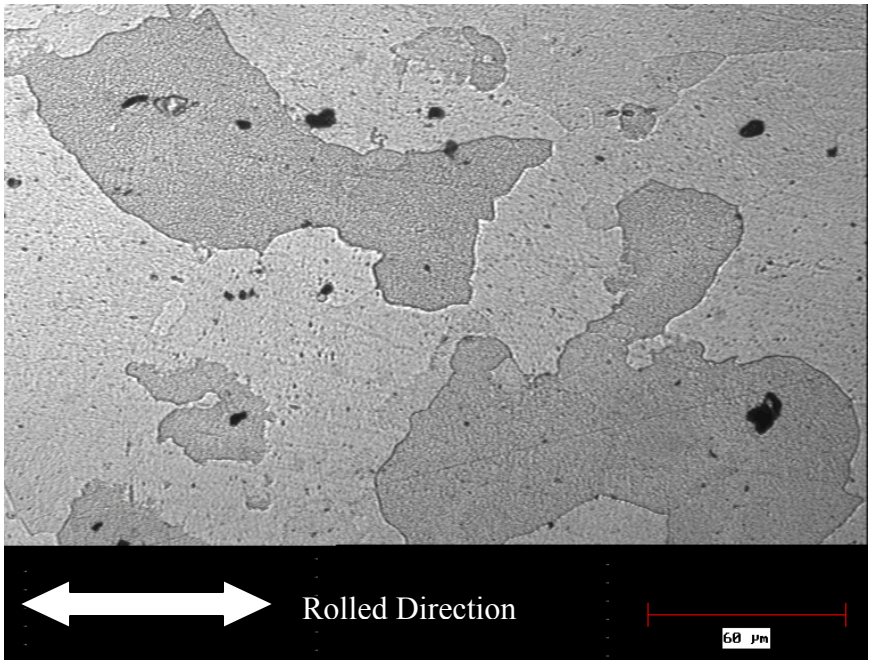

(b) 500x

Figure 26 – 7075-T6 Grain structure of flat sheet surface; etched with 0.5% HF solution followed separately with Keller's reagent. (photos MS-019 and -20)

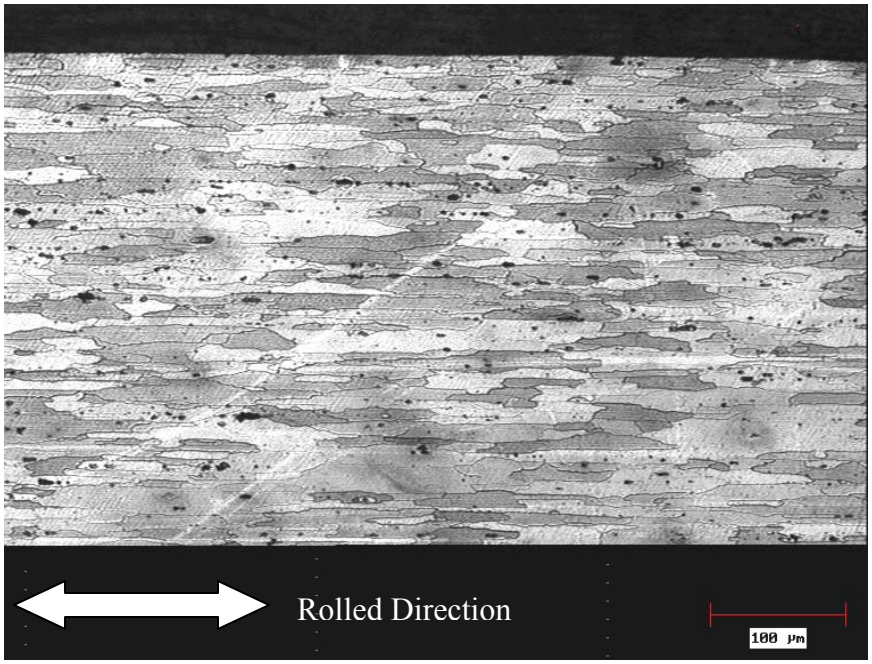

(a) 200x

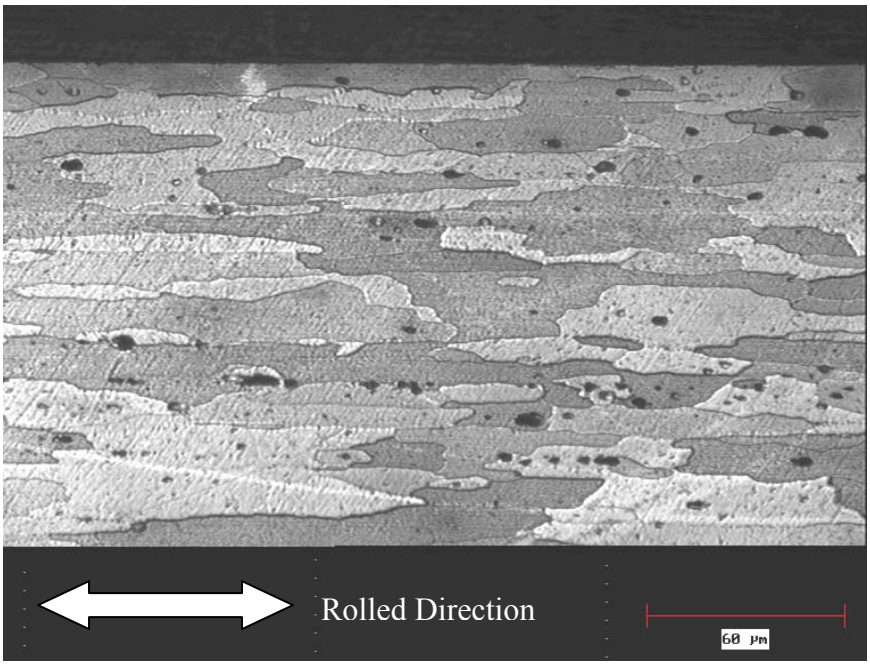

(b) 500x

Figure 27 – 7075-T6 grain structure, edge parallel to the rolled direction. Specimens were etched with 0.5% HF followed by Keller's reagent. The upper edge of the specimen is the free surface, which some fairly thin grains are noted to intersect. The grain size thickness ranges from about 5-25 µm and average about 10 µm. (photos MS-053/-054)

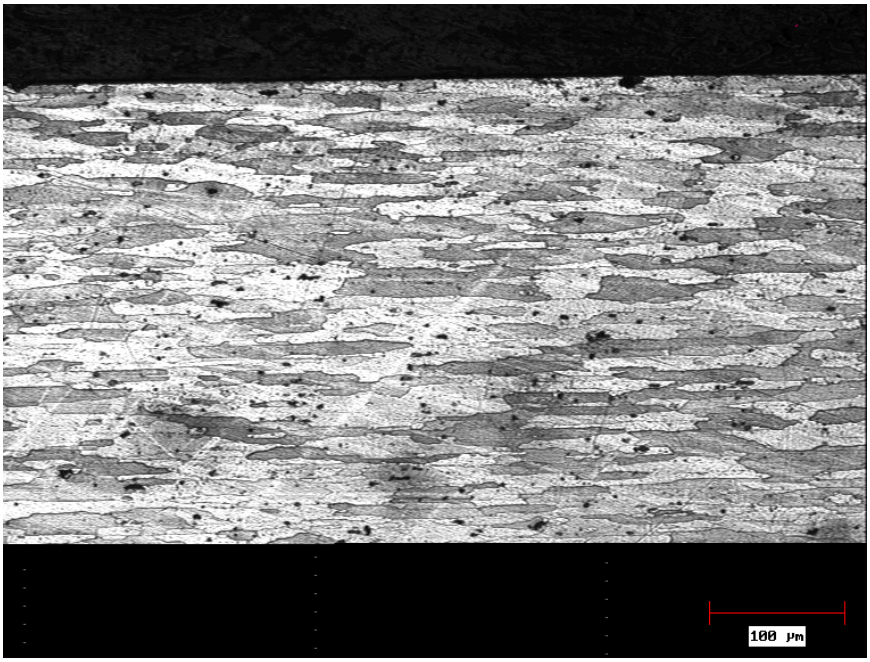

(a) 200x

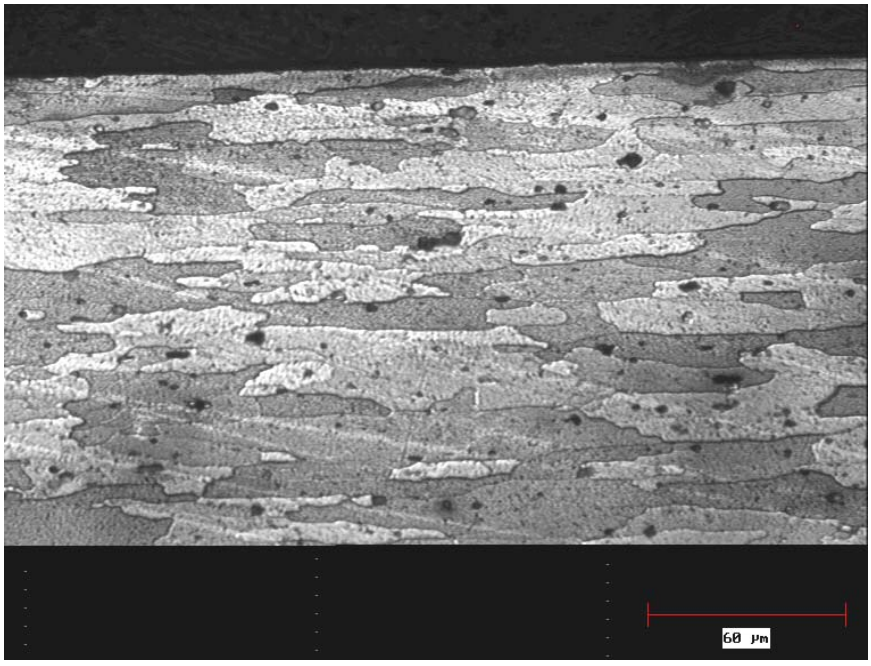

(b) 500x

Figure 28 – 7075-T6 grain structure, edge perpendicular to the rolled direction. Specimens were etched with 0.5% HF followed by Keller's reagent. The upper edge of the specimen is the free surface, which some fairly thin grains are noted to intersect. The grain size thickness ranges from about 5-25 µm and average about 10 µm. (photos MS-055/-056)

4.2 – Laser Cut and Machine Cut Specimens

All fatigue cracks from previous work originated at the specimen edges, in the as-received machine shop fabrication condition; typical views of the as-received finish are shown in Figure 29. The edges of the laser cut specimen is notably different compared to the machined edges and the fatigue testing documented lives are notably lower as compared to the machine cut specimens. The reason for this difference lies in the melting process associated with the laser cutting mechanism; this process alters the material properties enough to aid in earlier crack initiation and subsequent lower fatigue life but always initiates at an edge the same as its machine cut counterpart. The melting reaction on the 2024-T3 laser cut material is demonstrated by the drip edge in Figure 29 (e); this was also noted in the microstructure of Section 4.1.

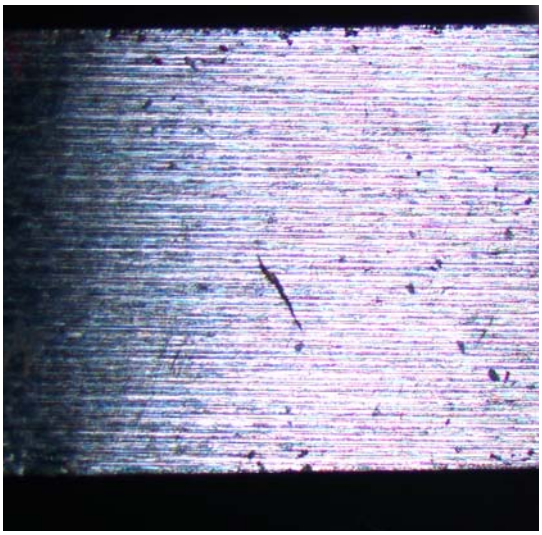

(a) 6061-T6 (photo EC-005)

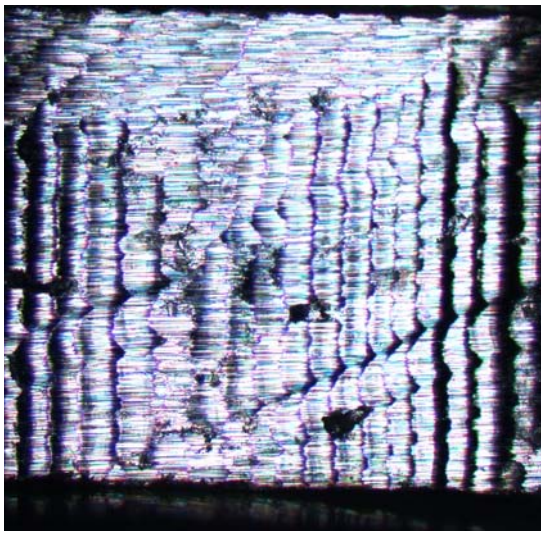

(b) 7075-T6 (photo EC-006)

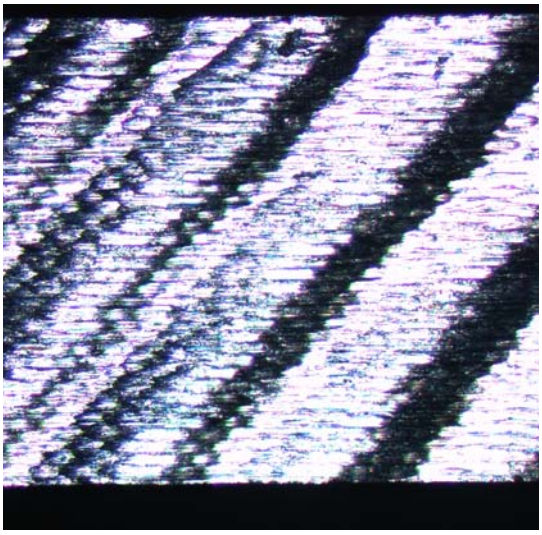

(c) 2024-T3 (photo EC-002)

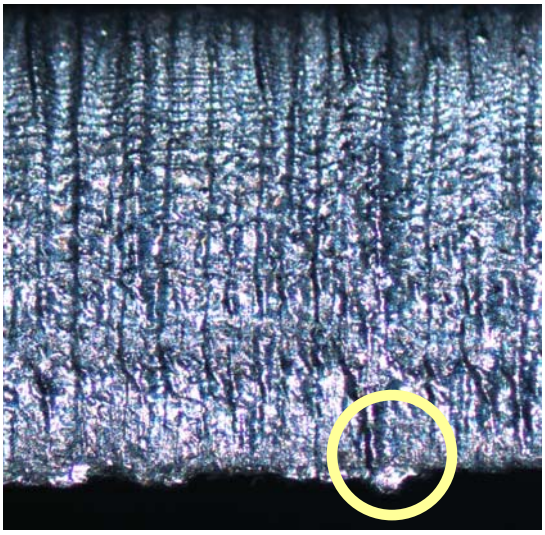

(d) Laser cut 2024 (photo EC-004)

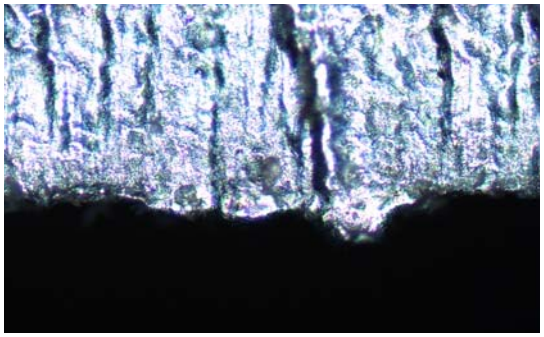

(e) Laser cut 2024-T3

Figure 29 – Edge conditions of various alloy specimens used in study (50x). the irregular surfaces of (b) and (c) are apparent chatter marks from machining. Photo (e) shows a closer view of the "drip" (circled area) along the lower edge of the laser cut specimen (d).

4.3 – Fatigue of Pristine Laser Cut and Machine Cut Specimens

As received laser and machine cut specimens were failed in fatigue using the Budd fatigue machine at 14 mm deflection; Figures 30 - 33 shows the fracture surface features. The general observation in these un-corroded pristine specimens is that of relatively smooth, unremarkable fracture surface. No corrosion is present on these specimens and note general lack of ratchet marks. Plots of the pristine failure data appear in appear in Figures 34 - 36.

Cracks on pristine specimens such as this have always been observed beginning at the edge in absence of pits or other defects that serve as crack initiation sites. Of note is the fact that laser cut specimens typically have a significantly lower fatigue life as compared to machined specimens [24 - 27]. Table 7 summaries fatigue life values for all alloys tested in this study; this fact is apparent in comparing 2024-T3 at the 14 mm deflection. The bar graph in Figure 37 relates the data for the pristine specimens of machine cut 2024-T3, 6061-T6, 7075-T6 and laser cut 2024-T3.

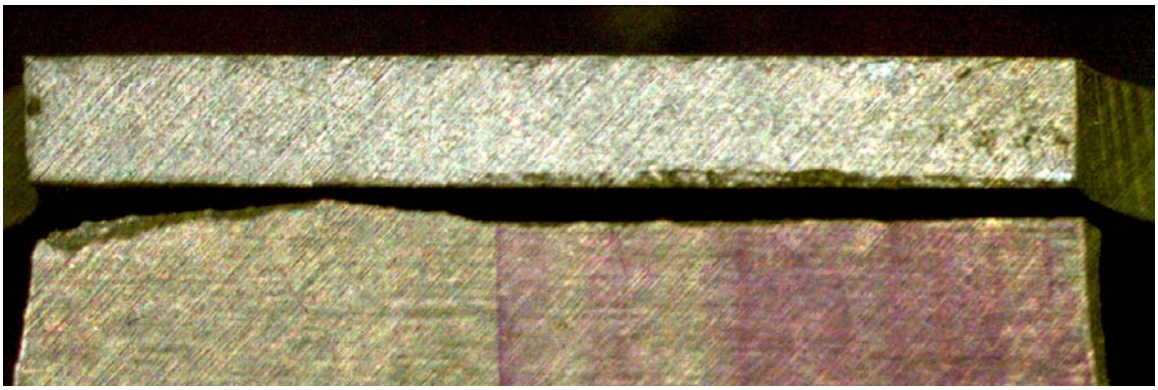

Figure 30 – Specimen T-20-6, 2024-T3 pristine (no corrosion) at 14 mm deflection, Nf = 1,014,300. No corrosion on this specimen and note no ratchet marks. Cracks on pristine specimens such as this always begin at the edge without pits or other defects that serve as crack initiation sites. (photo S-012)

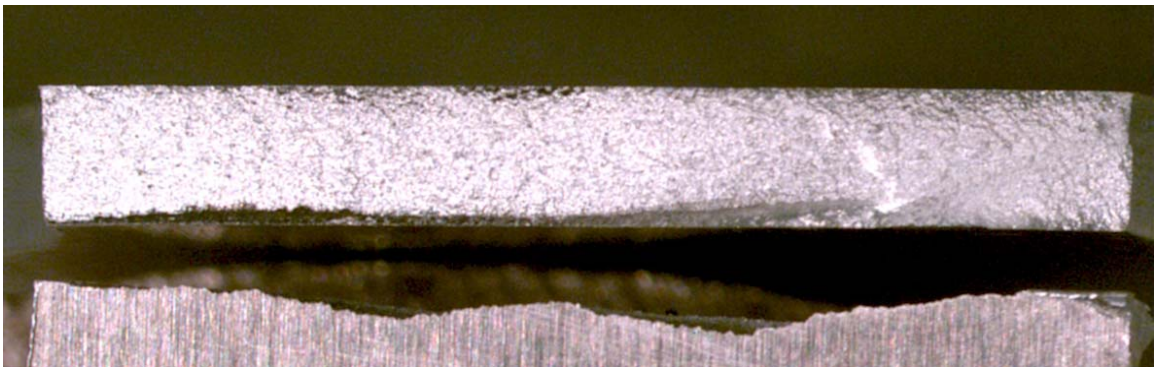

Figure 31 – Specimen L-1, 2024-T3 laser cut pristine (no corrosion) at 14 mm deflection, Nf = 126,000. No corrosion on this specimen and note no ratchet marks. Cracks on pristine specimens such as this always begin at the edge without pits or other defects that serve as crack initiation sites; laser cut specimens typically have a significantly lower fatigue life as compared to machined specimens. (photo # LPHS-001)

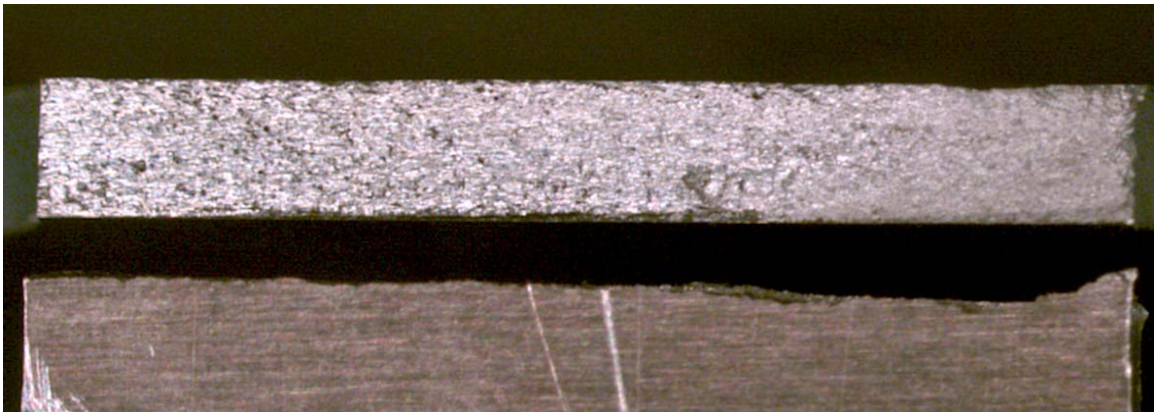

Figure 32 – 7075-T6 Specimen T-70-9 7075-T6 Pristine, cycled at 14 mm deflection, N_f = 298,700. No corrosion on this specimen and note no ratchet marks. (photo 7PS-001)

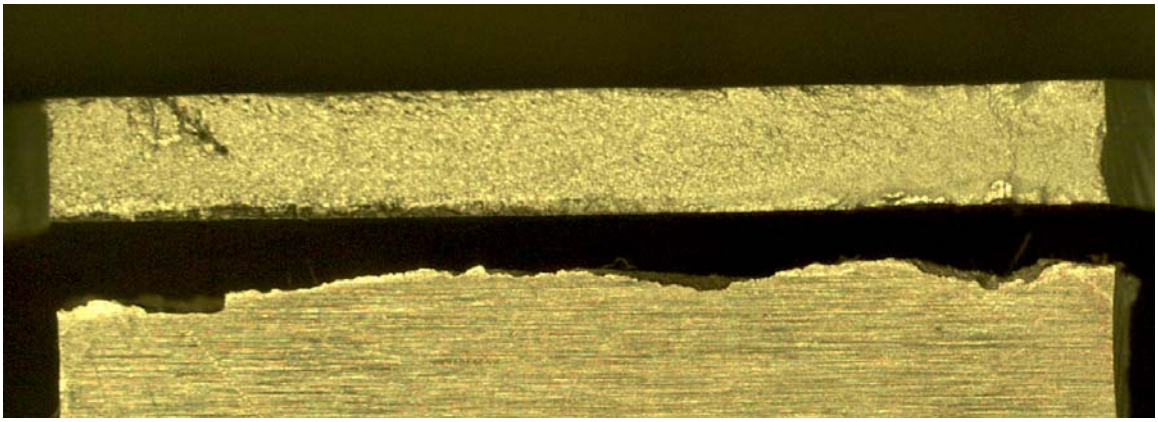

Figure 33 – 6061-T6 Specimen 60-1 Pristine, 14mm deflection, N_f = 206,300. No corrosion on this specimen; a ratchet mark appears near the left side possibly due to an inclusion. (photo 6S-1)

Table 7 – Summary of Pristine Specimen N_f Values

Defl, mm	2024-T3	2024-T3 laser cut	7075-T6	6061-T6
12			23,886,400	
13			2,923,300	
14	1,014,300	126,000	298,700	206,300
15	214,300		107,900	
16			105,300	116,300
17	181,100		65,500	66,900

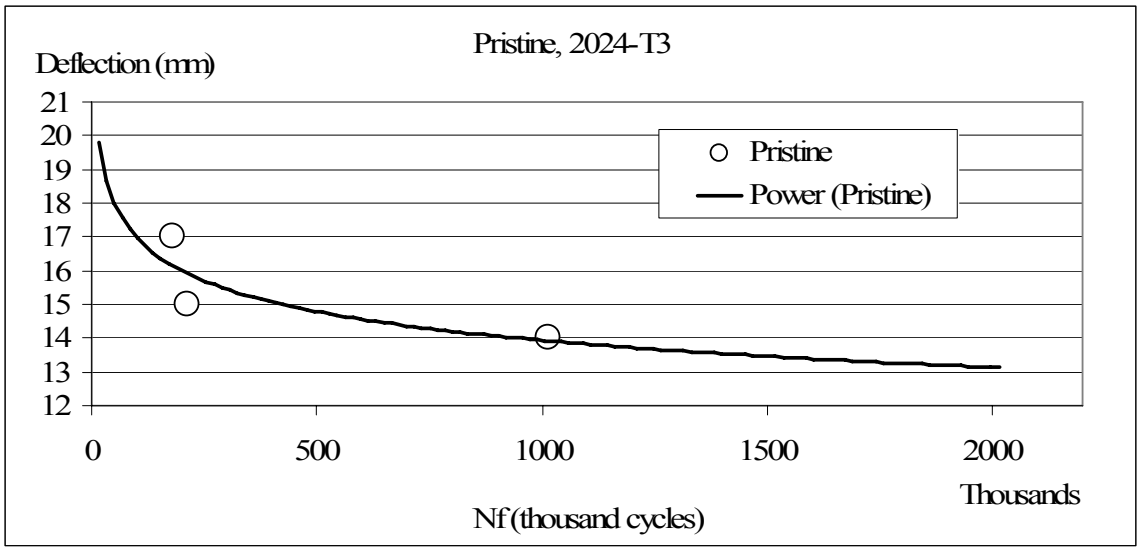

Figure 34 – Fatigue Data for Pristine (un-corroded) 2024-T3

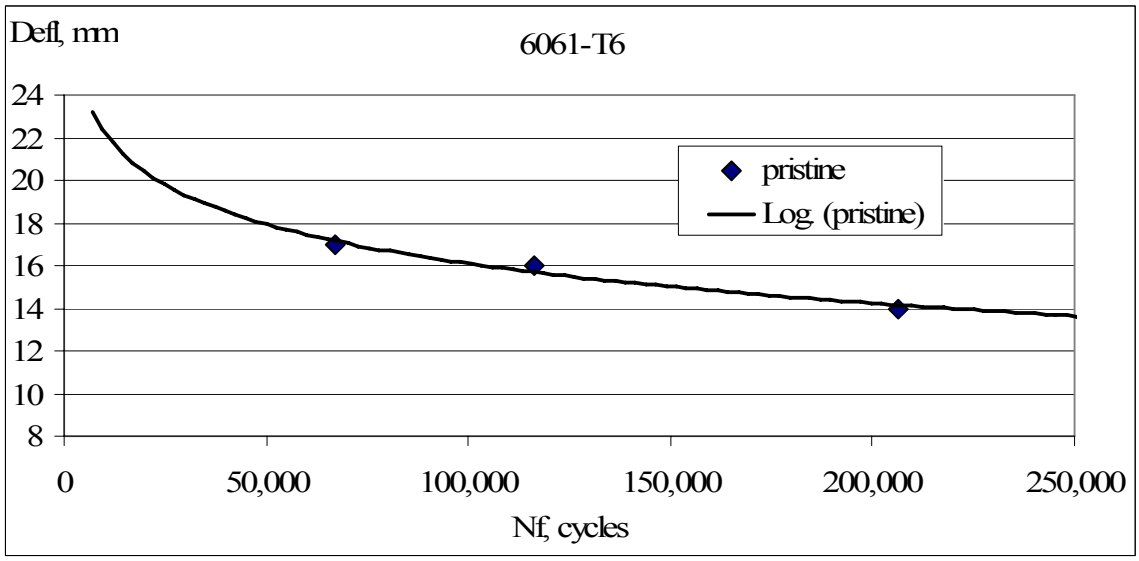

Figure 35 – Fatigue Data for 6061-T6 Pristine

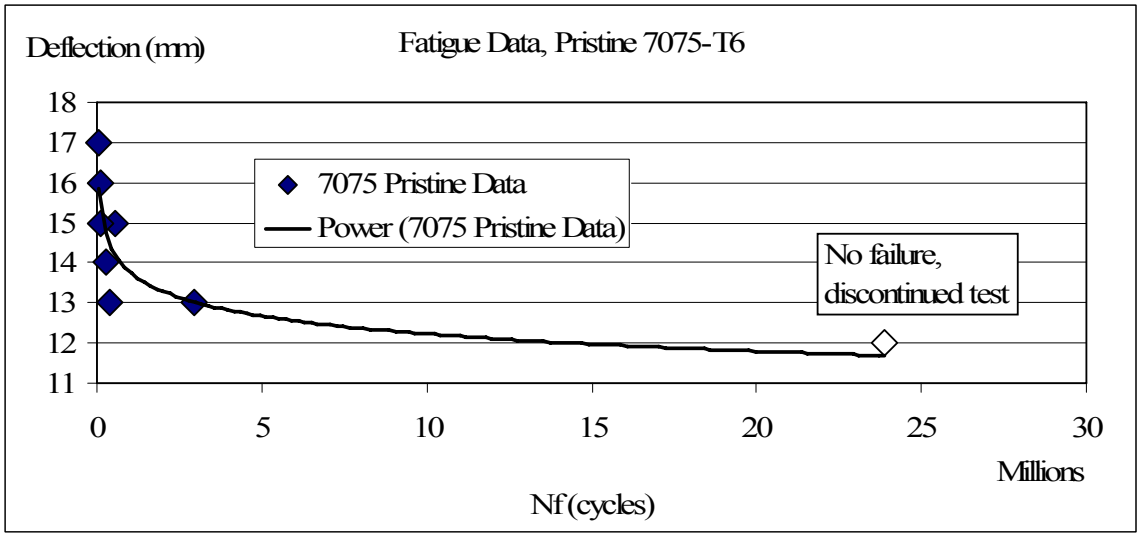

Figure 36 – Fatigue Data for 7075-T6 Pristine

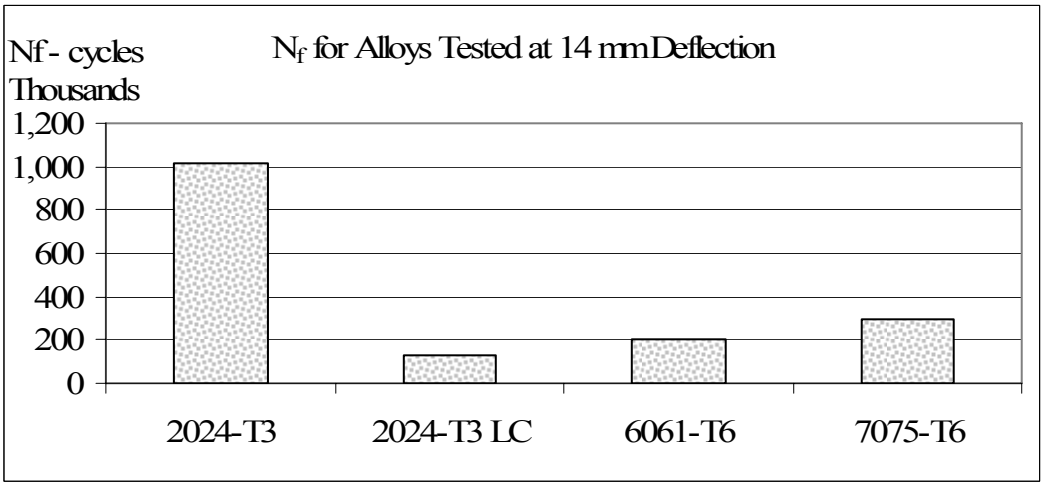

Figure 37 – Fatigue lives for all three alloys at 14 mm deflection. LC is laser cut.

4.4 – Corrosion Coupons

Figures 38 – 46 microscopically depict the degree of corrosion and pitting at specific time intervals and ratios of salt solution to hydrogen peroxide. As anticipated the corrosion attack of the specimens increased with time and higher concentrations of hydrogen peroxide. Pitting began on the 2024-T3 coupons sooner, as compared to the 7075-T6 and 6061-T6, which was expected due primarily to the increased copper content [31]. Active pitting into the surface was noted on the 2024-T3 at the 200:1 concentration and 30 minutes exposure. However the 7075-T6 and 6061-T6 materials were much more resistant to corrosion and higher concentration values of hydrogen peroxide was required to initiate pitting within the proposed test window. At a lower concentration of hydrogen peroxide a more general attack was noted and was often combined with a surface staining rather than pitting attack.

As seen in Figure 38 and 39, the 2024-T3 specimens displayed threshold pitting at the 200/1 ratio during the 30 min and 60 min tests. At the 50/1 hydrogen peroxide ratio, the pitting is very well formed and easily generated within a 30 min window. The other two alloys were much more resistant to pitting. The 7075 specimens in Figure 40 and 41 displayed essentially no pitting up to the 50/1 ratio, just a slight appearance of general corrosion. The 6061-T6 specimens, Figures 42 and 43, appeared slightly less resistant to corrosion than the 7075-T6; forming light pits at the 200/1 ratio but the heavier pits occurred best at the 50/1 ratio and the appearance was more akin to fields of light pits that began to coalesce into larger pitted areas. Further corrosion rate tests were done with 6061 and 7075 at lower ratios (40/1, 30/1 and 15/1) of hydrogen peroxide as shown in Figure 44 - 46; overall the best concentration was in the 40/1 to 30/1 range; the 15/1 ratio

is resulting in an excessive rate of corrosion in a relatively short amount of time. The ratio of 30/1 would be chosen to corrode all alloys for the most part. The degree of corrosion could be adjusted with lowering exposure time accordingly. The next section, some preliminary tests will be done to observe how the fatigue specimens will behave in both pre-corrosion and corroding-during scenarios.

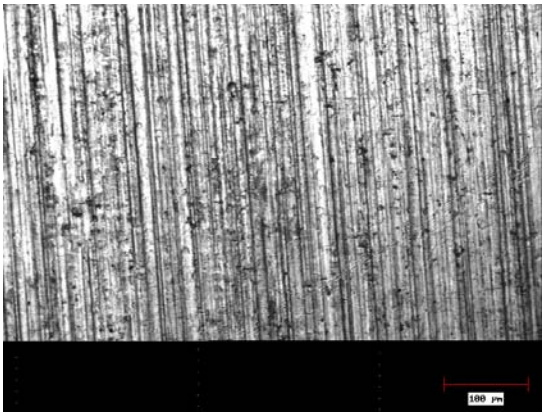

(a) Pristine

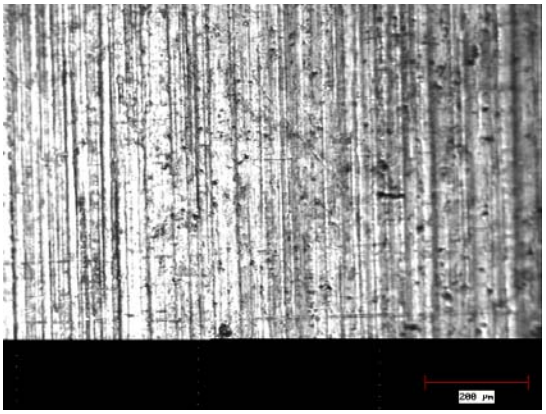

(b) 1/0 (zero H_2O_2)

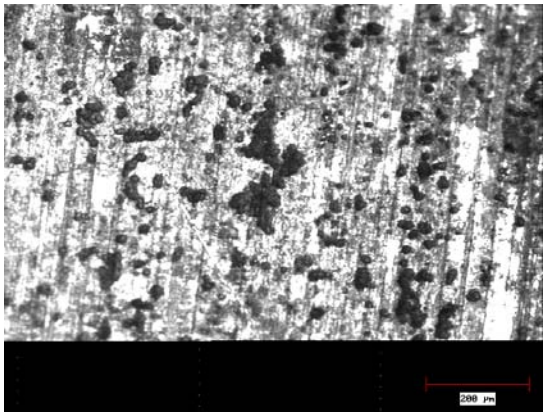

(c) 200/1

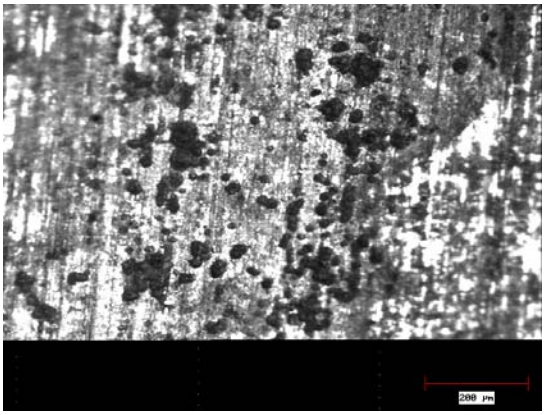

(d) 75/1

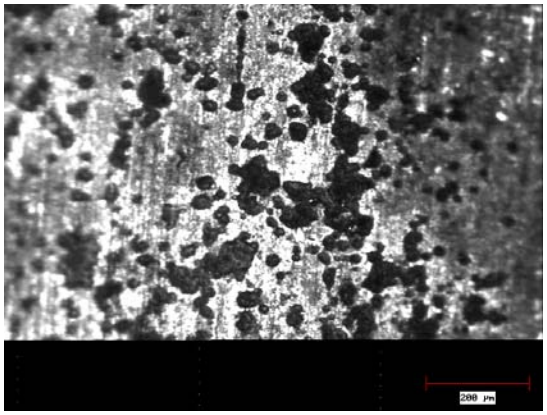

(e) 50/1

Figure 38 – 2024-T3, 30 minute exposure, at ratios of NaCl solution to H_2O_2 hydrogen peroxide (200x). Increasing pitting is apparent with escalating H_2O_2 concentration. Note the elongation of the pitting in the sheet rolled direction (vertical).

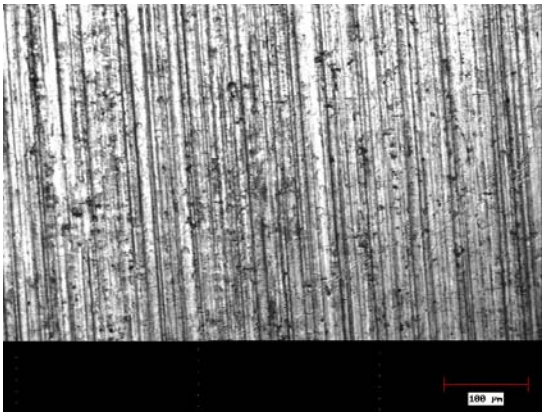

(a) Pristine

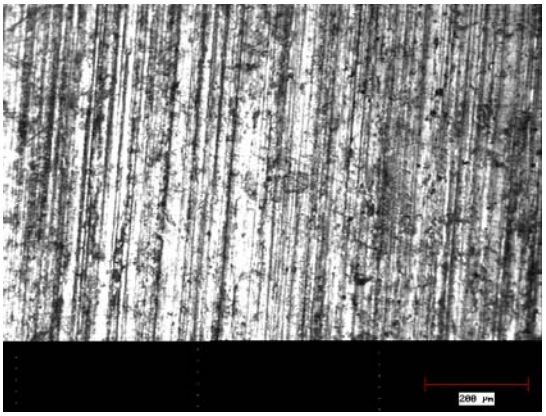

(b) 1/0 (zero H_2O_2)

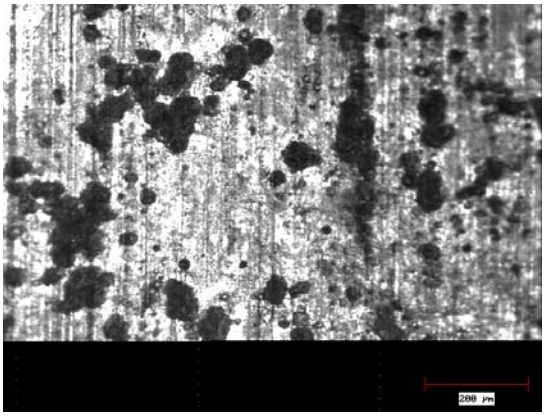

(c) 200/1

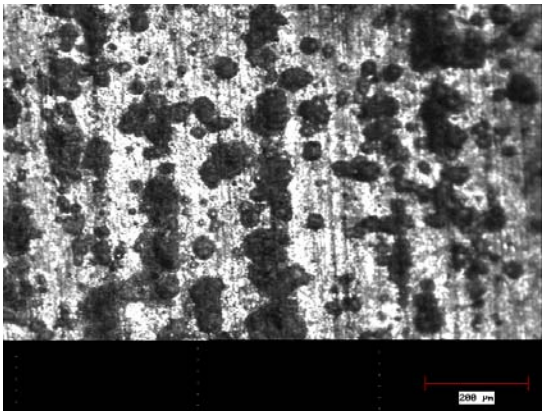

(d) 75/1

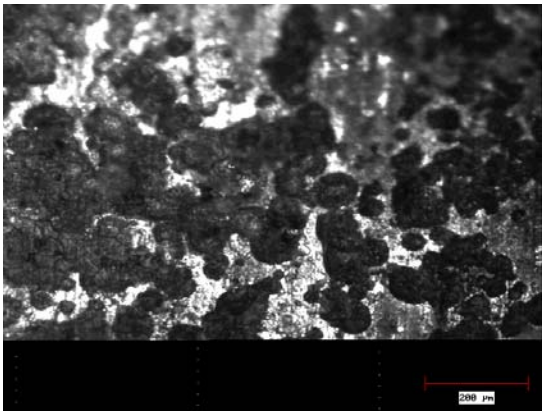

(e) 50/1

Figure 39 – 2024-T3, 60 minute exposure, at ratios of NaCl solution to H_2O_2 hydrogen peroxide (200x). Vibrant pitting is obvious with increasing H_2O_2. . Note the elongation of the pitting in the sheet rolled direction (vertical).

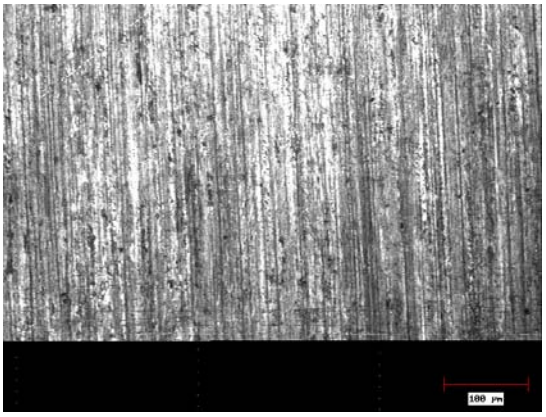

(a) Pristine

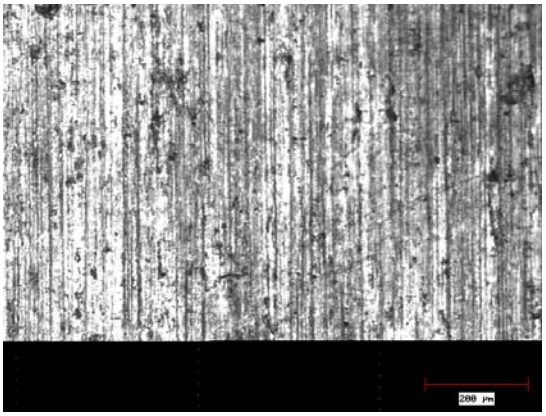

(b) 1/0 (zero H_2O_2)

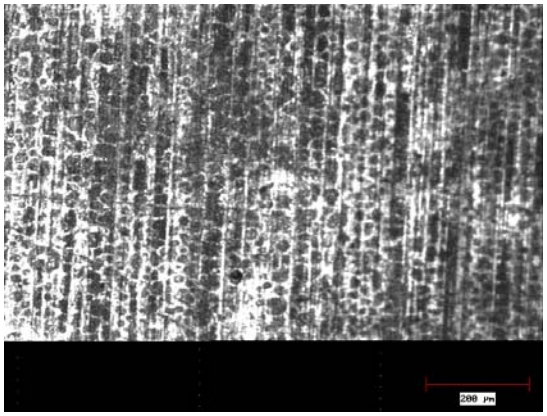

(c) 200/1

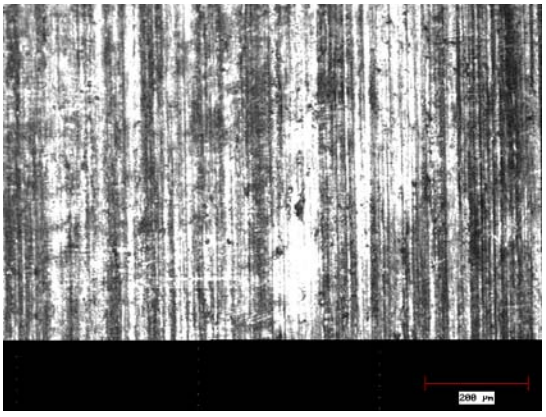

(d) 75/1

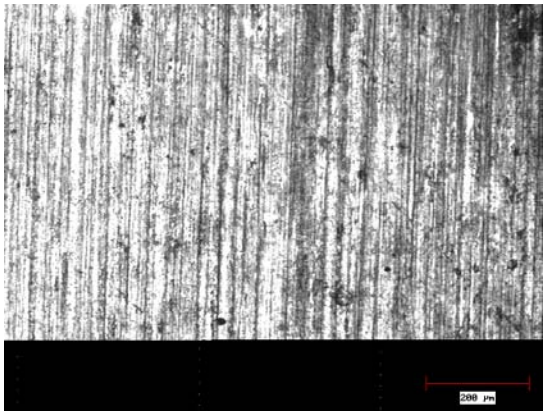

(e) 50/1

Figure 40 – 7075-T6, 30 minute exposure, at ratios of NaCl solution to H_2O_2 hydrogen peroxide (200x). Pitting is virtually nonexistent.

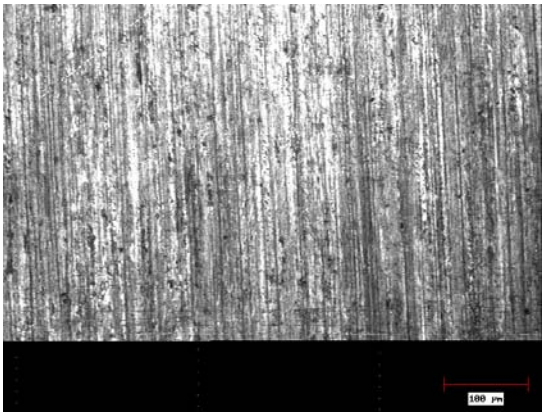

(a) Pristine

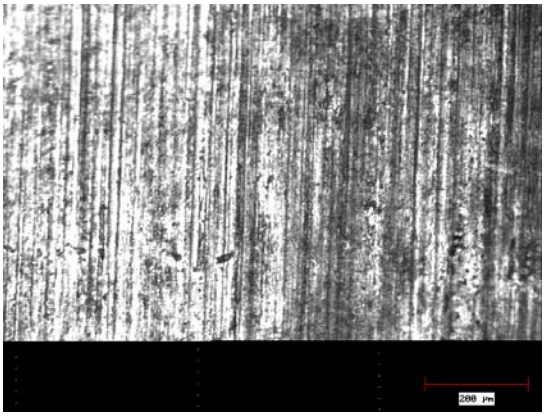

(b) 1/0 (zero H_2O_2)

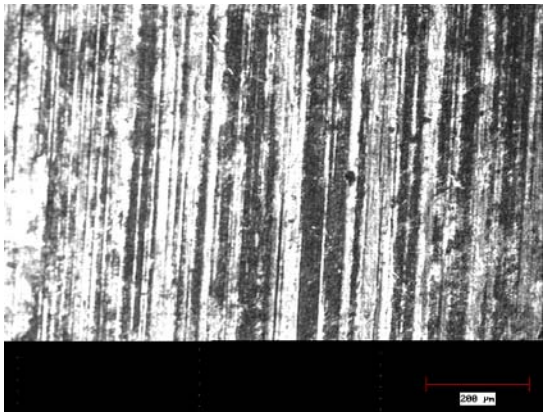

(c) 200/1

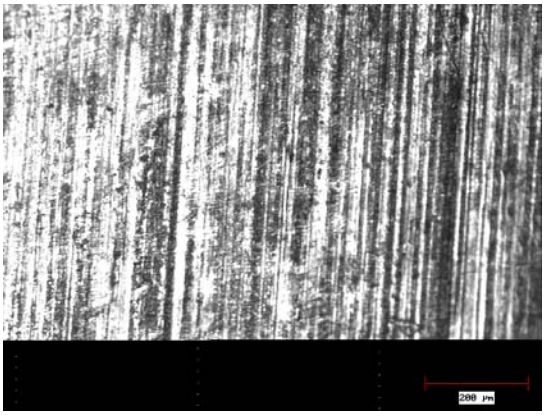

(d) 75/1

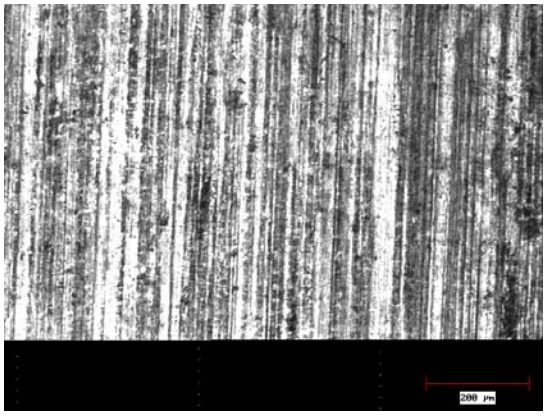

(e) 50/1

Figure 41 - 7075-T6, 60 minute exposure, at ratios of NaCl solution to H_2O_2 hydrogen peroxide (200x). Pitting is virtually nonexistent, slight general corrosion noted.

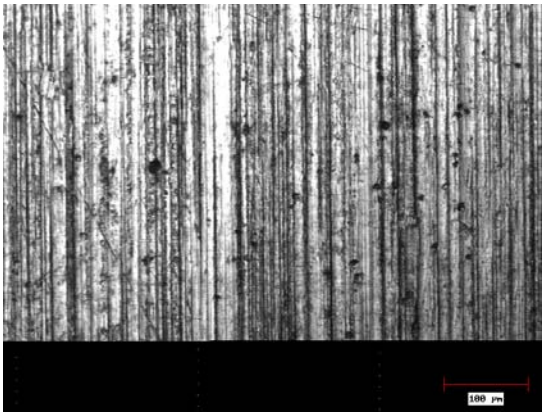

(a) Pristine

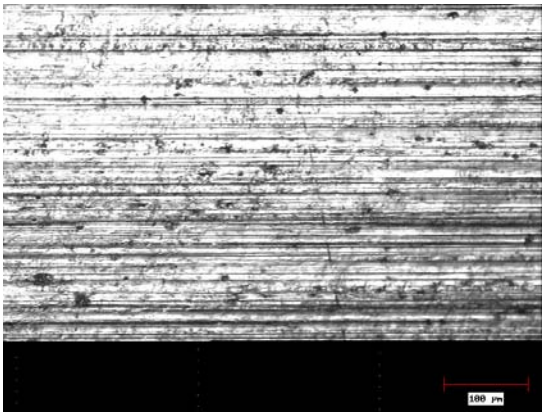

(b) 1/0 (zero H_2O_2)

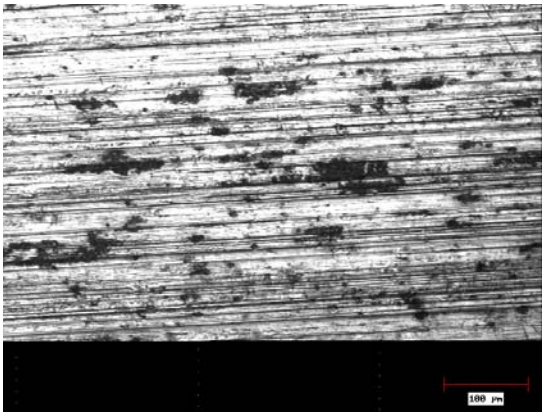

(c) 200/1

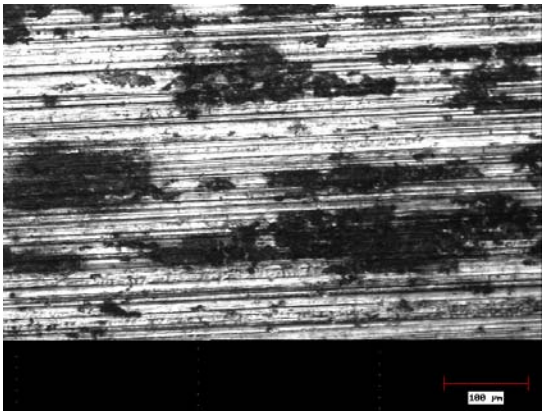

(d) 75/1

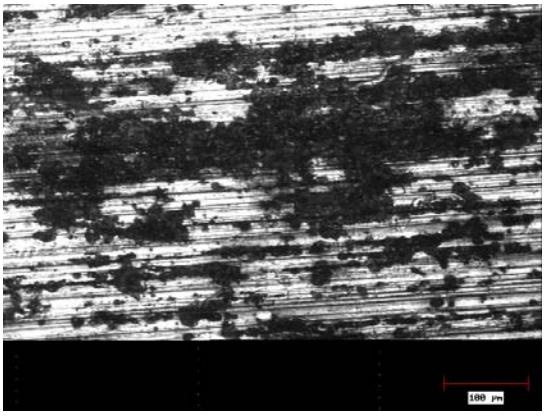

(e) 50/1

Figure 42 – 6061-T6, 30 minute exposure, at ratios of NaCl solution to H_2O_2 hydrogen peroxide (200x); pitting is steadily increasing as ratio is lowered. The larger dark regions as seen in (c) and (d) are pits merging into fields or groups. Note the elongation of the pitting in the sheet rolled direction (horizontal). (photos C-019 through C-022)

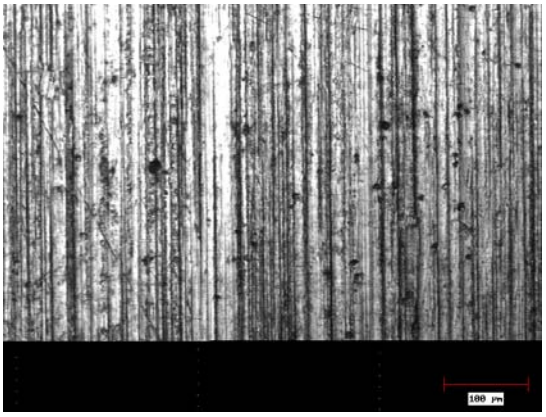

(a) Pristine

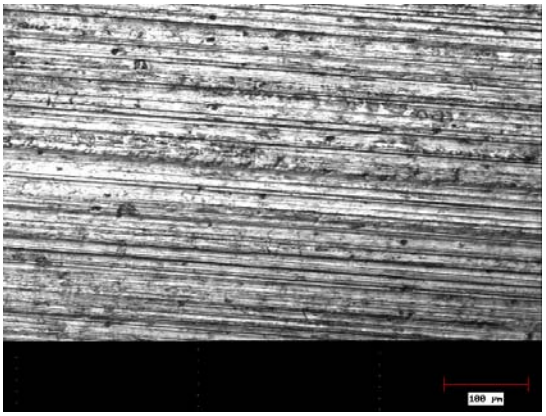

(b) 1/0 (zero H_2O_2)

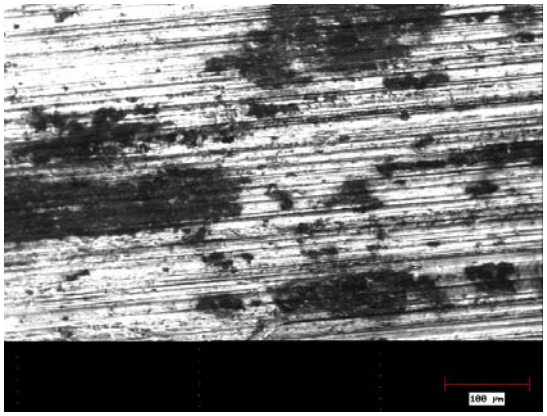

(c) 200/1

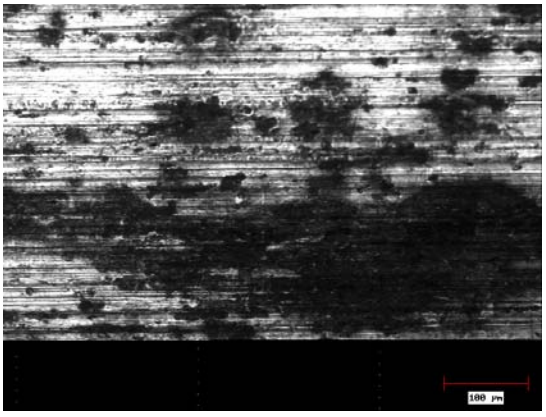

(d) 75/1

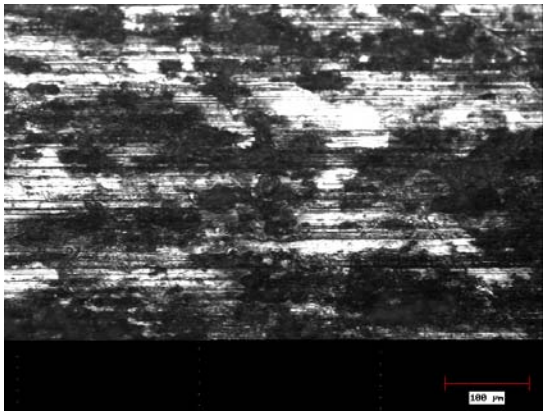

(e) 50/1

Figure 43 – 6061-T6, 60 minute exposure, at ratios of NaCl solution to H_2O_2 hydrogen peroxide (200x); further pitting as exposure time increases. The larger dark regions appear to be single pits merging into fields or groups. Note the elongation of the pitting in the sheet rolled direction (horizontal). (photos C-023 through C-026)

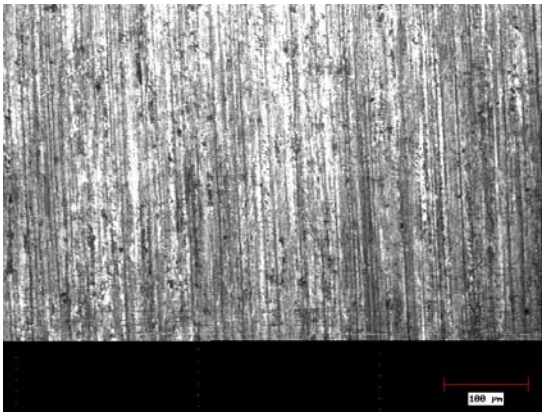

(a) Pristine

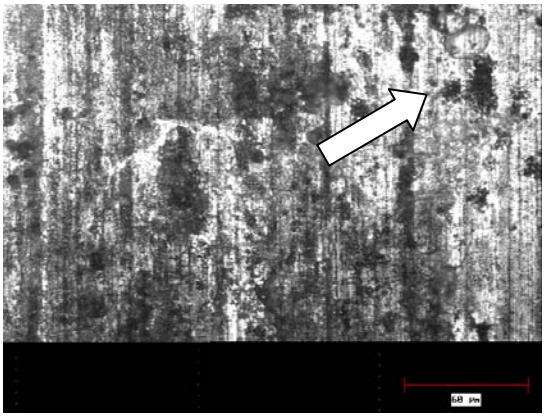

(b) 30/1 ratio, 15 min

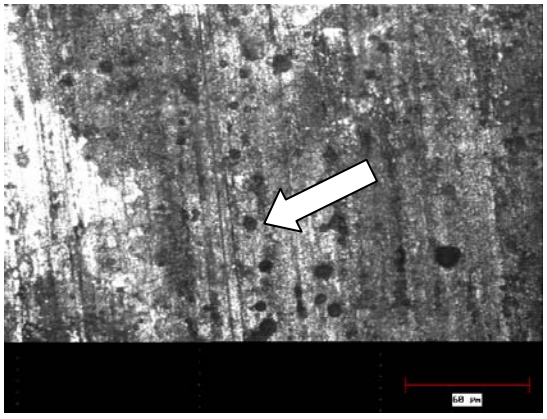

(c) 30/1 ratio, 30 min

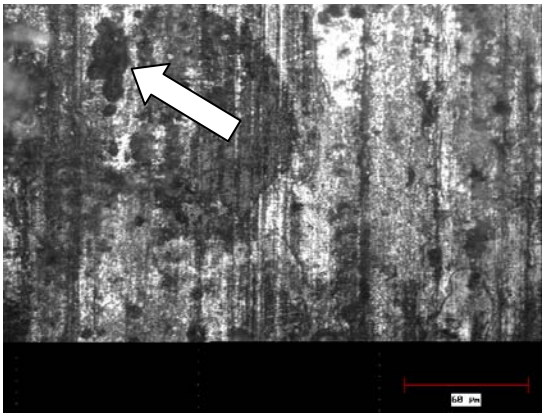

(d) 30/1 ratio, 60 min

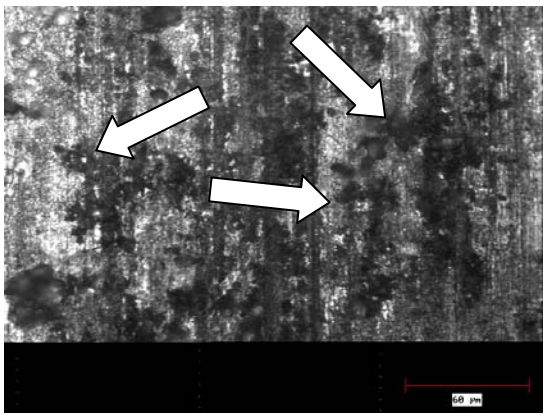

(e) 15/1 ratio, 30 min

Figure 44 – 7075-T6 exposure to ratios of 3.5% NaCl solution to H_2O_2 hydrogen peroxide (500x). as indicated by arrows, pitting is becoming evident at higher levels of H_2O_2.

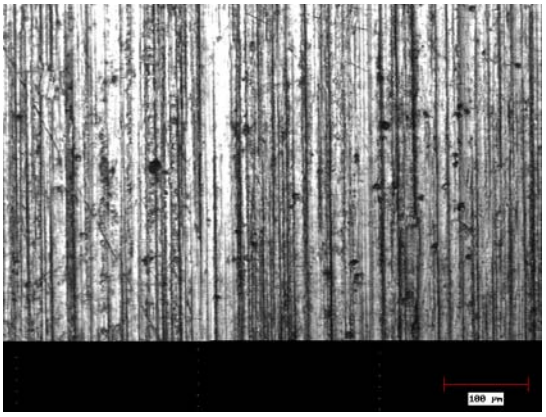

(a) Pristine

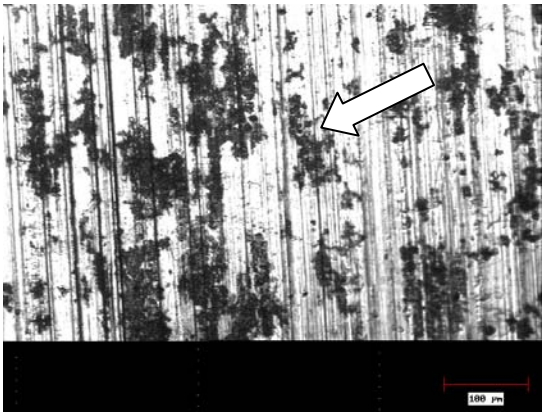

(b) 30/1 ratio, 15 min

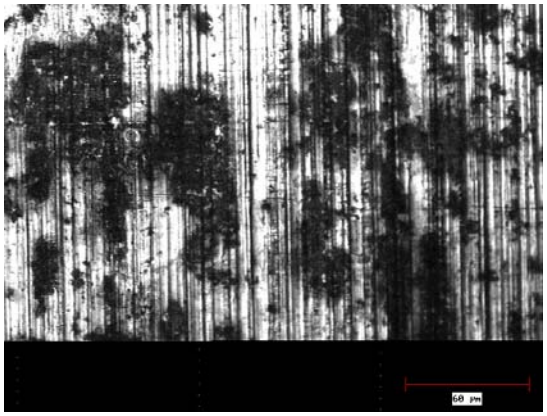

(c) 30/1 ratio, 30 min

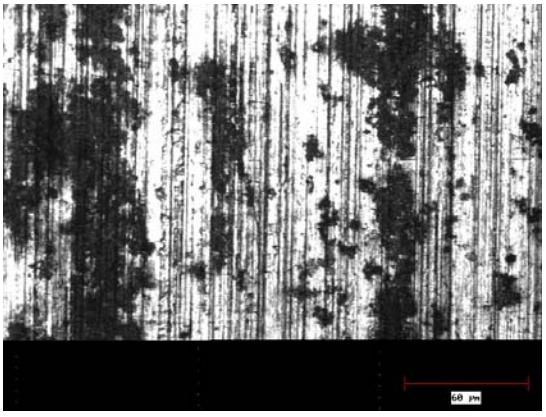

(d) 30/1 ratio, 90 min

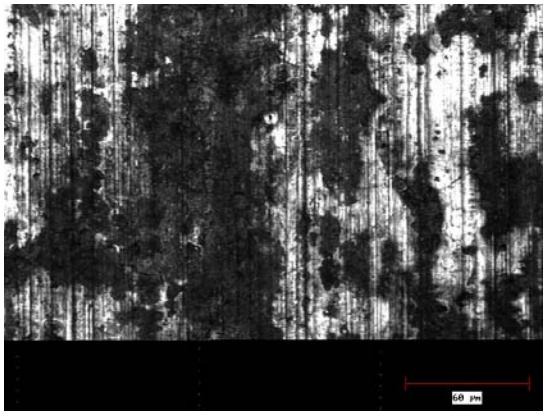

(e) 30/1 ratio, 120 min

Figure 45 – 6061-T6 exposure to ratios of 3.5% NaCl solution to H_2O_2 hydrogen peroxide (200x). Pitting is becoming evident at 30/1 ratio of H_2O_2 at the 15 minute exposure as shown in (a); as exposure time increases the pits coleses into the larger dark regions. Note the elongation of the pitting in the sheet rolled direction (vertical).

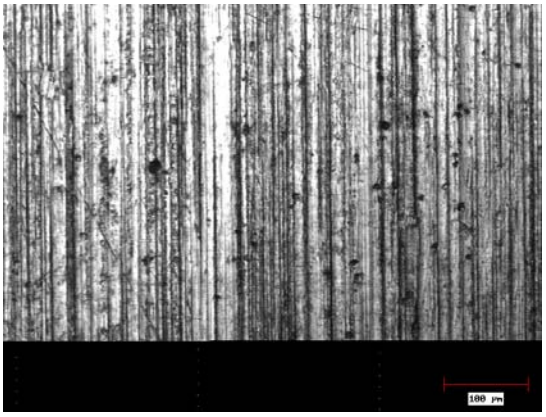

(a) Pristine

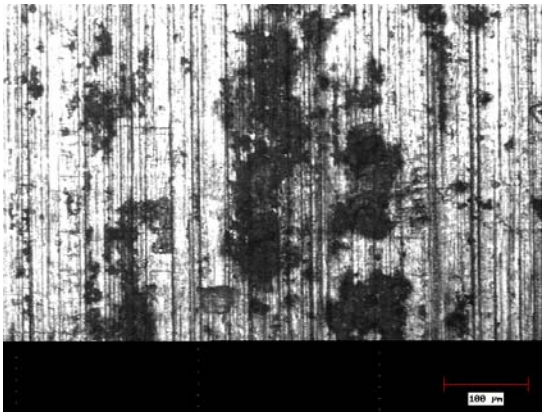

(b) 60/1 ratio, 60 min

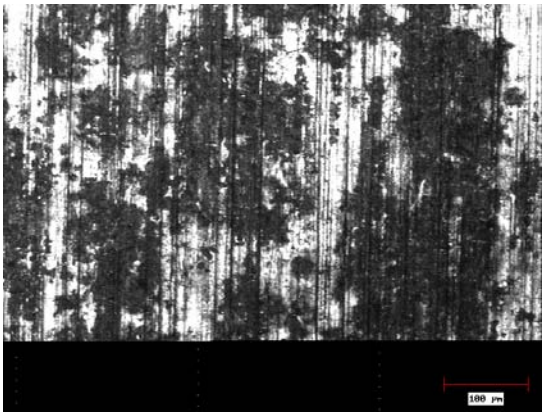

(b) 30/1 ratio, 60 min

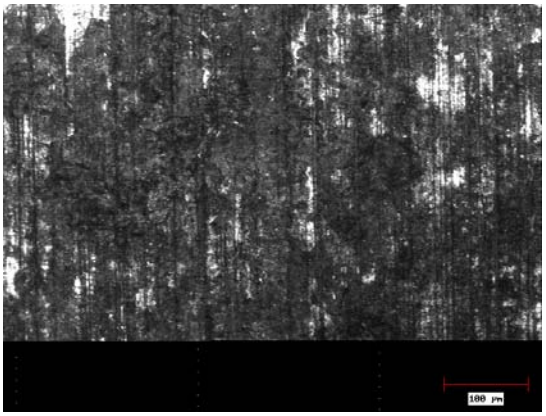

(c) 15/1 ratio, 60 min

Figure 46 – 6061-T6 exposure to ratios of 3.5% NaCl solution to H_2O_2 hydrogen peroxide (200x). Pitting is becoming evident at 60/1 and 30/1 ratios of H_2O_2 within the desired 60 min test window. Corrosion at the 15/1 ratio is becoming excessive as individual pits are coalescing into large fields and appears more like general corrosion than pitting. Note the elongation of the pitting in the sheet rolled direction (vertical).

4.5 - Corrosion Rates For Top and Bottom Sides of Sheet

It was noticed during the preliminary coupon testing that the corrosion rates of submerged specimens were often different from the top surface to the bottom surface. Specimens were placed vertically, so that all sides were equally exposed, in a 3.5% NaCL solution with H_2O_2 added as an accelerant. Figures 47 - 50 present the comparative difference between surfaces; it can be clearly seen that there is a significant difference in

each of the alloys in this study. Investigation into why this happens and any potential application or design considerations should be explored.

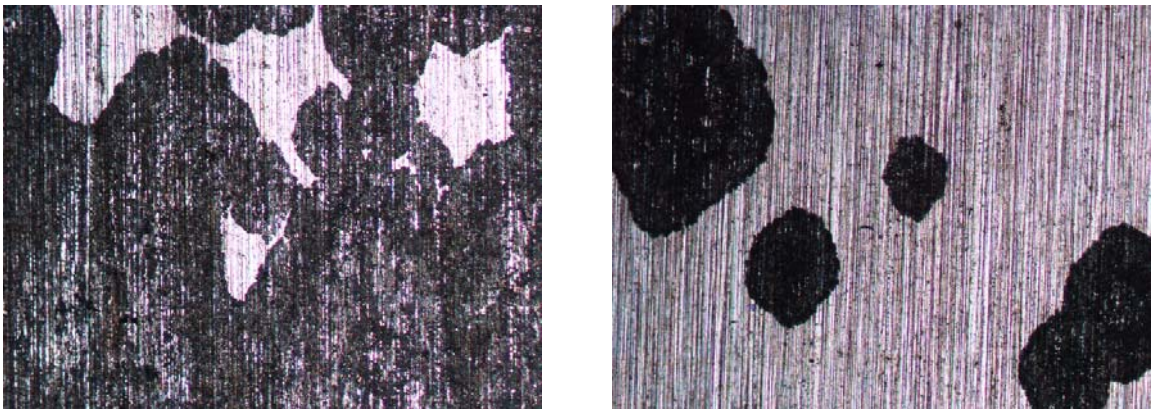

(a) top side (b) bottom side

Figure 47 – 2024-T3 corrosion each side of sheet, 3.5% NaCl at 30/1 ratio H_2O_2. Note the significant difference between the corrosion rates of the top and bottom. (photos CR-007/-008)

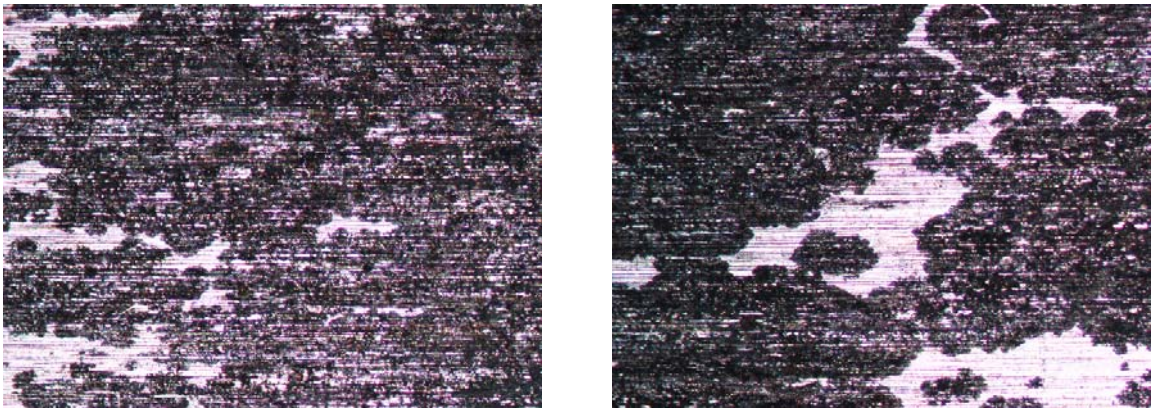

(a) top side (b) bottom side

Figure 48 – 2024-T3 laser cut corrosion each side of sheet, 3.5% NaCl at 30/1 ratio H_2O_2. Slight difference between the corrosion rates of the top and bottom. (photos CR-009/-010)

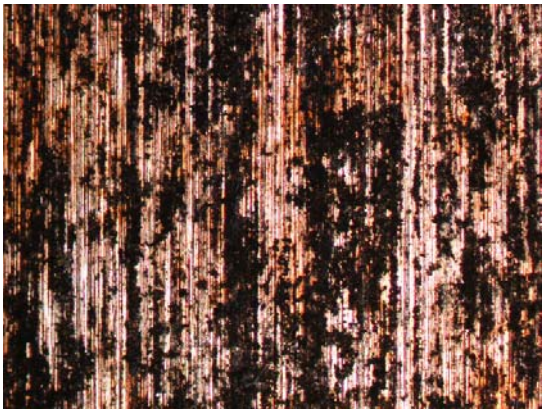

(a) top side

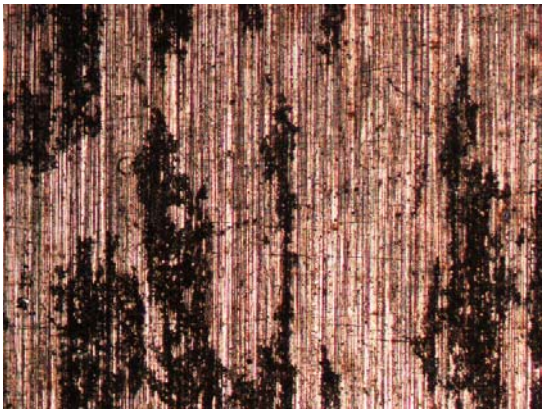

(b) bottom side

Figure 49 – 6061-T6 corrosion each side of sheet, 3.5% NaCl at 15/1 ratio H_2O_2. Notice the significant difference between the corrosion rates of the top and bottom sides. (photos CR-001/002)

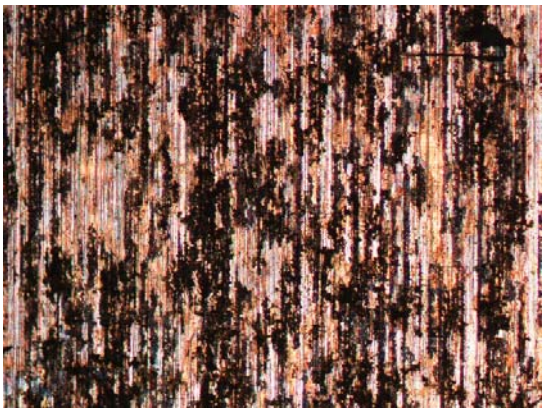

(a) top side

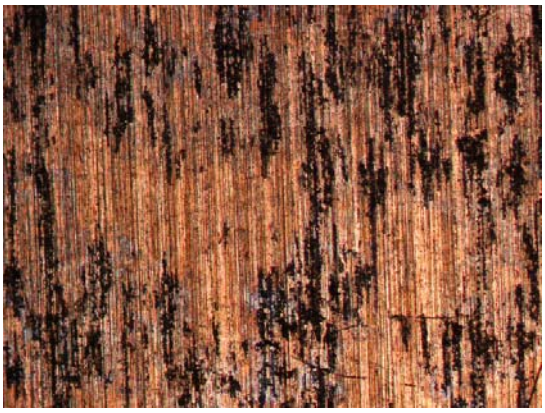

(b) bottom side

Figure 50 – 7075-T6 corrosion each side of sheet, 3.5% NaCl at 15/1 ratio H_2O_2. Notice the significant difference between the corrosion rates of the top and bottom sides (photos CR-003/-004)

4.6 – Initial Fatigue Data

Several initial experiments were run in order to assess how the corrosion would react to the specimens and the approximate cycles to failure. It was anticipated that the corrosion rate would increase under stress and a few samples were run to explore this aspect. Table 8 following summarizes the data gathered in 16 initial specimens. As stated earlier these tests were to develop a feel for corrosion fatigue behavior within the regime of an approximate 60 minute/100,000 cycle test window.

In general, any degree of corrosion pitting resulted in a substantial decrease in fatigue life. The corrosive solution to produce respectable pitting varied for each alloy but should exceed at least a 200/1 ratio of 3.5% NaCl solution to 30% hydrogen peroxide but a > 50/1 ratio yields much faster and aggressive result. The 7075-T6 and 6061-T6 alloys behaved very similar for the ratios tested; a 30/1 ratio works quite well and quickly yielding the desired degree of corrosion pitting in all circumstances. However, care has to be taken not to subject the specimen too long at any of these ratios or excessive corrosion will occur; the goal again, is identifying minimal criteria for fatigue crack initiation from corrosion pitting.

Table 8 – Initial Fatigue Data

Spec No.	Alloy	Method	Time, min	H_2O_2 Ratio	Defl, mm	Nf (cycles)	Comments
T-1	2024-T3	corr-during		15/1	17	22,300	
T-2	2024-T3	pre-corr	12	15/1	NA	not run	did not run because corrosion very heavy
T-3	2024-T3	pre-corr	7	15/1	15	95,600	
T-4	2024-T3	pre-corr	2	15/1	15	125,400	
T-5	2024-T3	pre-corr	1.5	15/1	13	2,479,100	terminated test before failure
T-6	7075-T6	corr-during		40/1	13	25,200	
T-7	7075-T6	pre-corr	60	40/1	13	31,200	
T-8	2024-T3	corr-during		40/1	17	25,200	dropped concentration due to excessive corr
T-9	7075-T6	pre-corr	30	15/1	15	51,300	
T-10	7075-T6	pre-corr	30	15/1	15	50,000	no failure, stopped short of T-9 to inspect for cracks
T-11	2024-T3	corr-during		400/1	15	38,700	
T-12	2024-T3	pre-corr	20	400/1	0	not run	T-11/-12 compared; deter. if cyclic stress acceler. corrosion
T-13	7075-T6	corr-during		400/1	15	60,800	
T-14	7075-T6	pre-corr	31	400/1	0	not run	T-13/-14 compared; deter. if cyclic stress acceler. corrosion
T-15	6061-T6	pre-corr	30	15/1	14	68,200	
T-16	6061-T6	pre-corr	30	15/1	14	60,000	no failure, stopped short of T-15 to inspect for cracks

4.7 – Metallography of Initial Fatigue Specimens

The detailed captions of Figures 51 - 57 that follow describe the observations of the initial fatigue experiments. Some of these specimens were corroded more heavily than needed, but as stated earlier, these experiments were to get a feel of the results of the corrosion-fatigue experimental methodology and to determine if the approach is valid as well as define areas to insert any procedural adjustments. It became obvious in these early gross experiments that fatigue lives were greatly affected by the amount of corrosion and that multiple cracks were beginning within the corroded regions. As seen in Section 4.3 the fracture surface of the pristine specimens were typically smooth but the specimens in Figures 51 - Figure 54 are rough and have somewhat vertical lines beginning at the top (tension) surface and traversing downward across the cross-section for at least half the thickness. Closer inspection of the specimens reveals smaller cracks throughout the fatigue zone running parallel to the primary fracture surface. These cracks are emanating from corrosion pits or inclusions and individually propagating, then link up as they progress, eventually forming the main fracture surface. These vertical lines on the fracture surface are ratchet marks and indicate where cracks have originated and linked up; thus forming the fracture surface. The presence of ratchet marks may be used as an indicator in determining if multiple fatigue cracks are present and compose the make-up of a fatigue failure.

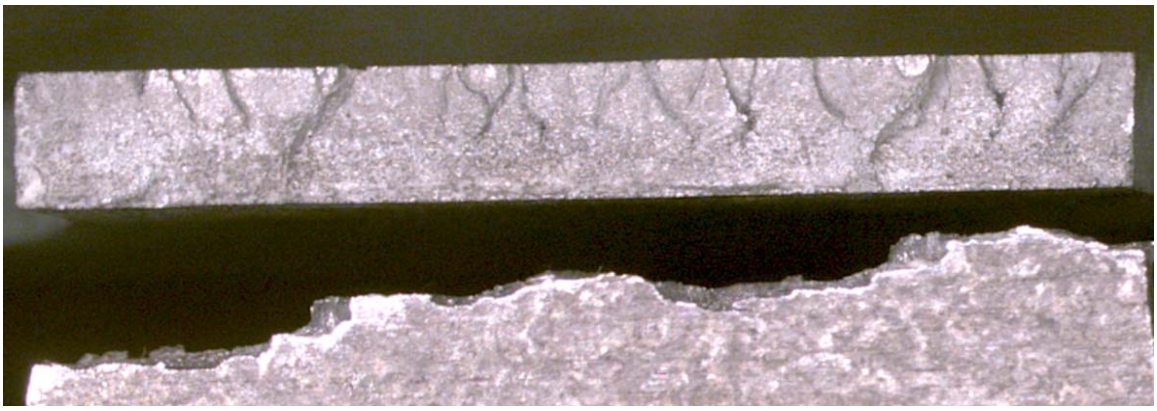

Figure 51 – Specimen T-1, 2024-T3 corroded during cyclic loading, exposed to 15/1 ratio 3.5% NaCl solution to H_2O_2 hydrogen peroxide, deflection = 17 mm (uncalibrated), Nf = 22300 cycles. The 15/1 ratio resulted in a high rate of corrosion and overrode any link to accelerated corrosion under cyclic loading conditions; pursuing threshold pitting would need to be accomplished at a much lower hydrogen peroxide ratio. Note approximately 20 ratchet marks; it appears there may be individual cracks that traversed much of the cross-section before linkage. (photo # TPS-003)

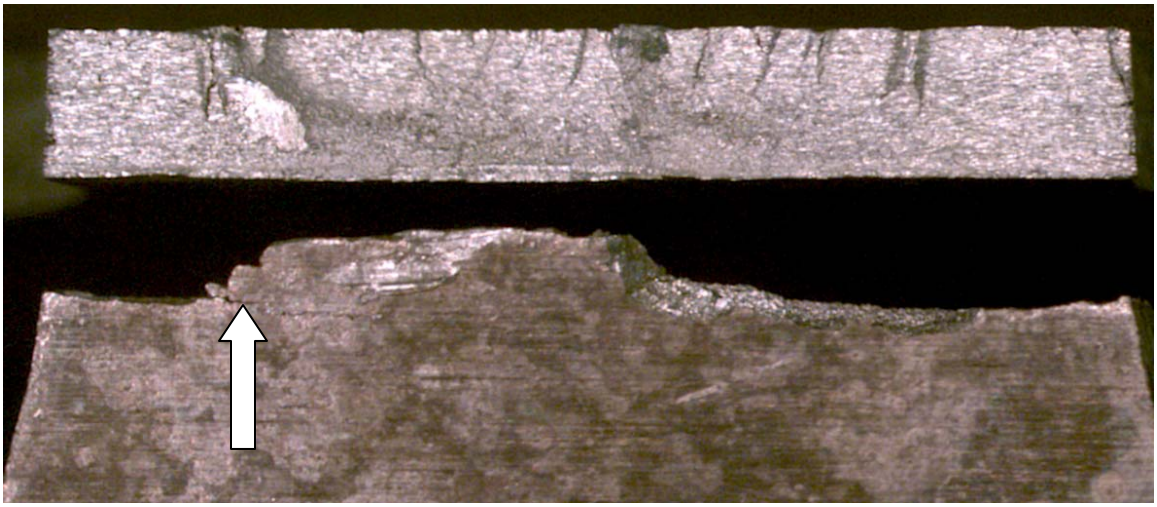

Figure 52 – Specimen T-7, 7075-T6, pre-corroded 60 minutes, exposed to 40/1 ratio 3.5% NaCl solution to H_2O_2 hydrogen peroxide, deflection = 13 mm (uncalibrated), Nf = 31,200 cycles. Cracks other than the primary fracture surface observable; one such is indicated by the arrow. Multiple ratchet marks indicate multiple cracks. (photo # TPS-005)

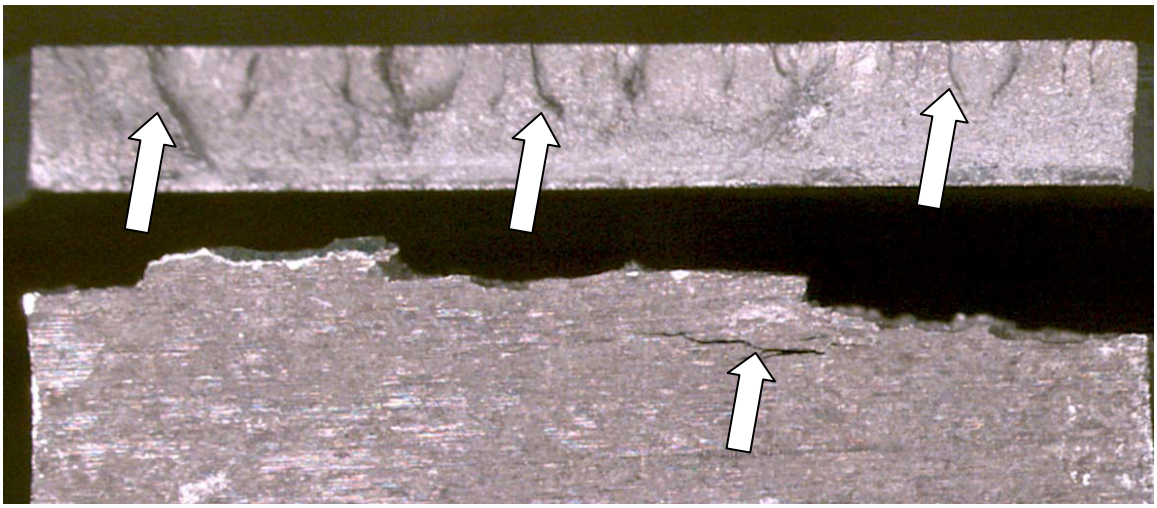

Figure 53 – Specimen T-8, 2024-T3 corroded during cyclic loading, exposed to 40/1 ratio 3.5% NaCl solution to H_2O_2 hydrogen peroxide, deflection = 17 mm (uncalibrated), N_f = 25200 cycles. Note the easily visible secondary crack (indicated by arrow) parallel to fracture surface; also there are many other less conspicuous secondary cracks. The end view of the fracture surface shows obvious signs of multiple ratchet marks (top arrows) indicating the cracks did not begin at the edges but is a result of multiple surface cracks linking together to form the fracture and thereby significantly reducing the fatigue life. (photo # TPS-004)

Figure 54 – Specimen T-9, 7075-T6 pre-corroded 30 minutes exposure to 15/1 ratio 3.5% NaCl solution to H_2O_2 hydrogen peroxide, deflection = 15 mm (uncalibrated), Nf = 51,300 cycles. (photo # TPS-002)

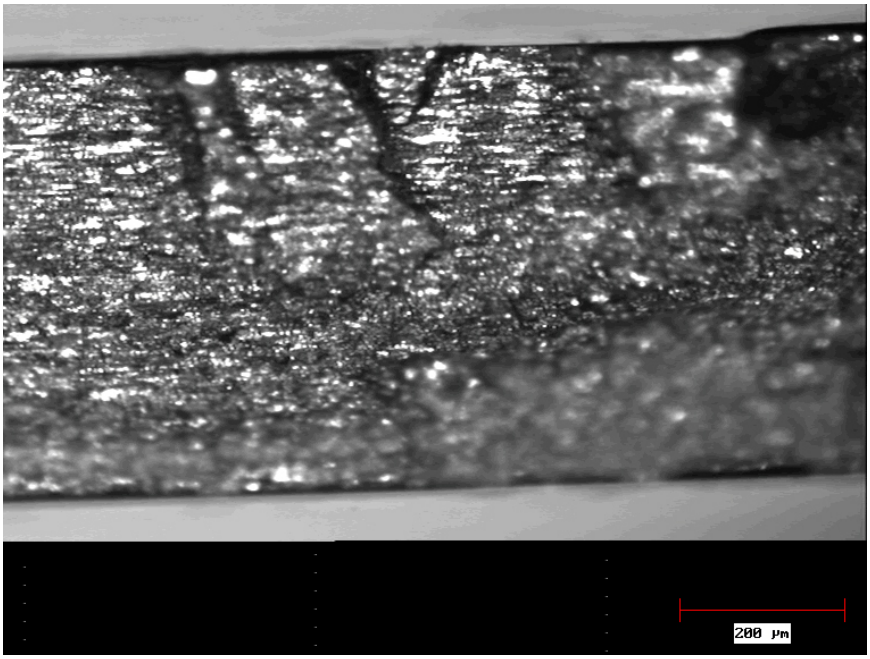

Figure 55 – Specimen T-7, 7075-T6 on edge showing closer view of ratchet marks, 50x, (photo T-7_2)

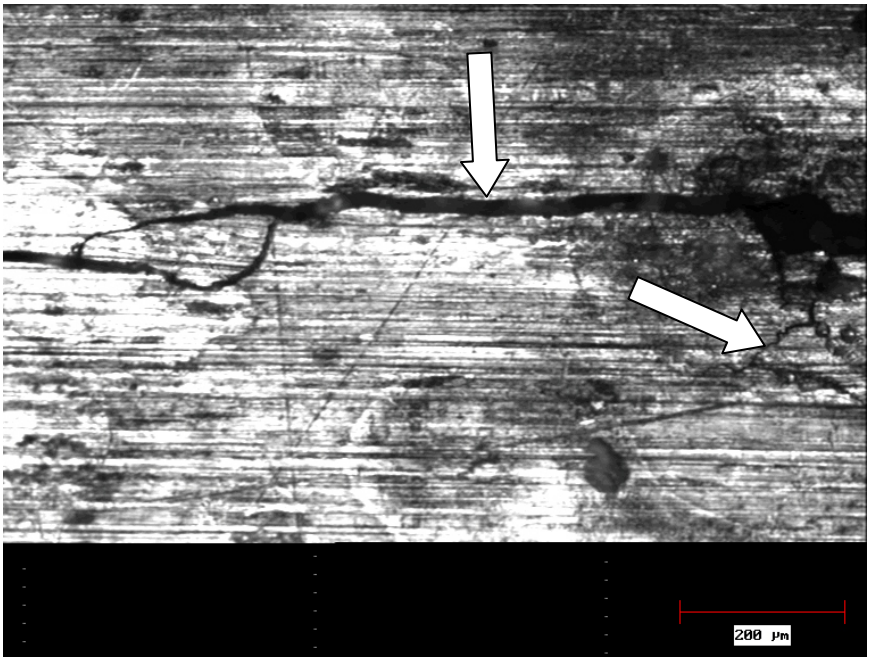

Figure 56 – Specimen T-7, 7075-T6, pre-corroded 60 minutes, exposed to 40/1 ratio 3.5% NaCl solution to H_2O_2 hydrogen peroxide, deflection = 13 mm (uncalibrated), Nf = 31,200 cycles. Cracks observed from a corrosion pit at right of frame. (photo # T-7_2DE)

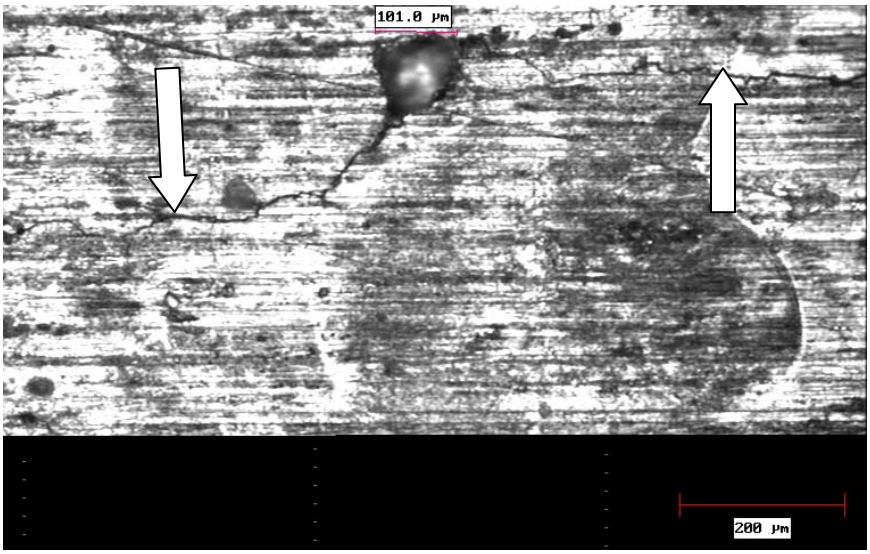

Figure 57 – Specimen T-7, 7075-T6, pre-corroded 60 minutes, exposed to 40/1 ratio 3.5% NaCl solution to H_2O_2 hydrogen peroxide, deflection = 13 mm (uncalibrated), Nf = 31,200 cycles. Cracks observed emanating from a corrosion pit formed at an inclusion at center of frame; crack runs lfet and right as indicated by arrows. (photo # T-7_3DE)

4.8 – Corrosion-During Cyclic Loading

The phenomenon of increased corrosion rates induced by cyclic loading was explored to ascertain if stress could actually function as an accelerant in the corrosive process. Two experiments using 2024-T3 and 7075-T6 were conducted using a relatively mild (400/1) ratio of 3.5% NaCl to hydrogen peroxide. The comparisons are displayed in Figures 58 and 59.

Other comparisons were made using 7075-T6 contrasting the corroded-during to pre-corroded behaviors and are shown in Figures 60 and 61. These specimens were corroded in the 3.5% NaCl solution without any hydrogen peroxide. The general observations indicate a very slight increase in corrosion rate in the corroded-during over that of the pre-corroded. The most notable contrast is in Figure 61, where the time was 298 minutes. This amount of time is an order of magnitude greater than the typical specimens tested so the degree of corrosion is understandably different. The timeframe of the tests with no or low ratios of hydrogen peroxide must increase greatly in order to bring about sufficient pitting. Oddly though the failures for the left and right specimens respectively were 595,600 and 335,800 cycles; this is opposite the expected results but could possibly be explained by the wide band of fatigue failures in general, indicating more tests before conclusions can be drawn confidently.

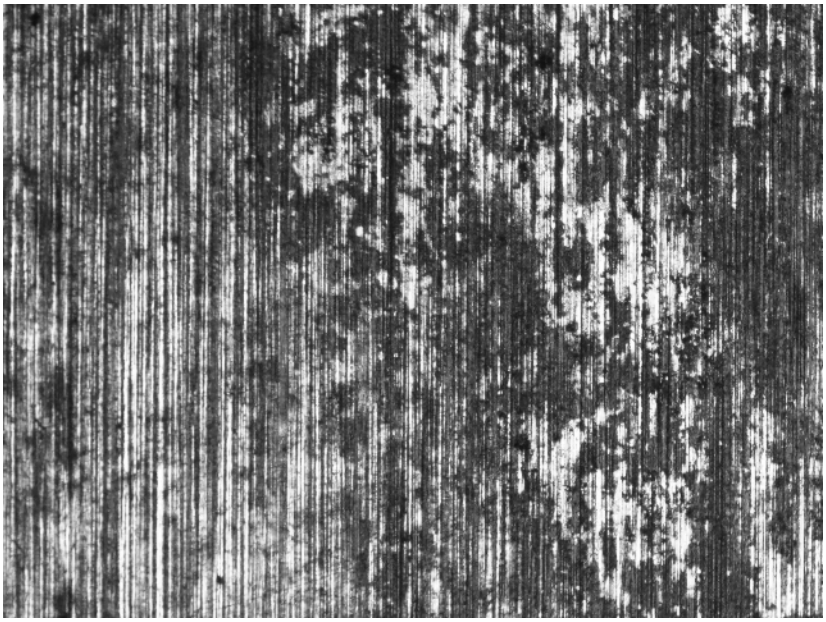

(a)

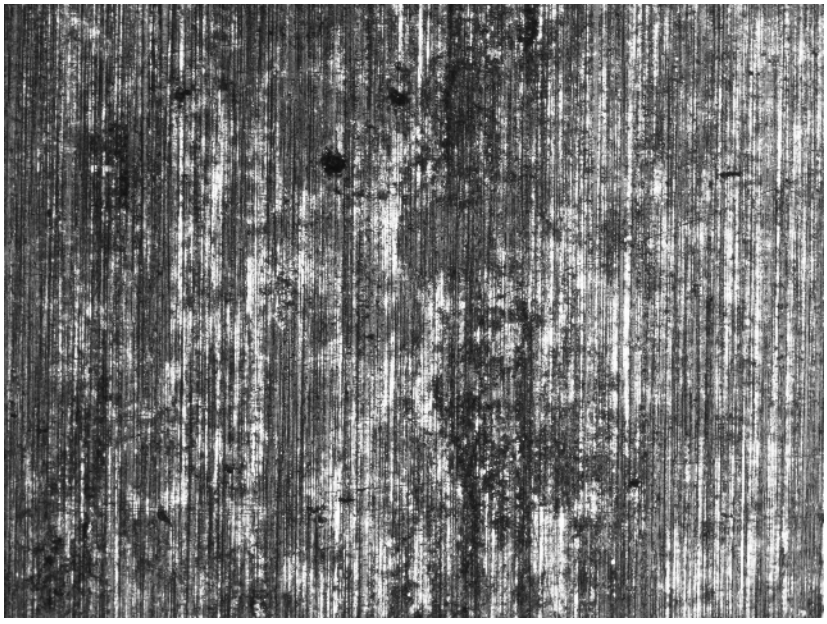

(b)

Figure 58 – 2024-T3, T-11 & T-12(50x) exposed to 400/1 ratio 3.5% NaCl solution to H_2O_2 hydrogen peroxide, (uncalibrated). (a) Specimen T-12, N = 0 (uncycled), pre-corroded for 19.4 minutes. (b) Specimen T-11, cycled at deflection = 15 mm to Nf = 38,700 or 19.4 minutes. Severity of general corrosion and pitting faintly higher in (b) cycled vs. (a) uncycled, indicating cyclic loading may exacerbate corrosion rate. (photos NH-018/-019)

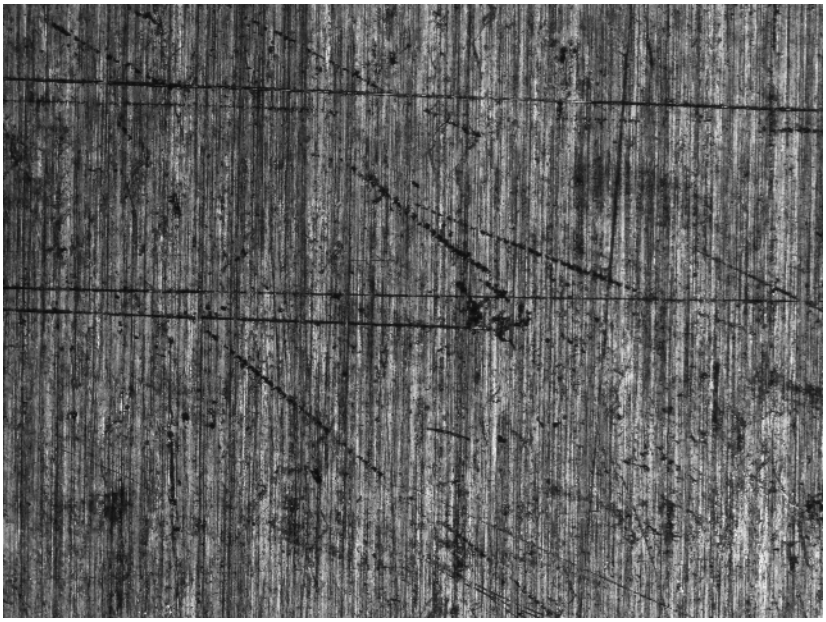

(a)

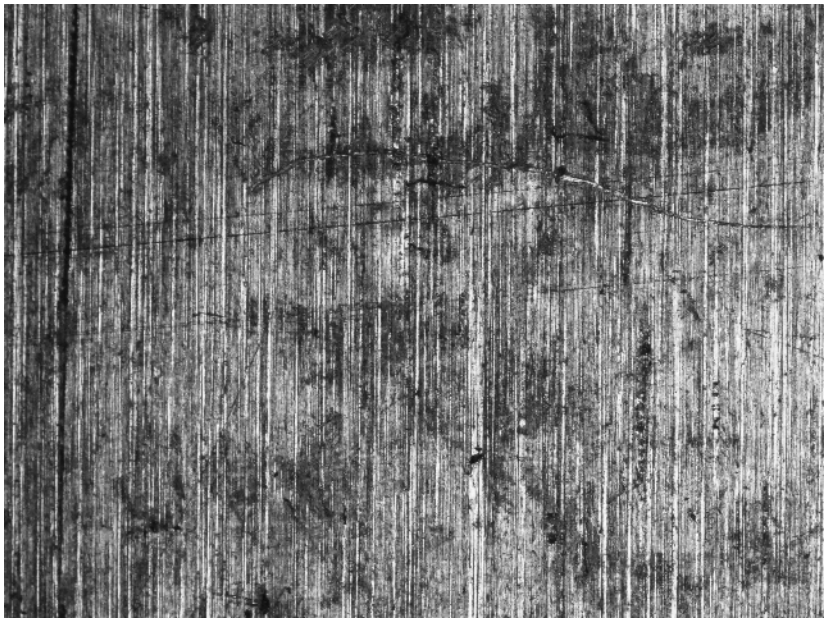

(b)

Figure 59 – 7075-T6, (50x) exposed to 400/1 ratio 3.5% NaCl solution to H_2O_2 hydrogen peroxide, (uncalibrated). (a) Specimen T-14, N = 0 (uncycled), pre-corrdeed for 30.4 minutes. (b) Specimen T-13, cycled at deflection = 15 mm to Nf = 60,800 or 30.4 minutes. Severity of general corrosion slightly higher in (b) cycled vs. (a) uncycled. Initiation of a few pits is evident as well. Difference indicates cyclic loading may accelerate/worsen corrosion rate.

Figure 60 – 7075-T6 Corrode-During and Pre-Corroded (50x). The left specimen in the photo (T-70-1, N_f = 49,600, Defl = 15 mm, 25 min) was corroded during cyclic loading and the right hand specimen (T-7P-1, N_f = 84,000) was pre-corroded 25 min. The difference between the two is negligible

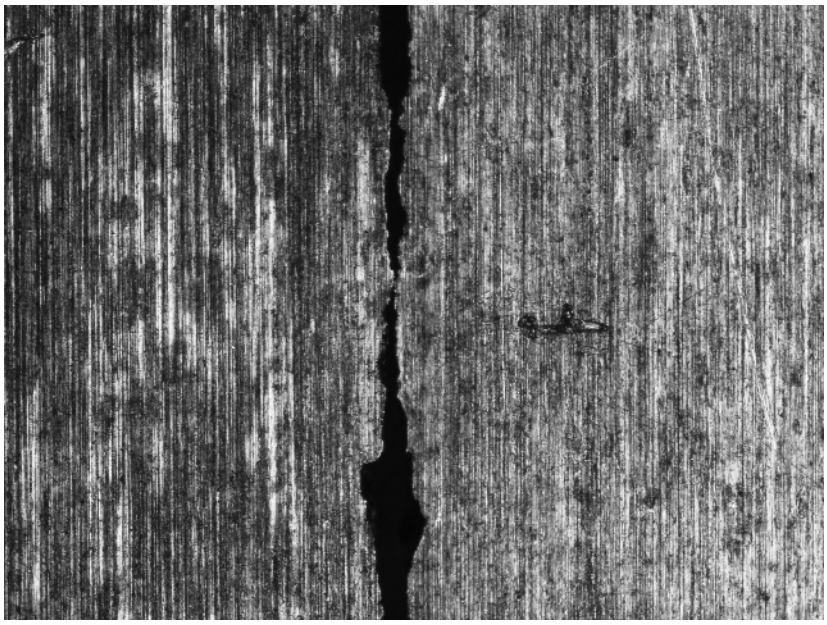

Figure 61 – 7075-T6 Corrode-During and Pre-Corroded (50x). The left specimen in the photo (T-70-4, N_f = 595,600, Defl = 13 mm, 298 min) was corroded during cyclic loading and the right hand specimen (T-7P-4, N_f = 335,800) was pre-corroded 298 min. The specimen at left is notably more corroded than the one on the right; however the corrosion is general with no obvious pitting

4.9 – Fatigue Data with only NaCl Solution

Several sets of specimens were run with only the 3.5% NaCl solution - that is, without the use of the hydrogen peroxide accelerant. The thrust of this series was to possibly utilize the effect of stress as a means of increasing the rate of corrosion and thereby replacing the hydrogen peroxide. Table 9 gives the bulk data recorded for this test specimens; the pristine values are given as well for comparison. Plots of the data are showing corrode-during and pre-corrosion are shown in Figures 62 - Figure 66, depicting results of experiments conducted with 2024-T3, 6061-T6 and 7075-T6. The pre-corroded specimens were done so as a direct comparison to the corrode-during specimens; the pre-corrosion times were equated to the time to failure of the corroded-during specimens.

The results were largely unremarkable, as the corrosion rate over the short time period was not near sufficient enough to shorten the fatigue lives but slightly, over pristine specimen values. There is a very slight difference in overall fatigue life reduction, which is logical, but the spread of data could reflect an explanation of this in normal distributions of fatigue life cycles to failure. Tables 10 - 12 gives the reduction in fatigue life of corroded specimens as they relate to the un-corroded pristine specimens; the average reduction in life for all alloys tested is 3.1 for corroded-during and 1.3 for pre-corroded. The addition of cyclic stress surely increased the susceptibility to earlier failure.

Table 9 – Fatigue Data on Pristine, Corrode-During Cyclic Loading and Pre-Corrode

Specimen	Method	NaCl Soln, %	H_2O_2, %	Alloy	N_f	Defl, mm	Comments
T-20-6	prist	0	0	2024-T3	1014300	14	
T-20-7	prist	0	0	2024-T3	214300	15	
T-20-5	prist	0	0	2024-T3	181100	17	
T-20-1	corr-dur	3.5	0	2024-T3	108500	15	
T-20-2	corr-dur	3.5	0	2024-T3	93000	16	
T-20-3	corr-dur	3.5	0	2024-T3	288100	14	
T-20-4	corr-dur	3.5	0	2024-T3	70000	17	
60-1	prist	0.0	0	6061-T6	206,300	14	
60-2	prist	0.0	0	6061-T6	116,300	16	
60-3	prist	0.0	0	6061-T6	66,900	17	
T-60-1	corr-dur	3.5	0	6061-T6	67,700	14	cycle time 34 min
T-60-2	corr-dur	3.5	0	6061-T6	34,700	16	cycle time 17 min
T-60-3	corr-dur	3.5	0	6061-T6	42,500	17	cycle time 21 min
T-6P-1	pre-corr	3.5	0	6061-T6	162,900	14	pre-corr 34 min
T-6P-2	pre-corr	3.5	0	6061-T6	123,900	16	pre-corr 17 min
T-6P-3	pre-corr	3.5	0	6061-T6	108,000	17	pre-corr 21 min
T-70-6	prist	0	0	7075-T6	23886400	12	No fail, terminated
T-70-7	prist	0	0	7075-T6	407100	13	failed within block
T-70-8	prist	0	0	7075-T6	2923300	13	failed within block
T-70-9	prist	0	0	7075-T6	298700	14	
T-70-10	prist	0	0	7075-T6	543100	15	failed within block
T-70-11	prist	0	0	7075-T6	107900	15	failed within block
T-70-12	prist	0	0	7075-T6	105300	16	
T-70-13	prist	0	0	7075-T6	65500	17	
T-70-1	corr-dur	3.5	0	7075-T6	49600	15	
T-70-2	corr-dur	3.5	0	7075-T6	56800	16	
T-70-3	corr-dur	3.5	0	7075-T6	117400	14	
T-70-4	corr-dur	3.5	0	7075-T6	595600	13	
T-70-5	corr-dur	3.5	0	7075-T6	2917800	12	failed within block
T-70-14	corr-dur	3.5	0	7075-T6	14700	17	
T-7P-1	pre-corr	3.5	0	2024-T3	84000	15	Pre-corr 25 min
T-7P-2	pre-corr	3.5	0	2024-T3	426100	16	28 m, failed at block
T-7P-3	pre-corr	3.5	0	2024-T3	7769100	14	Pre-corr 59 min
T-7P-4	pre-corr	3.5	0	2024-T3	335800	13	Pre-corr 298 min
T-7P-5	pre-corr	3.5	0	2024-T3	143900	17	Pre-corr 21 min

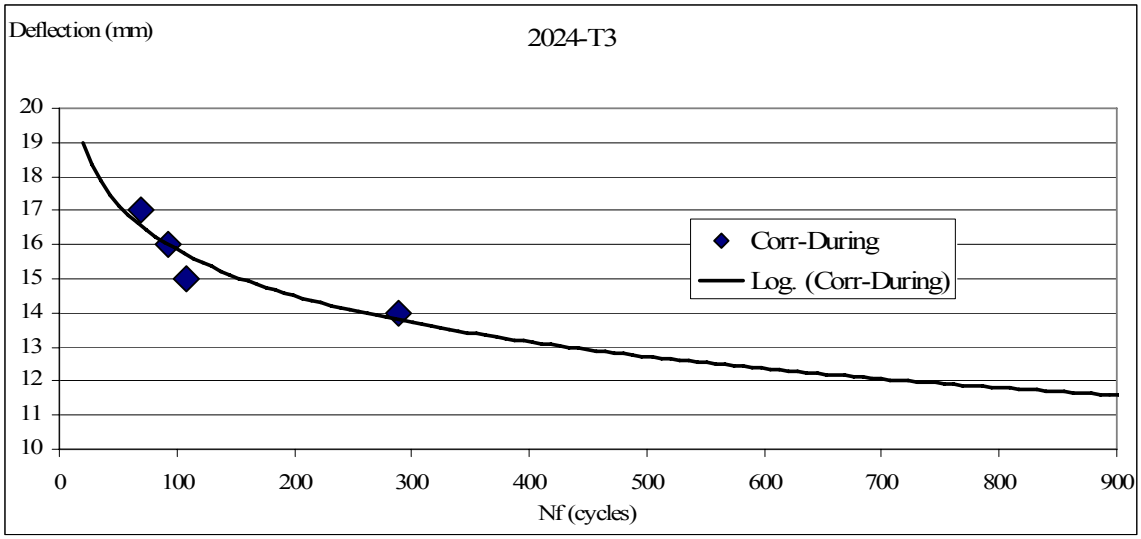

Figure 62 – Plot of Fatigue Data for 2024-T3 Corroded During Cyclic Loading

Table 10 – Life Reduction Factors of 2024-T3 in 3.5% NaCl Solution

Defl, mm	Corr-During N_f	Prist Nf	Nf Reduction Factor
14	288,100	1,014,300	3.5
15	108,500	214,300	2.0
17	70,000	181,100	2.6
		Average	2.3

Table 11 - Fatigue Life Reduction Factors for 6061-T6 in 3.5% NaCl Solution

Defl, mm	Corrode During, Nf	Pre-corr, Nf	Pristine, Nf	Corr-Dur Life Reduction Factor	Pre-corr Life reduction Factor
14	67,700	162,900	206,300	3.05	1.27
16	34,700	123,900	116,300	3.35	0.94
17	42,500	108,000	66,900	1.57	0.62
			Average	2.66	0.78

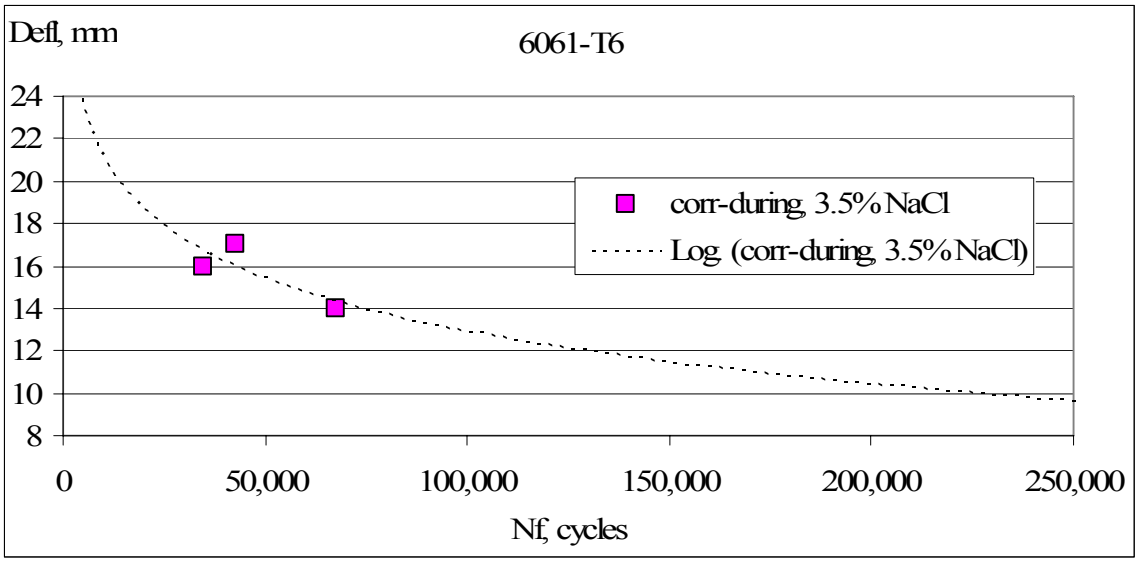

Figure 63 – 6061-T6 Corroded-During cyclic leading in 3.5% NaCl

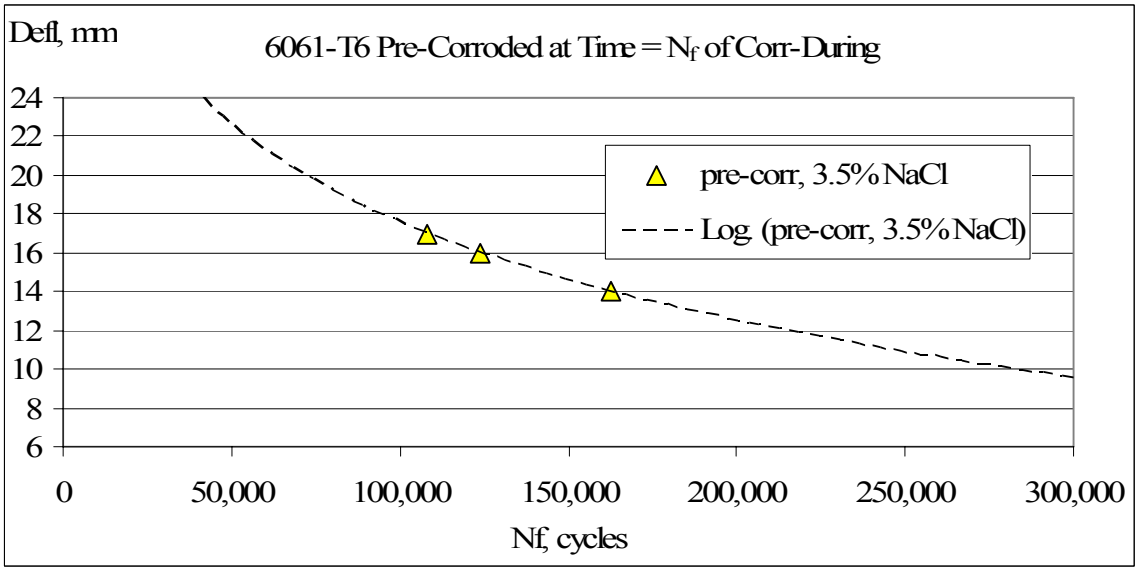

Figure 64 – 6061-T6 Pre-corroded Specimens; corrosion times equated to Corr-During N_f

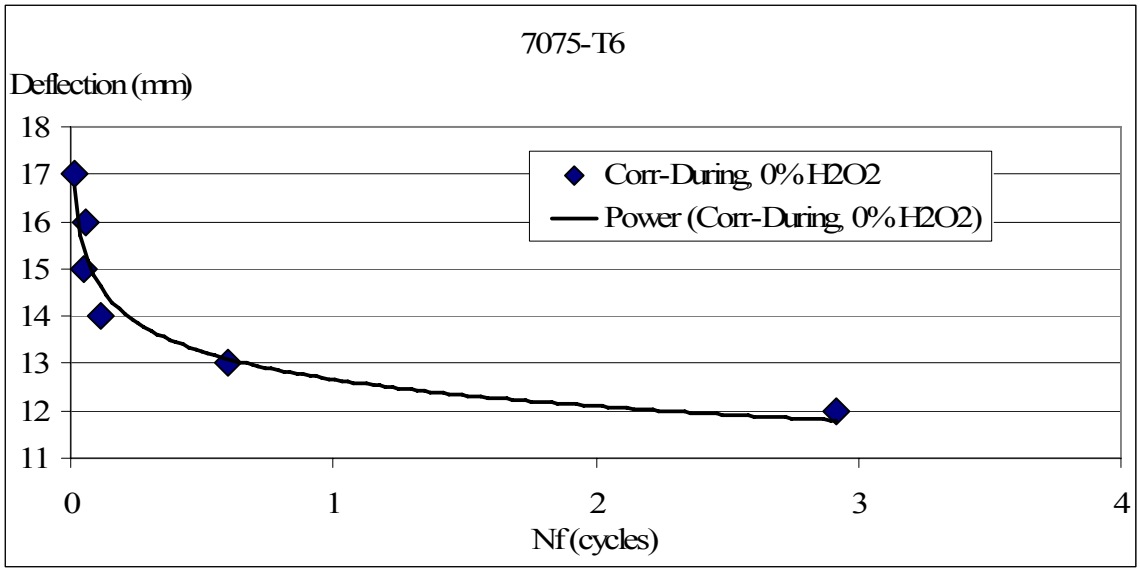

Figure 65 – 7075-T6 Corroded-During cyclic leading in 3.5% NaCl

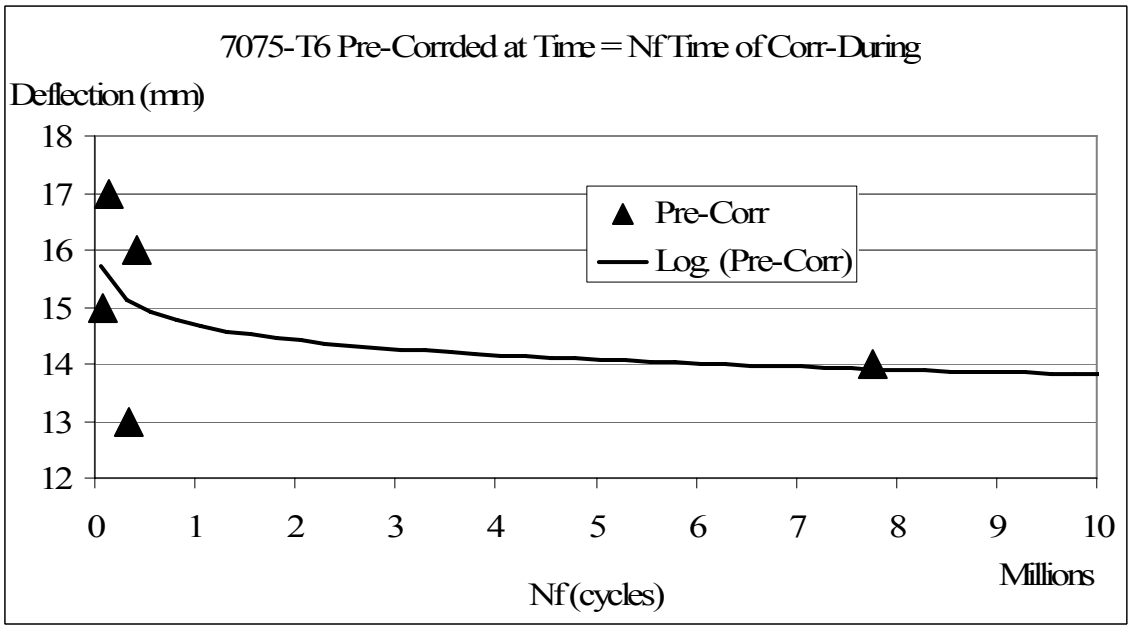

Figure 66 – 7075-T6 Pre-corroded Specimens; corrosion times equated to Corroded-During N_f

Table 12 – Fatigue Life Reduction Factors for 7075-T6 in 3.5% NaCl Solution

Defl, mm	Corrode During, Nf	Pre-corr, Nf	Pristine, Nf	Corr-Dur Life Reduction Factor	Pre-corr Life reduction Factor
12	2,917,800		23,886,400	8.19	
13	595,600	335,800	1,665,200	2.80	4.96
14	117,400	7,769,100	298,700	2.54	0.04
15	49,600	84,000	325,500	6.56	3.88
16	56,800	426,100	105,300	1.85	0.25
17	14,700	143,900	65,500	4.46	0.46
			Average	4.40	1.91

4.10 – Metallography of Fatigue Specimens with only NaCl

The images of the fatigue specimens failed using only 3.5% NaCL solution are shown in Figures 67 - 76. The obvious note in the 2024-T3 and 7075-T6 specimens is the general lack of corrosion pitting or other features of multiple sites fatigue crack initiation. In general these specimens subject to the NaCL solution appeared much the same as a pristine specimen. However the 6061-T6 specimens began to exhibit signs of secondary cracks off the primary fracture surface. Surprisingly the pristine specimen at the 17 mm deflection also had secondary cracking. The secondary cracking, indicating multiple fatigue initiation sites, was present in all three regimes of 6061-T6: pristine, corroded-during cyclic loading and pre-corroded.

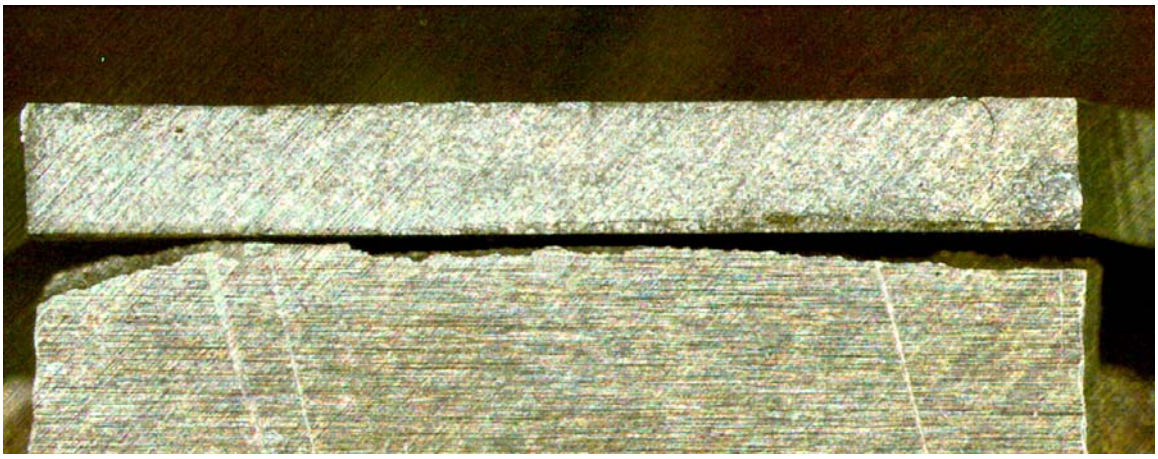

Figure 67 – Specimen T-20-1, 2024-T3 corrode-during in 3.5% NaCl, Defl = 15 mm, Nf = 49,600. Photo is typical of most specimens in this series; smooth and uneventful, no ratchet marks. (photo S-001)

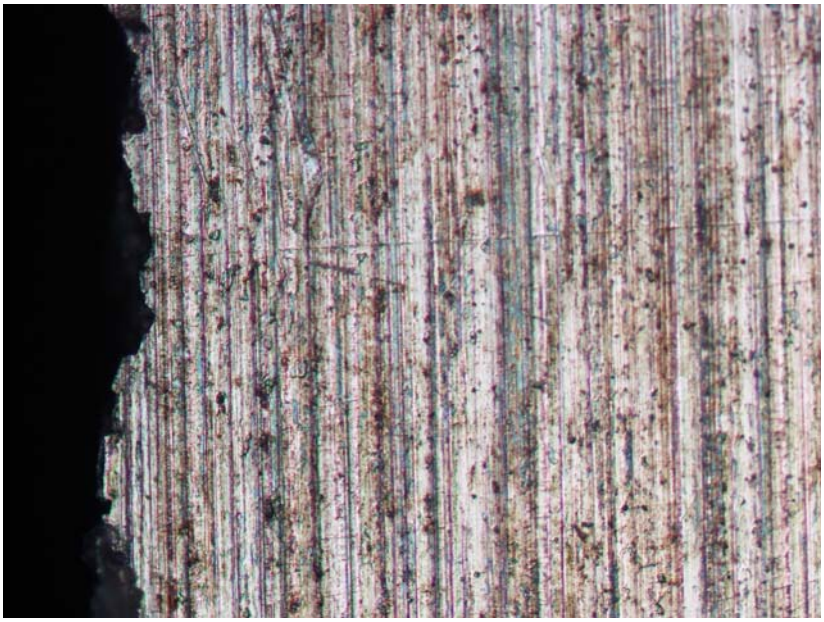

Figure 68 – 2024-T3, Specimen T-20-1 corrode-during in 3.5% NaCl (200x), Defl = 15 mm, Nf = 49,600 (photo NH-001)

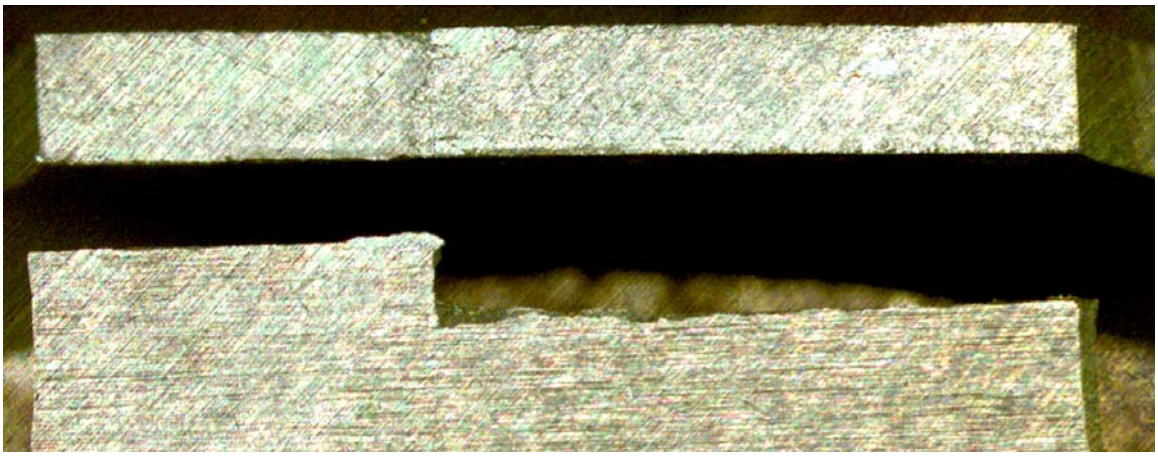

Figure 69 – Specimen T-20-4, corrode-during in 3.5% NaCl, Defl = 15 mm, Nf = 595,600. No obvious ratchet marks; jog in the center possibly due to two edge cracks meeting. However a secondary crack is noted in the Figure below; indicating the possibility of secondary cracking. (photo S-003)

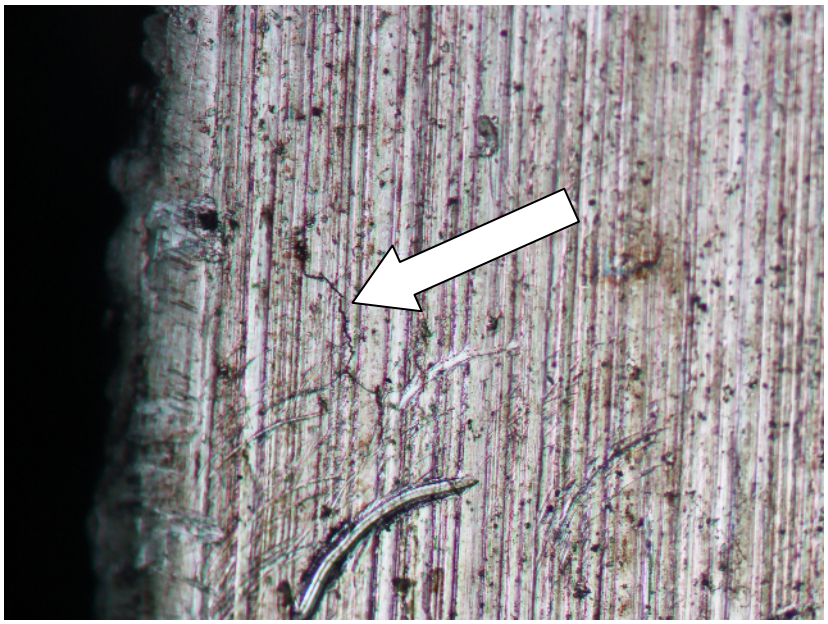

Figure 70 – 2024-T3 Specimen T-20-4 corrode-during in 3.5% NaCl (200x), Defl = 13 mm, Nf = 595,600. Note the small crack parallel to the fracture surface. (photo NH-006)

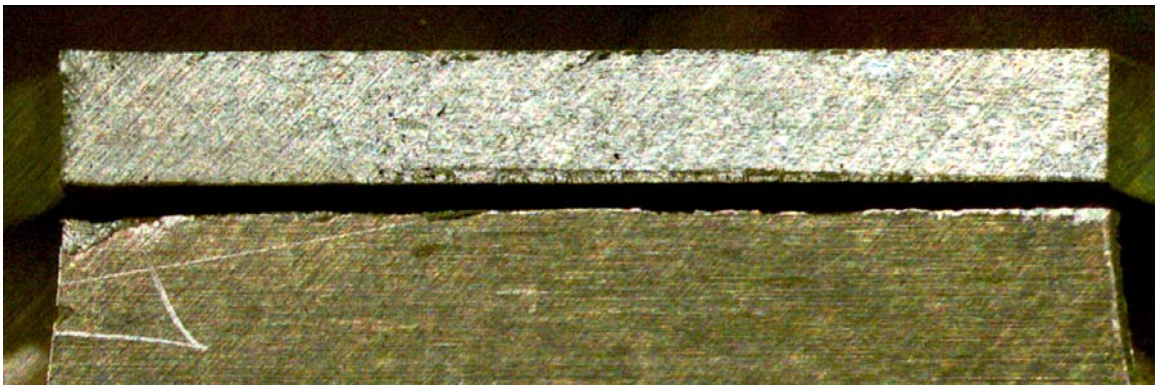

Figure 71 – Specimen T-70-1, 7075-T6, Nf = 49,600 cycles, Defl = 15 mm. Fracture surface is smooth and unremarkable; no ratchet marks. (photo S-006)

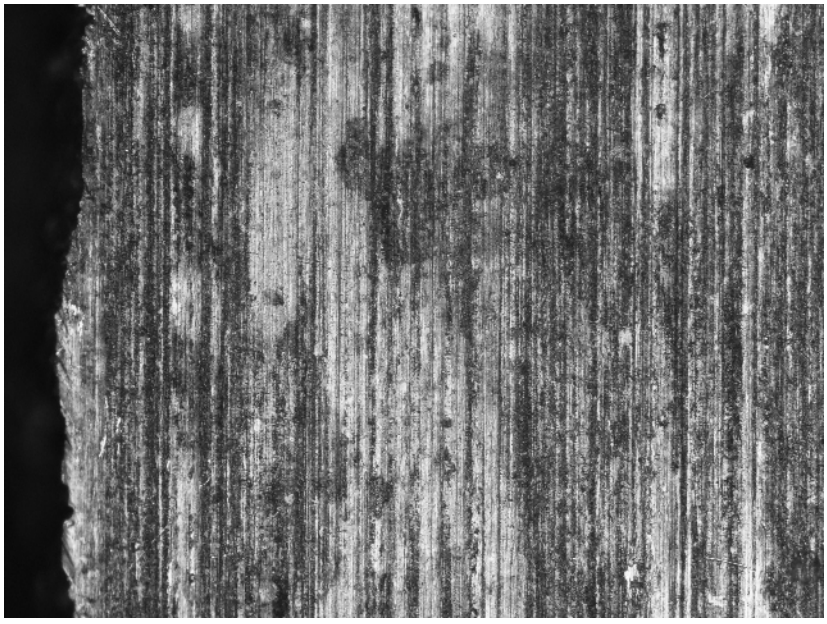

Figure 72 – 7075-T6 Specimen T-70-4 corrode-during in 3.5% NaCl (200x), Defl = 17 mm, Nf = 700,000. Surface appears to be coming slightly corroded. (photo NH-011)

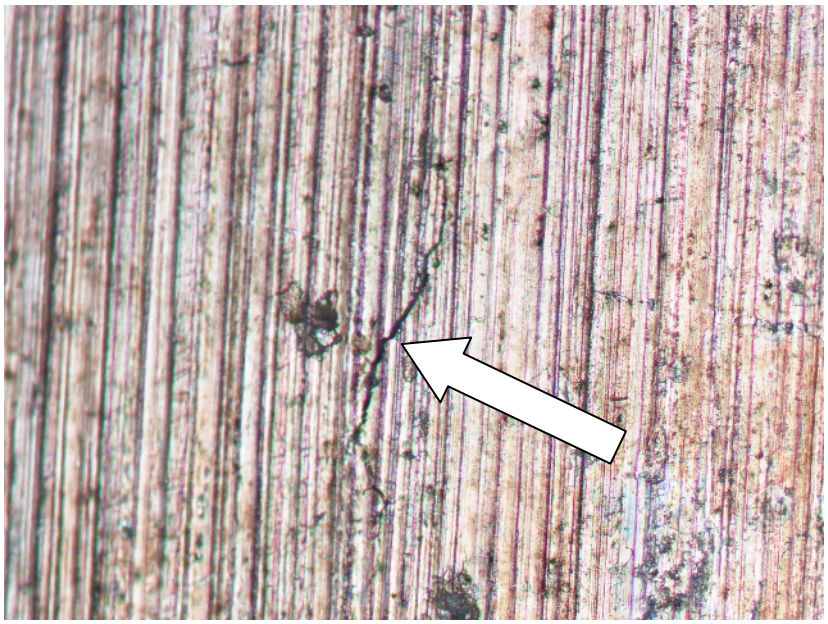

Figure 73 – Specimen 60-3 pristine (200x) 6061-T6, Defl = 17 mm, Nf = 66,900. Note the secondary crack off the primary fracture surface; this is highly unusual for pristine specimen to initiate cracks other than at an edge. (photo NH-031)

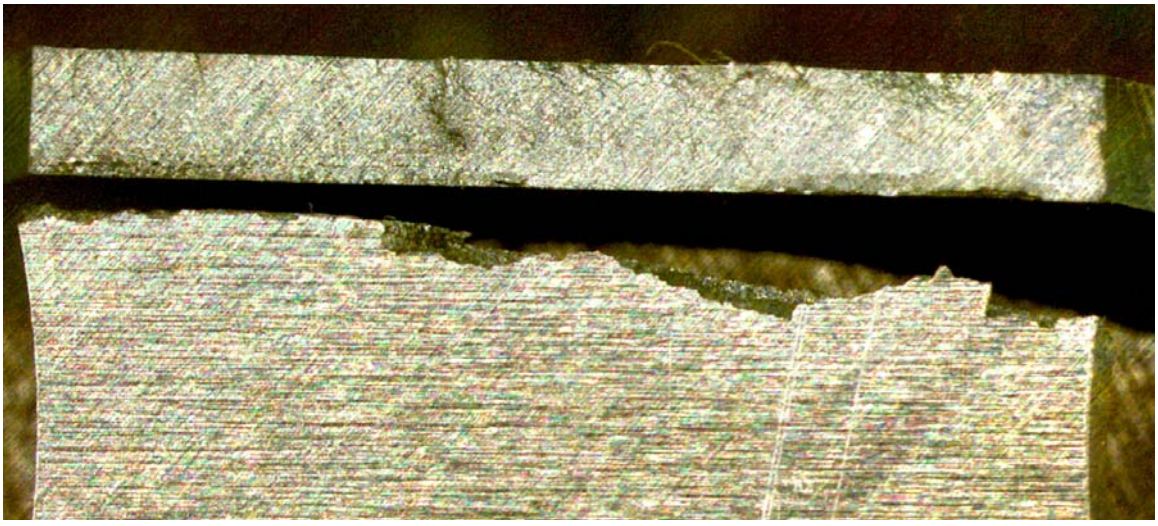

Figure 74 – Specimen T-60-3, (200x) 6061-T6, Defl = 17 mm, Nf = 42,500, corrode-during in 3.5% NaCl. Note ratchet marks indicating multiple fatigue crack initiation sites. (photo S-014)

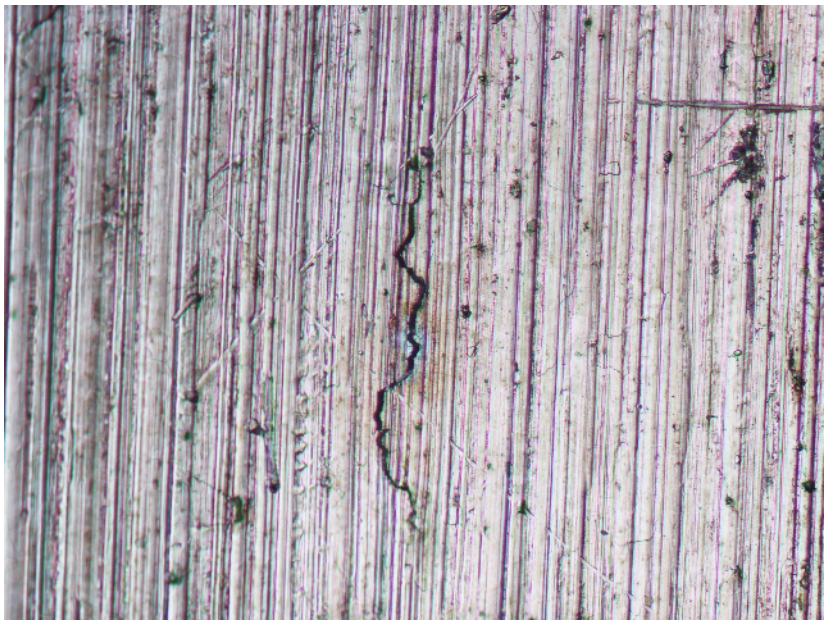

Figure 75 – T-60-3 Specimen (200x) 6061-T6, Defl = 17 mm, Nf = 42,500. Note the secondary crack off the primary fracture surface; source is not apparent but it could have occurred at an inclusion or constituent, exacerbated by corrosion-during cyclic loading. (photo NH-027)

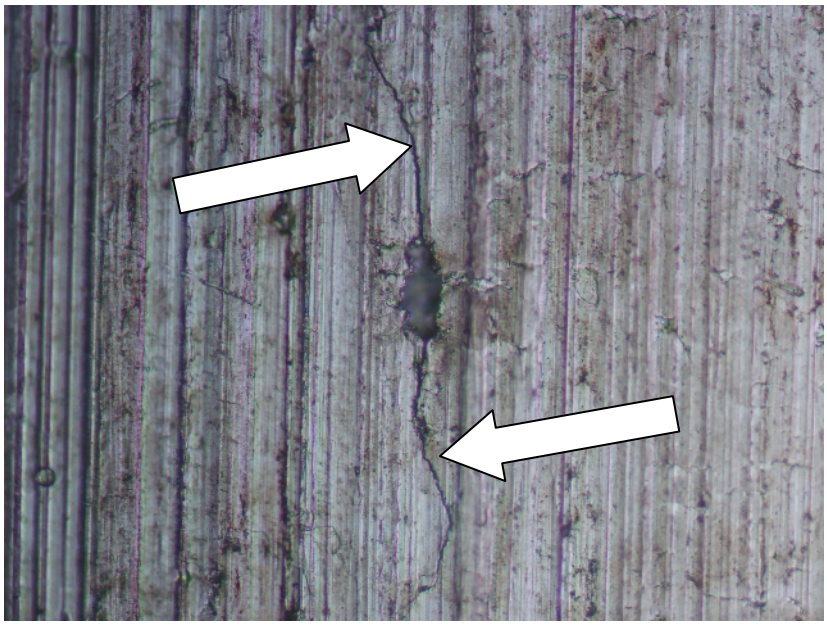

Figure 76 – T-6P-2 Specimen (200x) 6061-T6, Defl = 16 mm, Nf = 123,900. Note the secondary crack off the primary fracture surface at what appears to be an inclusion or void. (photo NH-029)

4.11 – Pitting For Fatigue Crack Initiation by Pre-Corrosion

Machine cut specimens of 2024-T3, 7075-T6 and 6061-T6 along with laser cut 2024-T3 specimens were fatigue tested to failure with varying degrees of pre-corrosion. A deflection of 14 mm was chosen for the test deflection and will give a sufficiently long life averaging near 100,000 cycles and ranging 30-60 minutes to N_f for all specimens. Table 13 gives the recorded data for each specimen tested. Figure 77- 82 plots the Pre-Corrosion Time vs. N_f and Pit Depth vs. N_f. The corrosive solution used was 3.5% NaCl and H_2O_2 at various ratios; but most commonly 30/1.

It was noted during the pre-corrosion, accomplished over several days, the corrosive solution aggressiveness seemed to gradually diminish with each passing day as indicated by it taking longer exposure times to yield suitable pitting. Not much was noticed within a few days but if over a week went by it became obvious. It was determined the hydrogen peroxide component of the solution would go “flat” over time. This was consistent with a Note discovered within the ASTM G110 [66] specification.

Table 13 – Data, Pre-corroded Specimens, 14 mm Deflection

Spec. No.	Alloy	N_f (cycles)	Pre-corr time	Ratio H_2O_2	Comments
LPH-2	2024 LC	73,200	70	30/1	
LPH-3	2024 LC	86,200	45	30/1	
LPH-1	2024 LC	114,500	15	30/1	
L-1	2024 LC	126,000	0	0	
LPH-4	2024 LC	82,000	10	30/1	diff batch of corr sol
LPH-5	2024 LC	114,900	5	30/1	diff batch of corr sol
60-1	6061-T6	206,300	0	0	
6PH-4	6061-T6	76,500	15	30/1	
6PH-3	6061-T6	110,000	30	30/1	
6PH-1	6061-T6	84,200	90	30/1	
6PH-2	6061-T6	47,200	120	30/1	
7PH-1	7075-T6	31700	60	30/1	
7PH-2	7075-T6	30000	30	30/1	
7PH-3	7075-T6	41300	15	30/1	
7PH-4	7075-T6	34800	10	30/1	
7PH-5	7075-T6	47900	15	60/1	
7PH-6	7075-T6	64200	30	120/1	
7PH-7	7075-T6	51900	240	120/1	
T-70-9	7075-T6	298700	0	0	

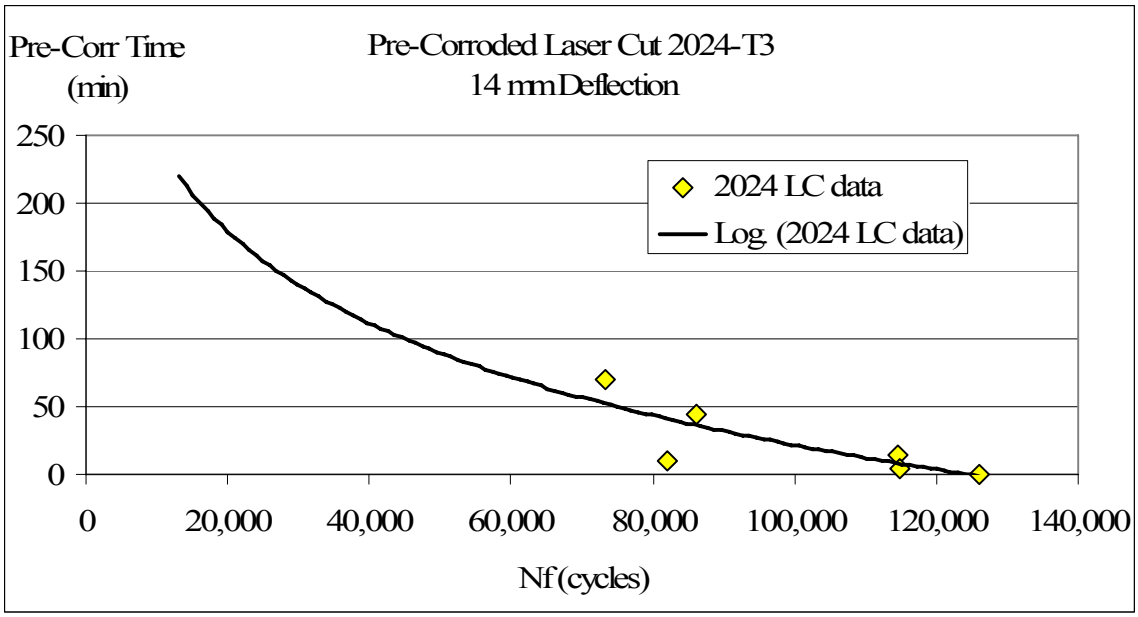

Figure 77 – Pre-Corroded 2024-T3 laser cut, cycled at 14 mm deflection

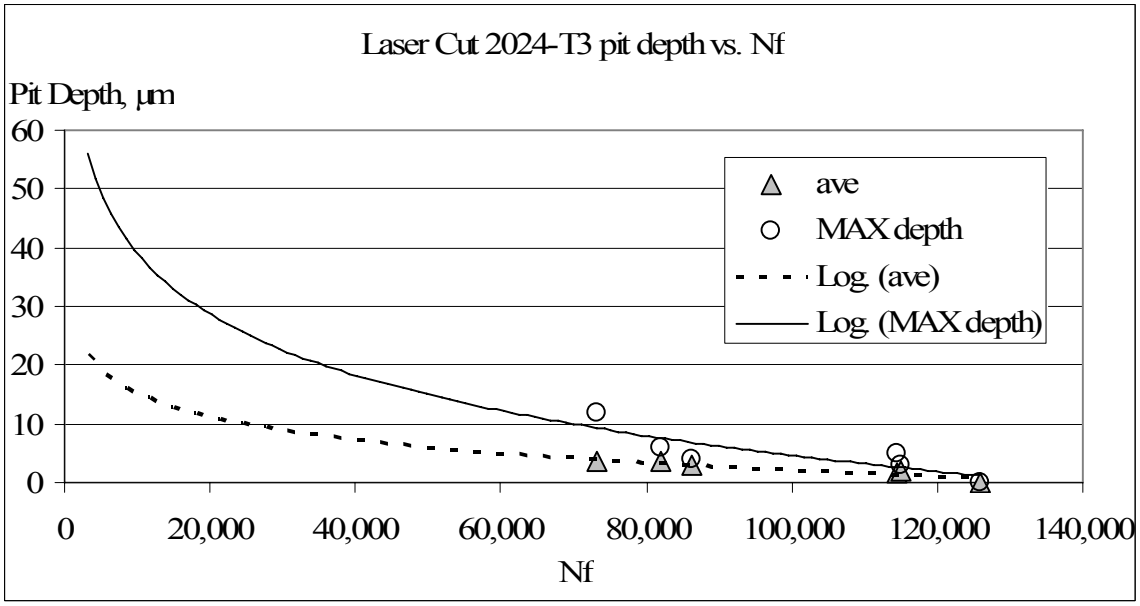

Figure 78 – Pit Depth, Pre-Corroded 2024-T3 laser cut, cycled at 14 mm deflectio

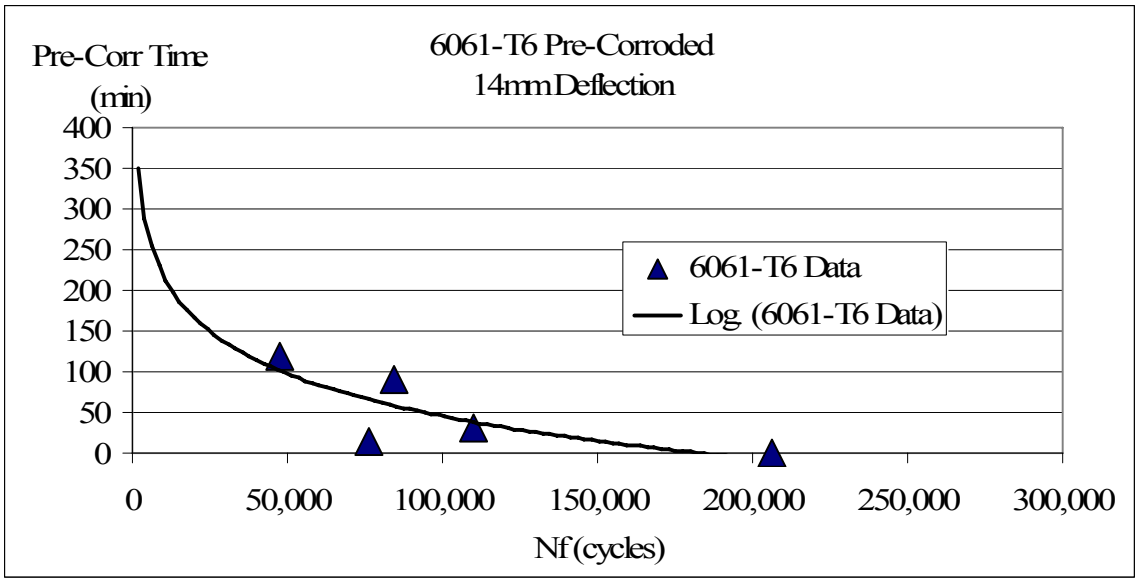

Figure 79 – Corrosion Time, Pre-Corroded 6061-T6 cycled at 14 mm deflection

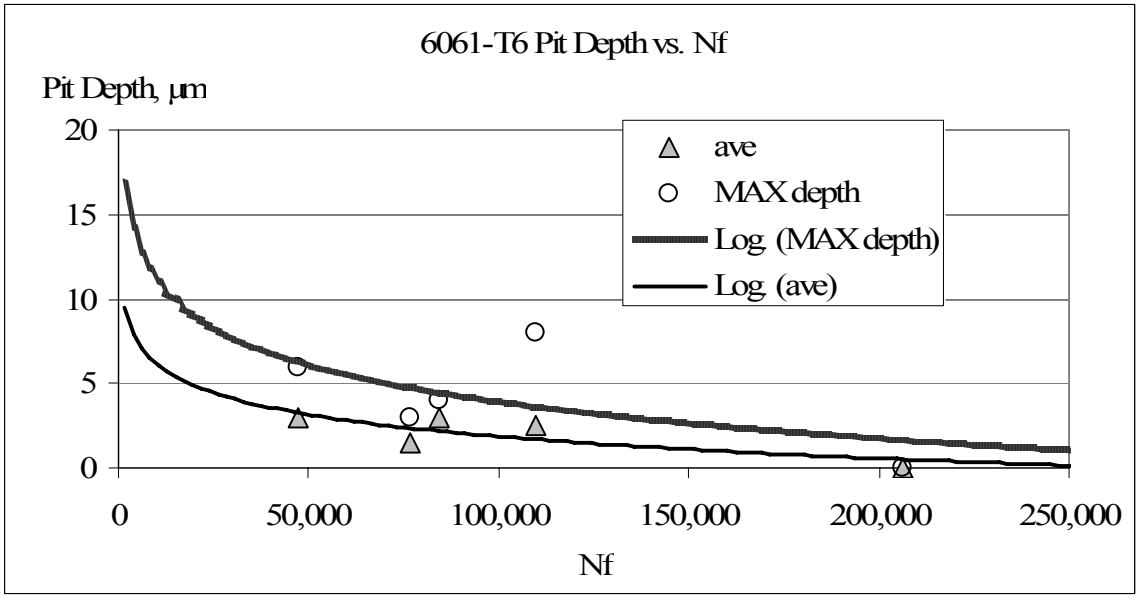

Figure 80 – Pit Depth Pre-Corroded 6061-T6 cycled at 14 mm deflection

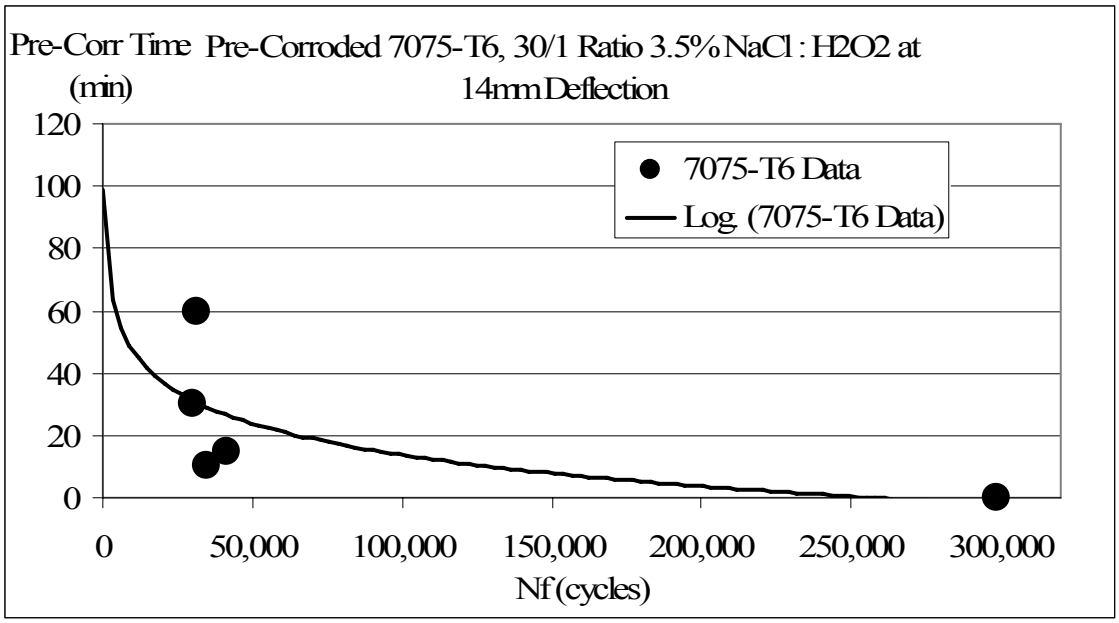

Figure 81 – Pre-corroded 7075-T6; Cycles vs. Corrosion Time; 14 mm deflection

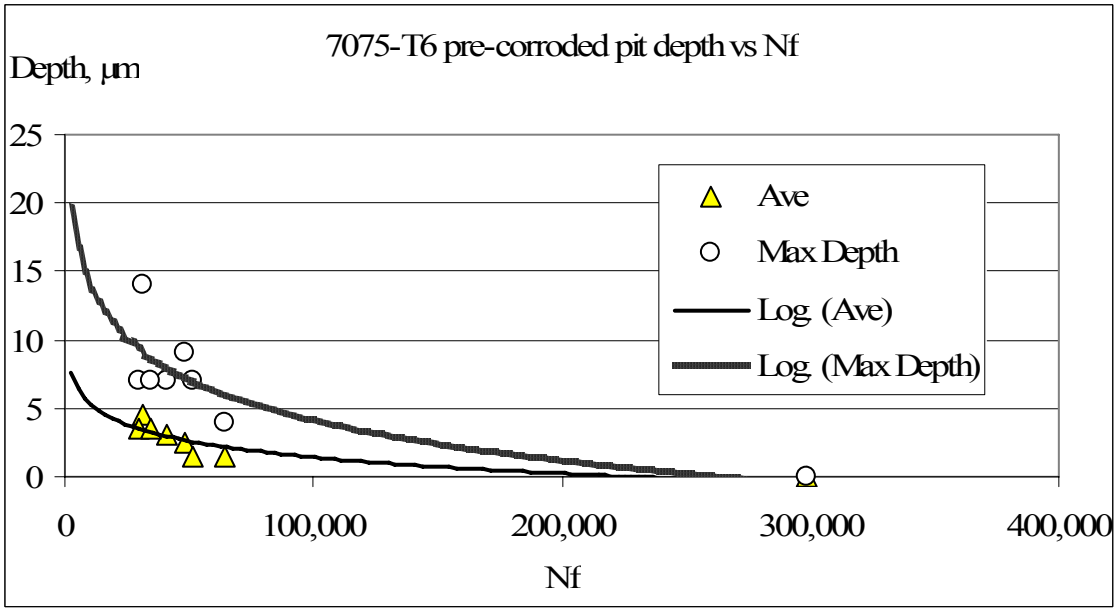

Figure 82 – Pre-corroded 7075-T6; Cycles vs. Pit Depth; 14 mm deflection

4.12 – Metallography of Pitted Specimens by Pre-Corrosion

The specimens are presented in Figures 83 - 110 below, highlighting any noteworthy features. Indications of secondary cracking abound in most specimens as witnessed by the presence of ratchet marks along the fracture surface, indicating multiple crack initiations. These ratchet marks generally traverse downward from the top (tension) surface about half the cross-section in the heavier corroded specimens. The lighter the corrosion magnitude, the lesser the distance the ratchet marks traveled down the fracture surface; in these minimal cases the pits are nearing the pit-crack threshold such as in Figure 87 and 107.

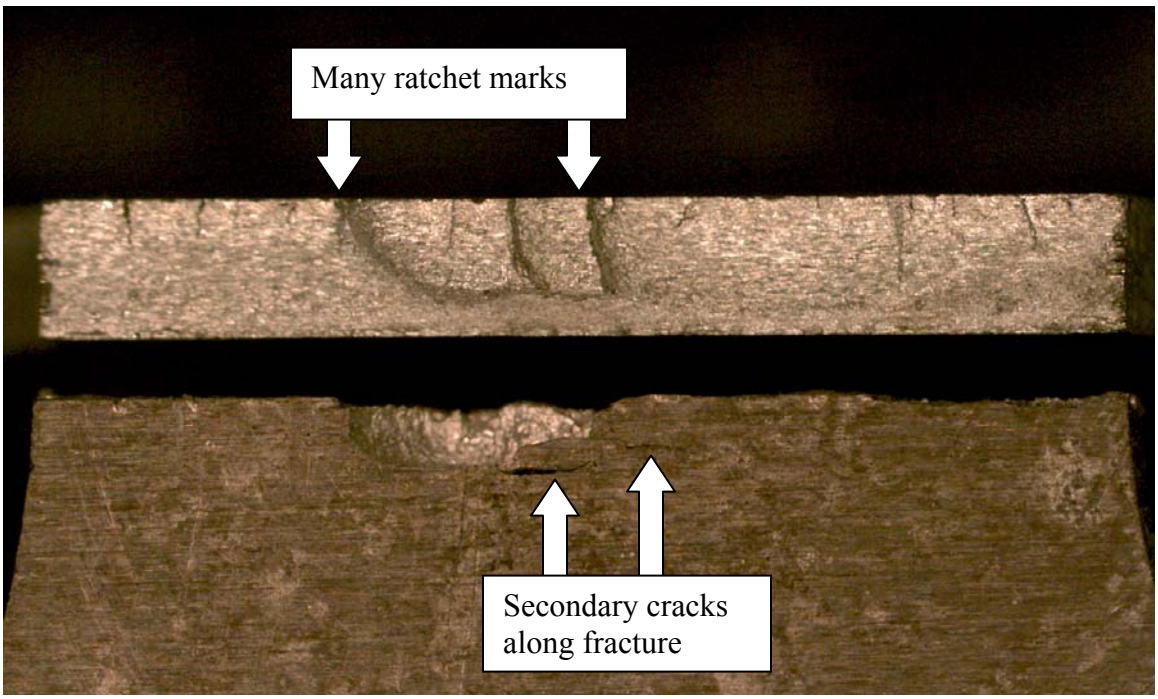

Figure 83 – Specimen 7PH-1, 7075-T6 pre-corroded 60 minutes in a 30/1 ratio of 3.5% NaCl solution to H_2O_2 hydrogen peroxide at 14 mm deflection, Nf = 31,700. Many secondary cracks can be seen along the fracture surface forming at pits, multiple ratchet marks (approximately 17 ea) can be seen originating at the top (tension) surface. (photo # PHS-009)

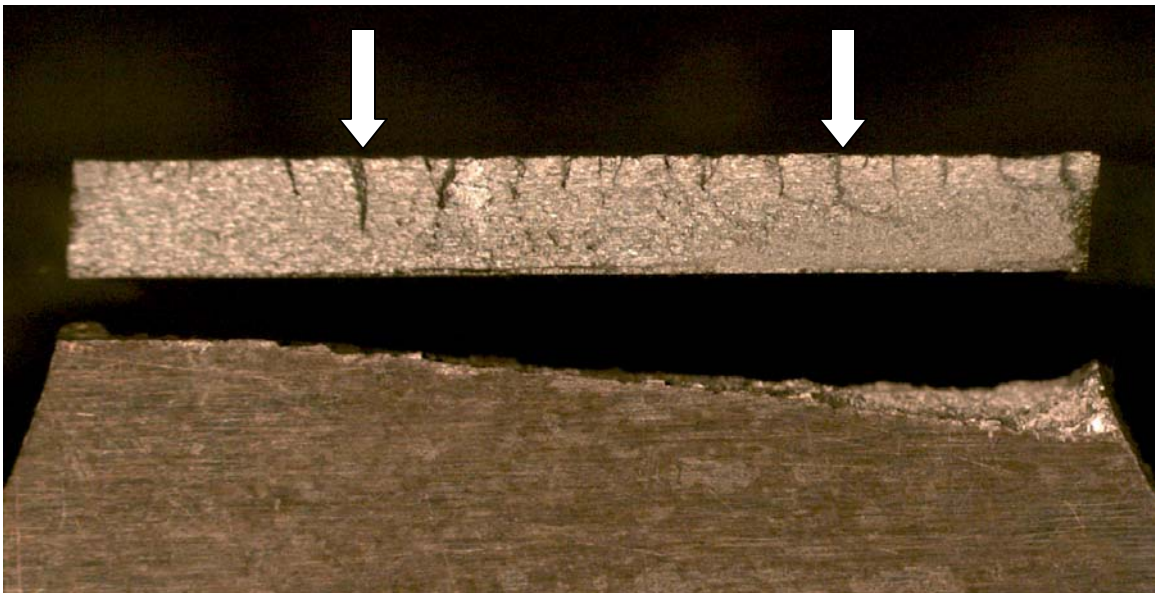

Figure 84 – Specimen 7PH-2, 7075-T6 pre-corroded 30 minutes in a 30/1 ratio of 3.5% NaCl solution to H_2O_2 hydrogen peroxide at 14 mm deflection, Nf = 30,000. Multiple ratchet marks (approximately 20 ea) can be seen originating at the top (tension) surface. (photo # PHS-010)

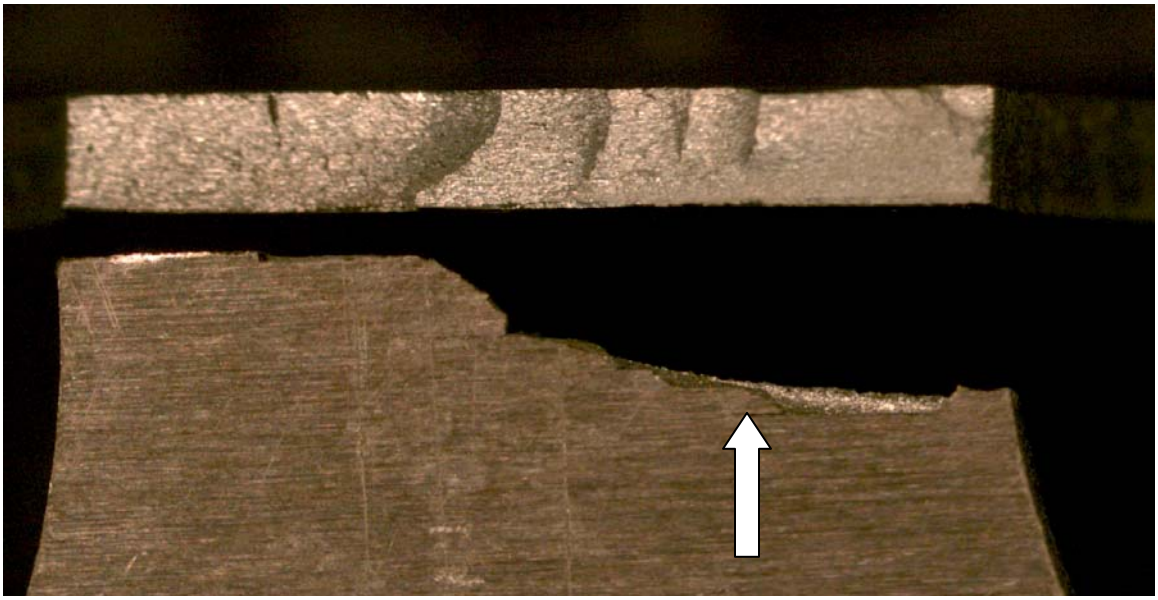

Figure 85 – Specimen 7PH-3, 7075-T6 pre-corroded 15 minutes in a 30/1 ratio of 3.5% NaCl solution to H_2O_2 hydrogen peroxide at 14 mm deflection, Nf = 41,300. A secondary crack can be seen along the fracture surface forming at pits, multiple ratchet marks (approximately 6 ea) can be seen originating at the top (tension) surface. (photo # PHS-011)

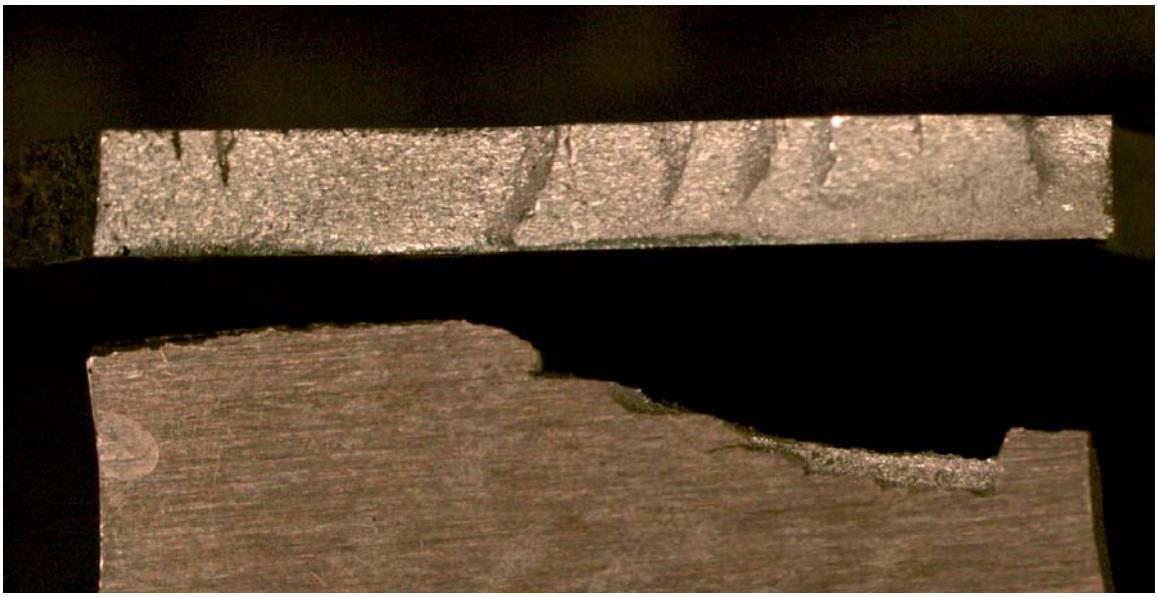

Figure 86 – Specimen 7PH-4, 7075-T6 pre-corroded 10 minutes in a 30/1 ratio of 3.5% NaCl solution to H_2O_2 hydrogen peroxide at 14 mm deflection, Nf = 34,800. Multiple ratchet marks (approximately 9 ea) can be seen originating at the top (tension) surface. (photo # PHS-008)

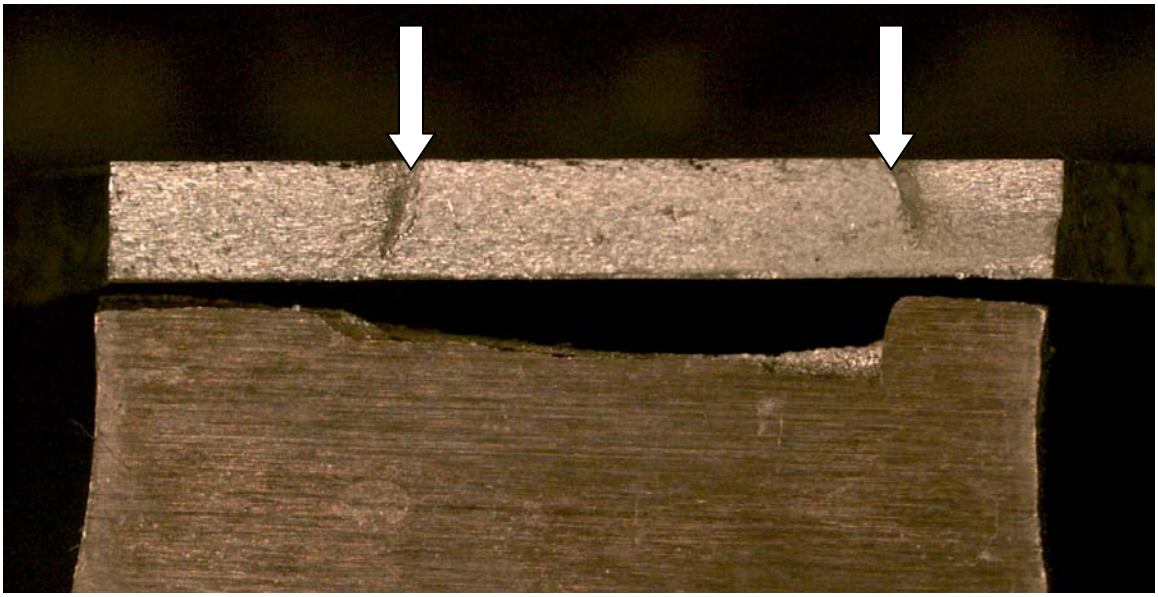

Figure 87 – Specimen 7PH-5, 7075-T6 pre-corroded 15 minutes in a 60/1 ratio of 3.5% NaCl solution to H_2O_2 hydrogen peroxide at 14 mm deflection, Nf = 47,900. Multiple ratchet marks (approximately 4 ea however the 2 obvious are indicated with arrows) can be seen originating at the top (tension) surface – this is greatly reduced from the previous specimens indicating the minimum corrosion pitting value is in close proximity. (photo # PHS-012)

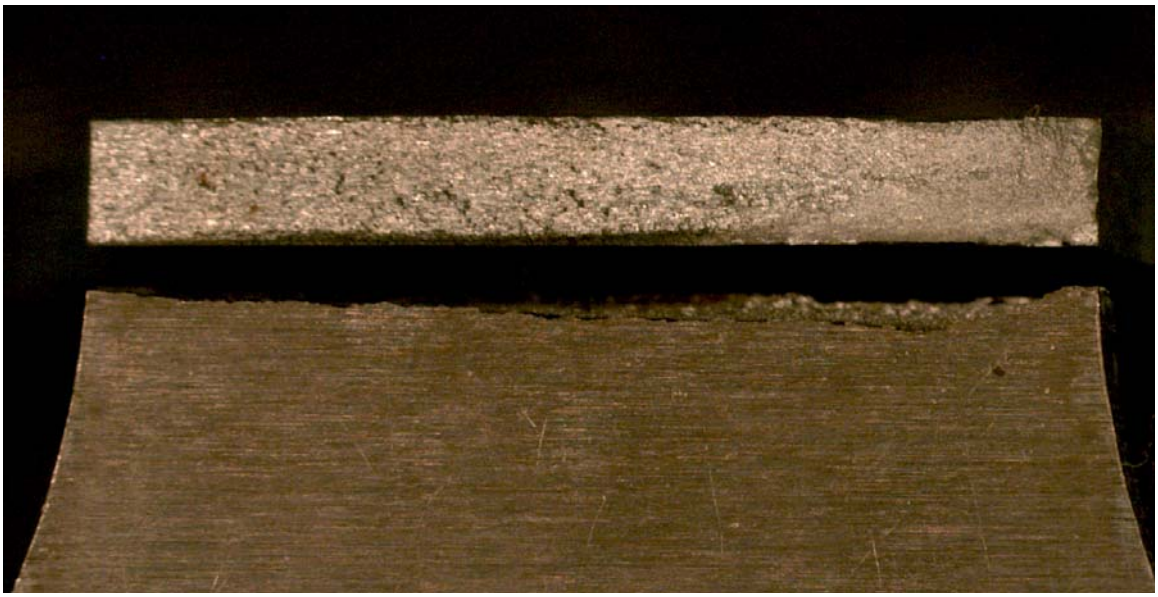

Figure 88 – Specimen 7PH-6, 7075-T6 pre-corroded 30 minutes in a 120/1 ratio of 3.5% NaCl solution to H_2O_2 hydrogen peroxide at 14 mm deflection, Nf = 64,200. No discernable ratchet marks can be seen originating at the expected top (tension) surface – this is greatly reduced from the previous specimens indicating the minimum corrosion pitting value required to generate ratchet marks must be more severe. (photo # PHS-013)

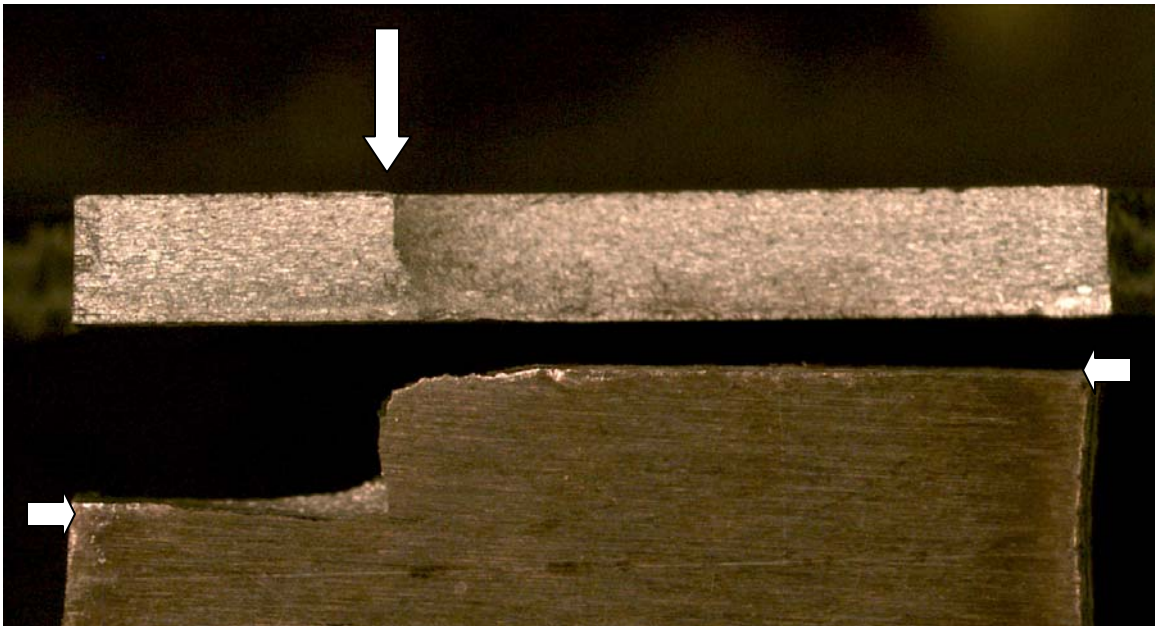

Figure 89 – Specimen 7PH-7, 7075-T6 pre-corroded 240 minutes in a 120/1 ratio of 3.5% NaCl solution to H_2O_2 hydrogen peroxide at 14 mm deflection, Nf = 51,900. Only one ratchet mark is apparent, however, it appears this is a result of cracks originating at each edge and meeting near center at the "ratchet" mark. (photo # PHS-014)

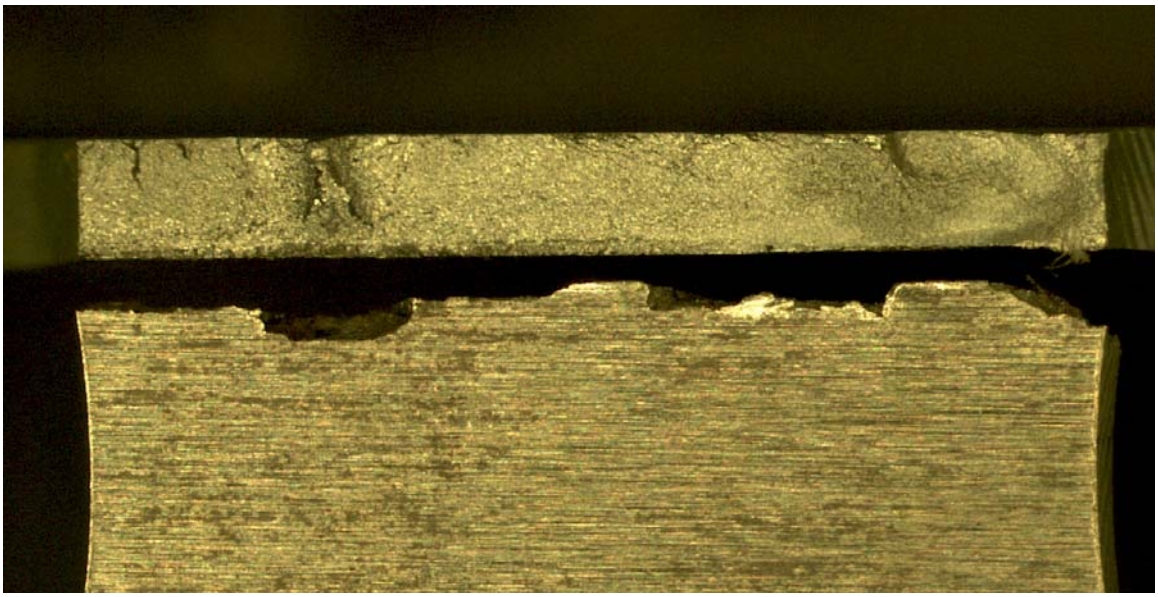

Figure 90 – Specimen 6PH-1, 6061-T6 pre-corroded 90 minutes in a 30/1 ratio of 3.5% NaCl solution to H_2O_2 hydrogen peroxide at 14 mm deflection, Nf = 84,200. Multiple ratchet marks (approximately 10 ea) can be seen originating at the top (tension) surface indicating multiple fatigue crack initiations. (photo # PHS-015)

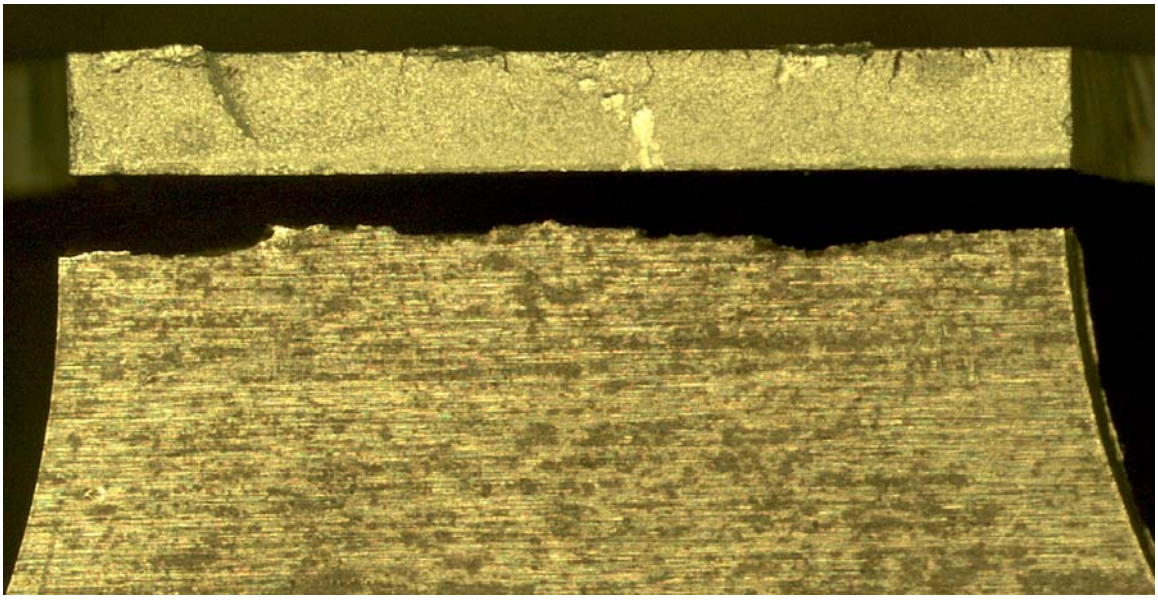

Figure 91 – Specimen 6PH-2, 6061-T6 pre-corroded 120 minutes in a 30/1 ratio of 3.5% NaCl solution to H_2O_2 hydrogen peroxide at 14 mm deflection, Nf = 47,200. Multiple ratchet marks (approximately 11 ea) can be seen originating at the top (tension) surface indicating multiple fatigue crack initiations. (photo # PHS-017)

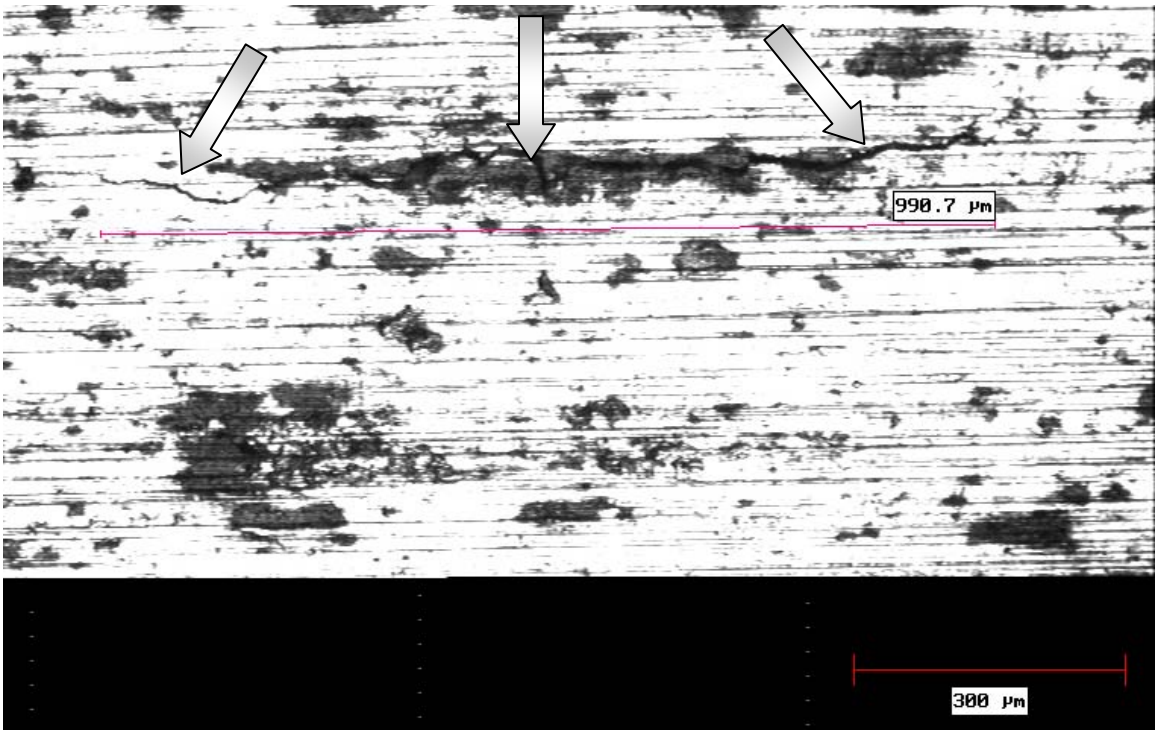

Figure 92 – Specimen 6PH-2, 6061-T6 pre-corroded 120 minutes in a 30/1 ratio of 3.5% NaCl solution to H_2O_2 hydrogen peroxide at 14 mm deflection, Nf = 47,200. An interior crack away from primary fracture surface initiating in a pitted region; again reinforcing the observation that visible corrosion pitting results in crack initiation and a subsequent reduction in N_f. (photo # PH-028)

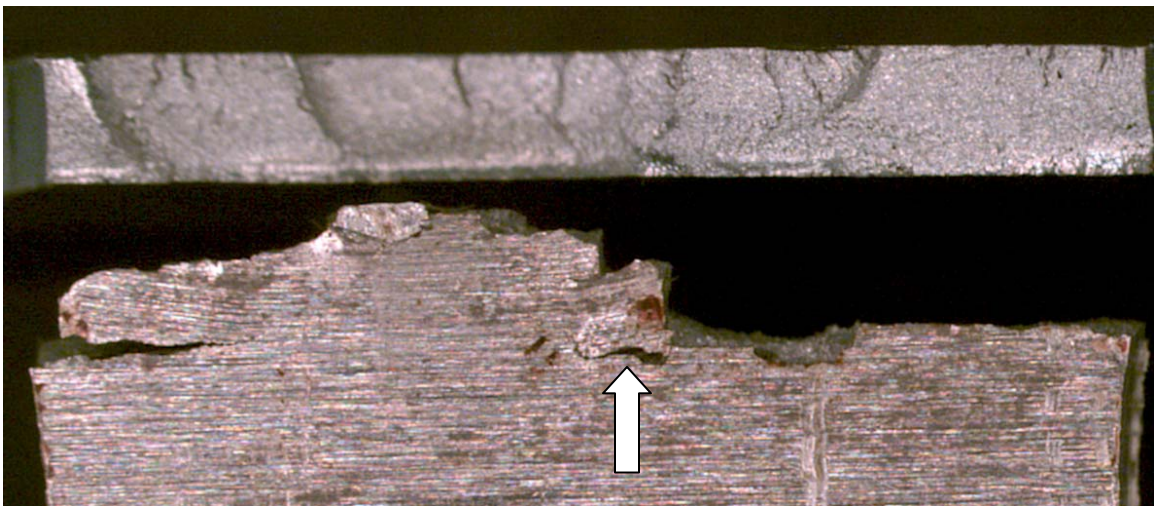

Figure 93 – Specimen 6PH-3, 6061-T6 pre-corroded 30 minutes in a 30/1 ratio of 3.5% NaCl solution to H_2O_2 hydrogen peroxide at 14 mm deflection, Nf = 110,000. Multiple ratchet marks (approximately 15 ea) can be seen originating at the top (tension) surface indicating multiple fatigue crack initiations. Arrow indicates an easily visible secondary crack. (photo # PHS-016)

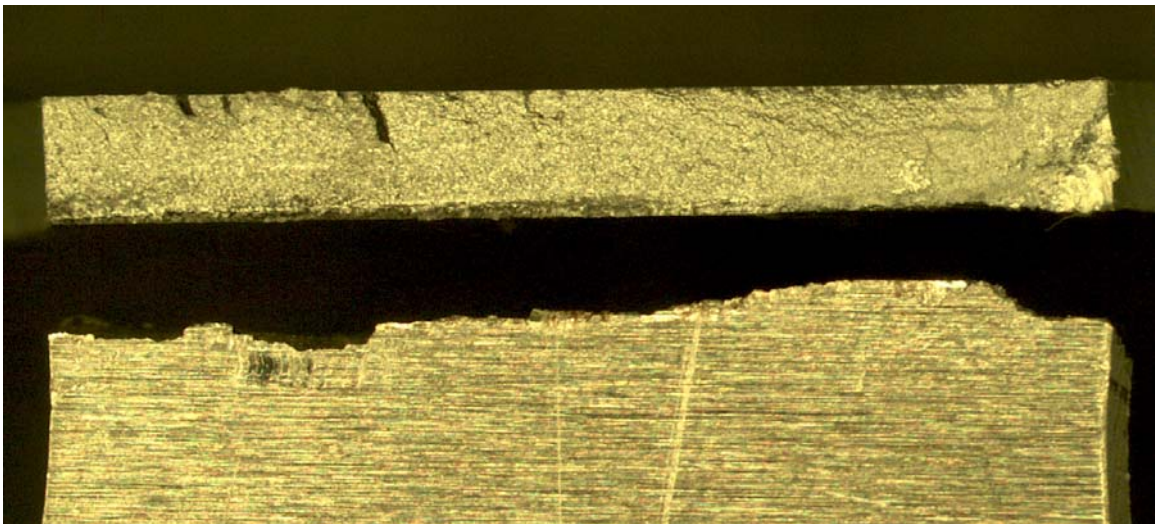

Figure 94 – Specimen 6PH-4, 6061-T6 pre-corroded 15 minutes in a 30/1 ratio of 3.5% NaCl solution to H_2O_2 hydrogen peroxide at 14 mm deflection, Nf = 76,500. Multiple ratchet marks (approximately 7 ea) can be seen originating at the top (tension) surface indicating multiple fatigue crack initiations. (photo # PHS-018)

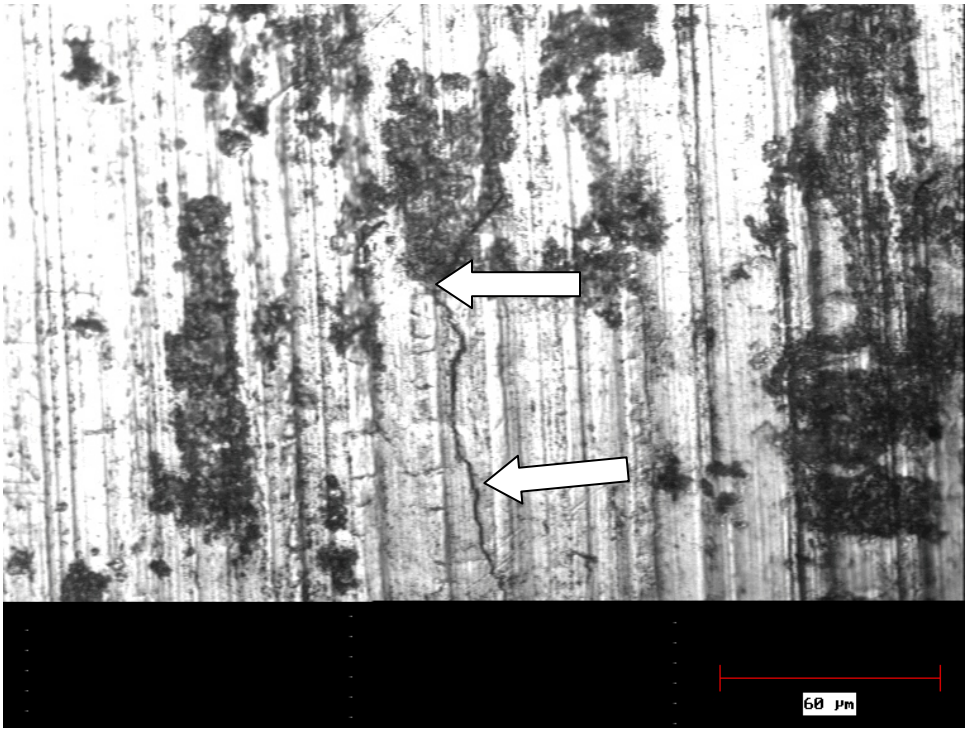

Figure 95 – Specimen 6PH-4, 6061-T6 pre-corroded 15 minutes in a 30/1 ratio of 3.5% NaCl solution to H_2O_2 hydrogen peroxide at 14 mm deflection, Nf = 76,500. Crack can be seen running through corrosion pits away from primary fracture surface. (photo # PH-030)

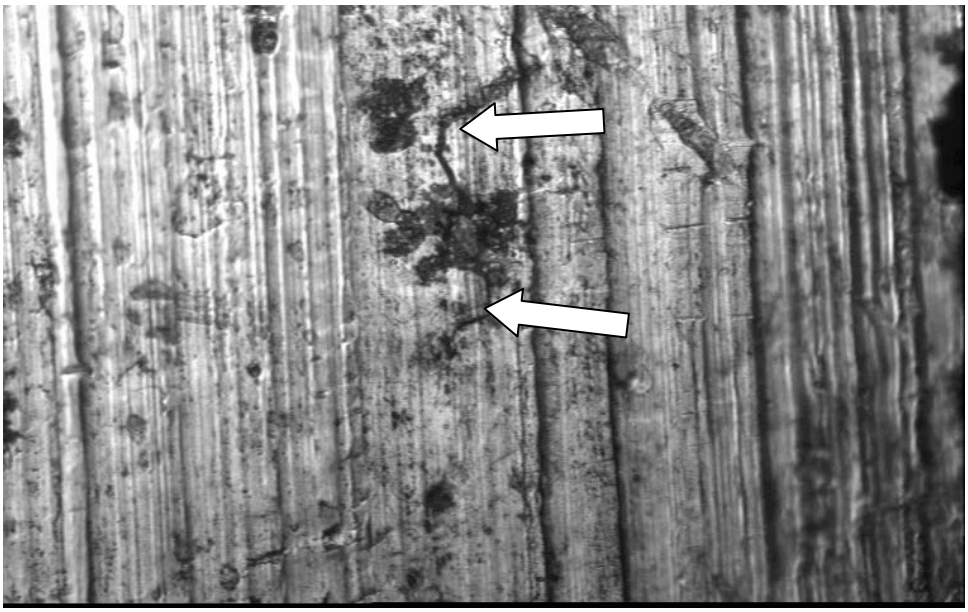

Figure 96 – Specimen 6PH-4, 6061-T6 pre-corroded 15 minutes in a 30/1 ratio of 3.5% NaCl solution to H_2O_2 hydrogen peroxide at 14 mm deflection, Nf = 76,500. Crack can be seen here beginning to initiate at a corrosion pit away from primary fracture surface; ample corrosion pitting is present in order to initiate secondary cracking as seen by ratchet marks in Figure 42. (photo # PH-031)

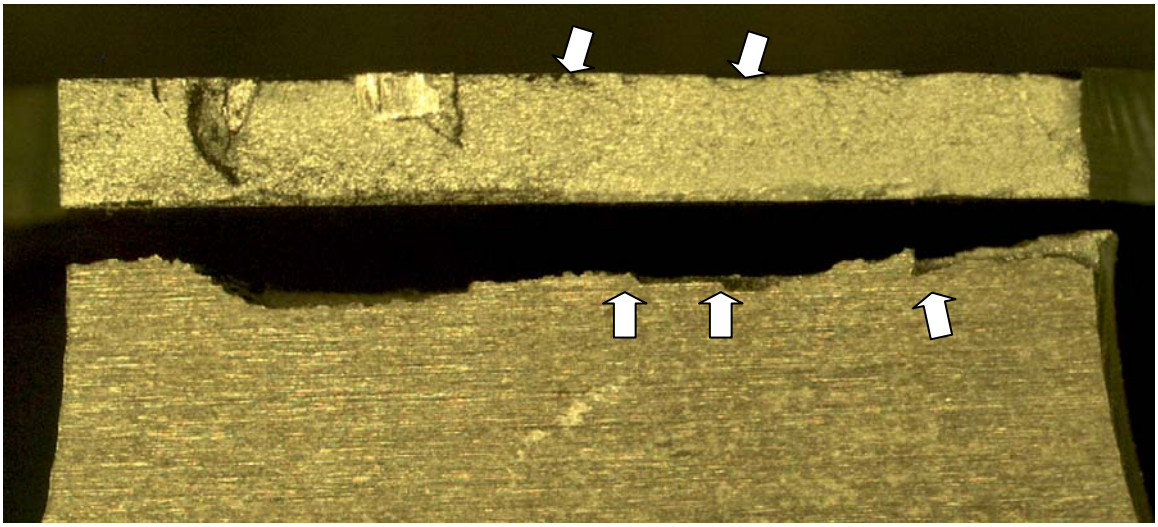

Figure 97 – Specimen 2PH-1, 2024-T3 pre-corroded 5 minutes in a 30/1 ratio of 3.5% NaCl solution to H_2O_2 hydrogen peroxide at 14 mm deflection, Nf = 128,600. Multiple ratchet marks (approximately 16 ea), most of them shallow, can be seen originating at the top (tension) surface indicating multiple fatigue crack initiations. The shallowness of the ratchet marks is a good indicator the degree of pitting is near a minimum. (photo # PHS-019)

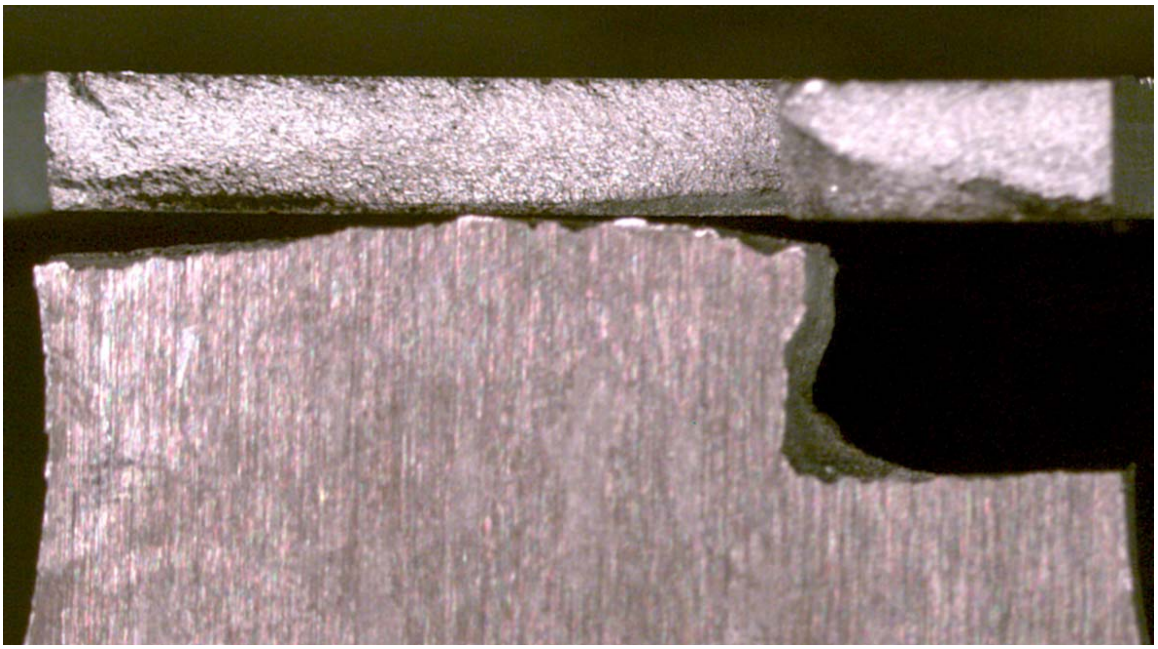

Figure 98 – Specimen LPH-1, 2024-T3 laser cut pre-corroded 15 minutes in a 30/1 ratio of 3.5% NaCl solution to H_2O_2 hydrogen peroxide at 14 mm deflection, Nf = 114,500. Possibly several small ratchet marks but main impression of this failure is that of two offset edge cracks that jogged near center to meet and complete the fracture surface. (photo # LPHS-002)

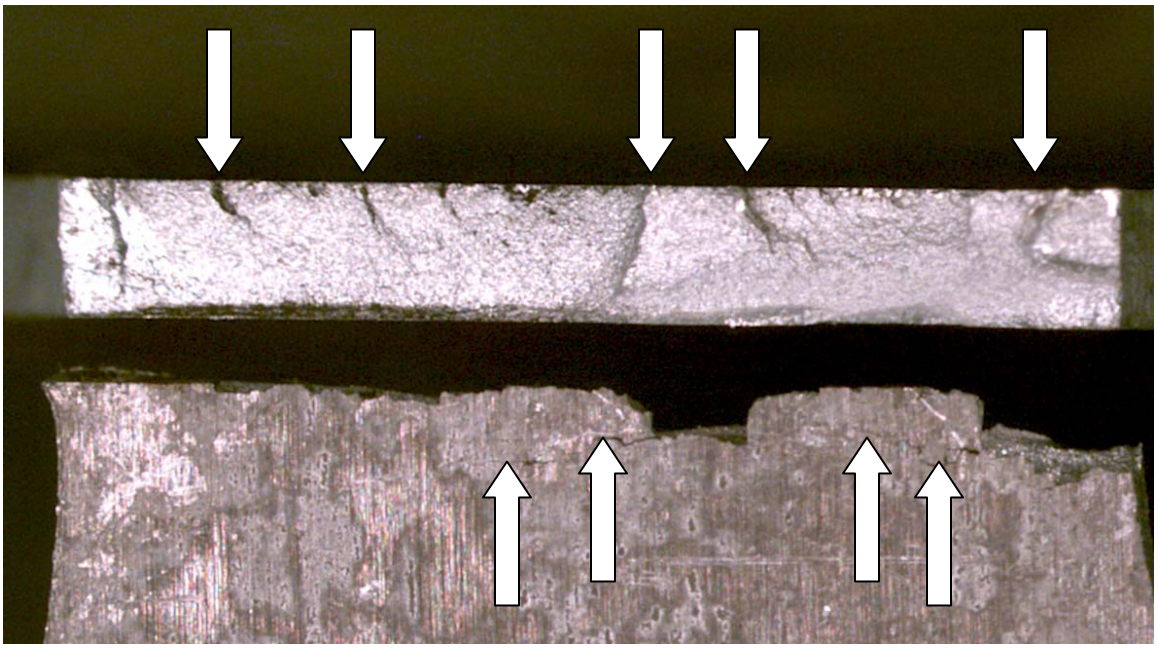

Figure 99 – Specimen LPH-2, 2024-T3 laser cut pre-corroded 70 minutes in a 30/1 ratio of 3.5% NaCl solution to H_2O_2 hydrogen peroxide at 14 mm deflection, Nf = 73,200. Multiple ratchet marks (approximately 14 ea) can be seen originating at the top (tension) surface indicating multiple fatigue crack initiations. Several cracks initiating from corrosion pits also observed running basically parallel to the primary fracture surface (lower section). (photo # LPHS-003)

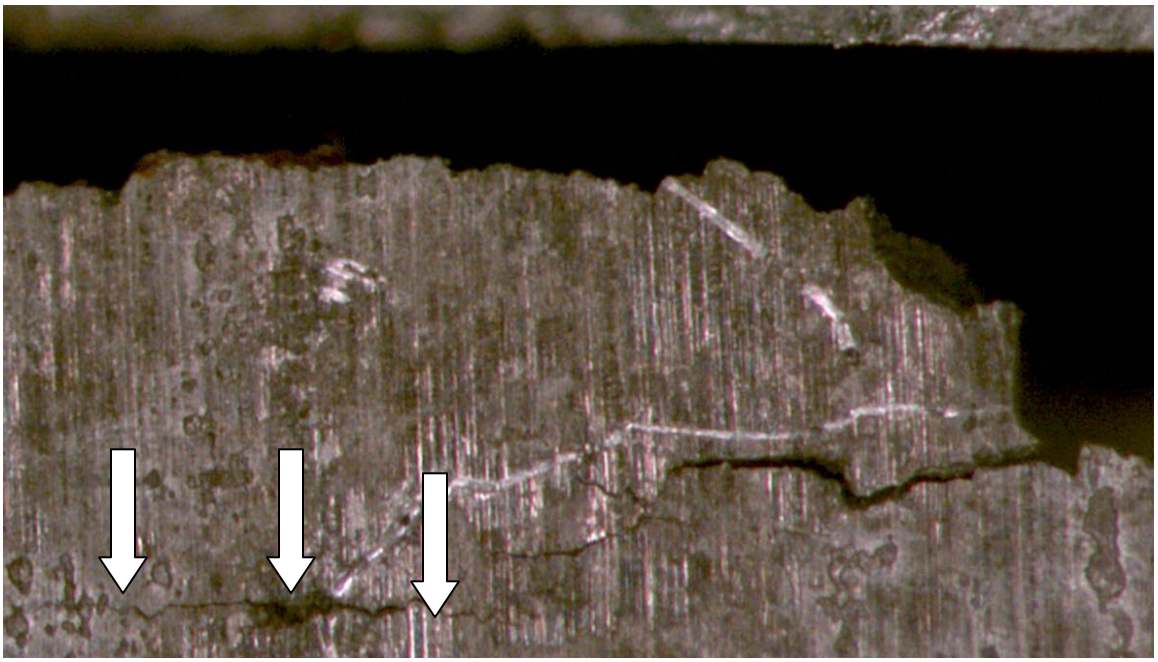

Figure 100 – Specimen LPH-2, 2024-T3 laser cut pre-corroded 70 minutes in a 30/1 ratio of 3.5% NaCl solution to H_2O_2 hydrogen peroxide at 14 mm deflection, Nf = 73,200. Closer view (50x) of secondary cracks, noted in Figure x above, running parallel to primary fracture surface – arrows indicate another fatigue crack traversing left and right from a pit (center arrow); crack has not yet linked to the larger crack at right. (photo # LPHS-004)

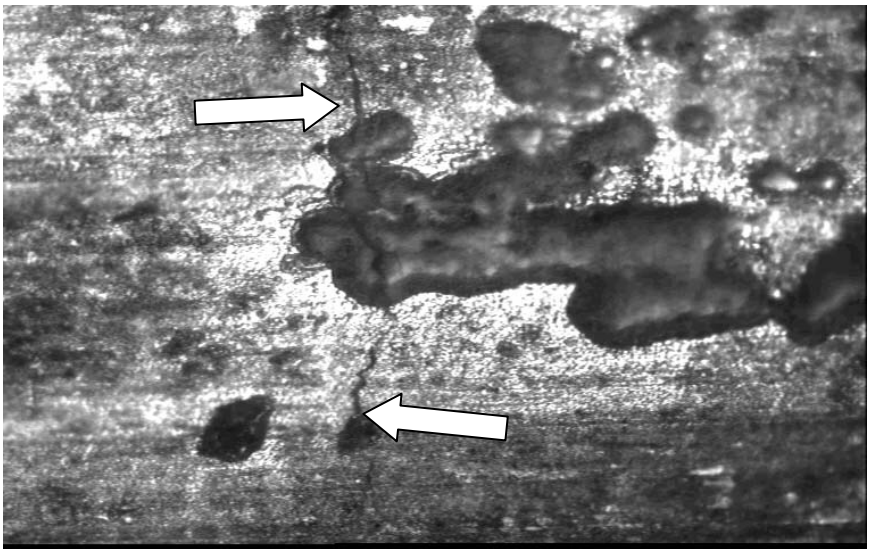

Figure 101 – Specimen LPH-2, 2024-T3 laser cut pre-corroded 70 minutes in a 30/1 ratio of 3.5% NaCl solution to H_2O_2 hydrogen peroxide at 14 mm deflection, Nf = 73,200. Crack shown (500x) originates from 4-5 μm corrosion pits well away from edges. (photo # PH-033)

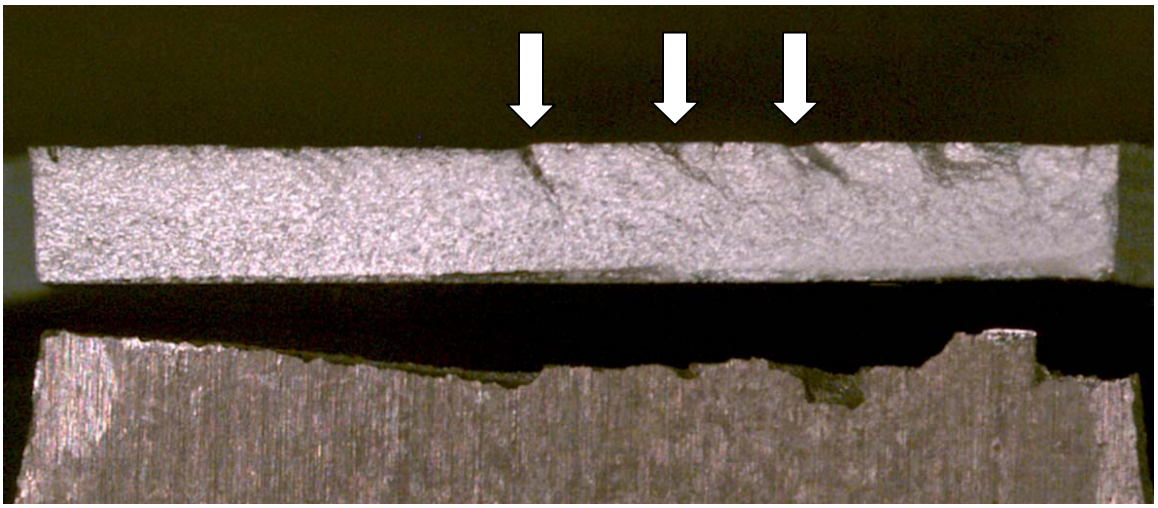

Figure 102 – Specimen LPH-3, 2024-T3 laser cut pre-corroded 45 minutes in a 30/1 ratio of 3.5% NaCl solution to H_2O_2 hydrogen peroxide at 14 mm deflection, Nf = 86,200. Multiple ratchet marks (approximately 10 ea) can be seen originating at the top (tension) surface indicating multiple fatigue crack initiations. (photo # LPHS-006)

Figure 103 – Specimen LPH-4, 2024-T3 laser cut pre-corroded 10 minutes in a 30/1 ratio of 3.5% NaCl solution to H_2O_2 hydrogen peroxide at 14 mm deflection, Nf = 73,200. Multiple ratchet marks (approximately 23 ea) can be seen originating at the top (tension) surface indicating multiple fatigue crack initiations – ratchet marks penetrate the surface about 1/3 -1/2 of thickness. One crack noted originating at the right-hand edge. (photo # LPHS-007)

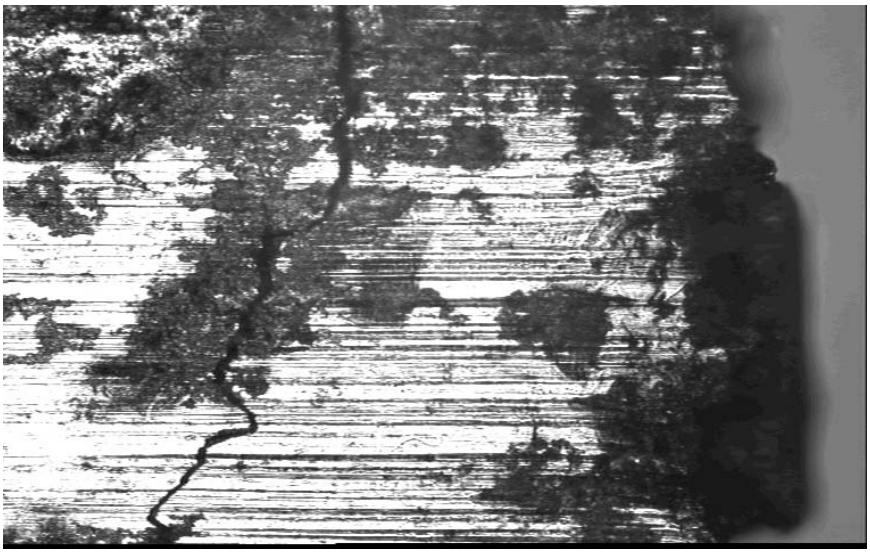

Figure 104 – Specimen LPH-4, 2024-T3 laser cut pre-corroded 10 minutes in a 30/1 ratio of 3.5% NaCl solution to H_2O_2 hydrogen peroxide at 14 mm deflection, Nf = 82,000. Closer view (200x) of surface near fracture zone of Figure x above – a crack parallel to the fracture surface can easily be seen linking fields. (photo # LPH-009)

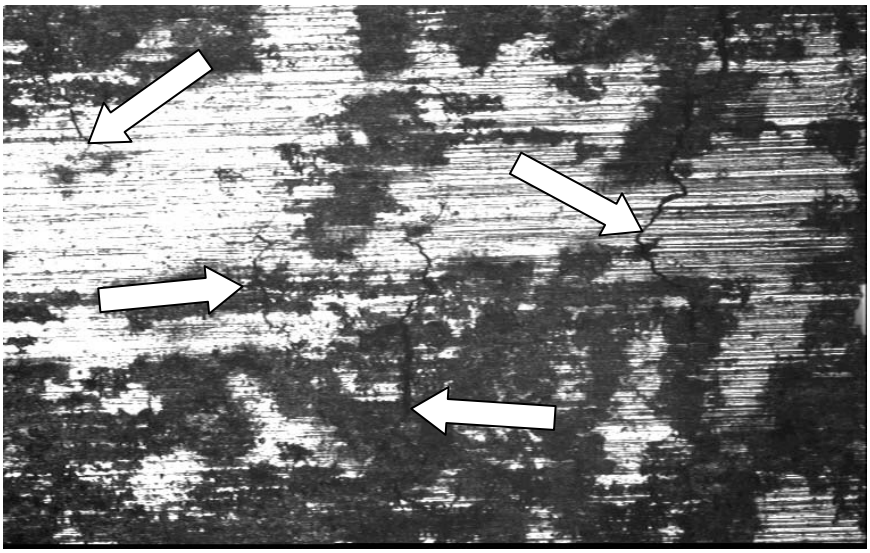

Figure 105 – Specimen LPH-4, 2024-T3 laser cut pre-corroded 10 minutes in a 30/1 ratio of 3.5% NaCl solution to H_2O_2 hydrogen peroxide at 14 mm deflection, Nf = 82,000. Closer view (100x) of surface near fracture zone of Figure x above – at least 4 separate cracks can easily be seen originating from corrosion pits well away from edges, strongly supporting the evidence of transition of fatigue crack origination away from edges to corrosion pits within the high stress zone. (photo # LPH-010)

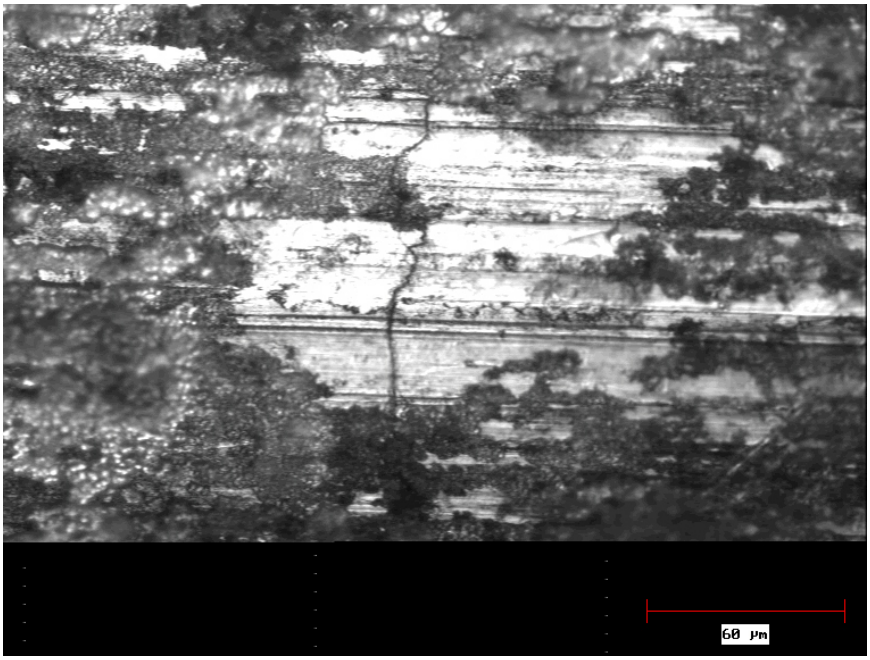

Figure 106 – Specimen LPH-4, 2024-T3 laser cut pre-corroded 10 minutes in a 30/1 ratio of 3.5% NaCl solution to H_2O_2 hydrogen peroxide at 14 mm deflection, Nf = 82,000. Cracking away from primary fracture surface (500x) – crack originates from a 4 µm deep corrosion pit well away from edges and propagates toward other pits. (photo # PH-034)

Figure 107 – Specimen LPH-5, 2024-T3 laser cut pre-corroded 5 minutes in a 30/1 ratio of 3.5% NaCl solution to H_2O_2 hydrogen peroxide at 14 mm deflection, Nf = 114,900. Multiple ratchet marks (approximately 24 ea) can be seen originating at the top (tension) surface indicating multiple fatigue crack initiations – ratchet marks are relatively shallow and penetrate vertically into the surface less than about 1/4 of thickness on average. Two cracks noted by arrow, originating at the right-hand edge. (photo # LPHS-009

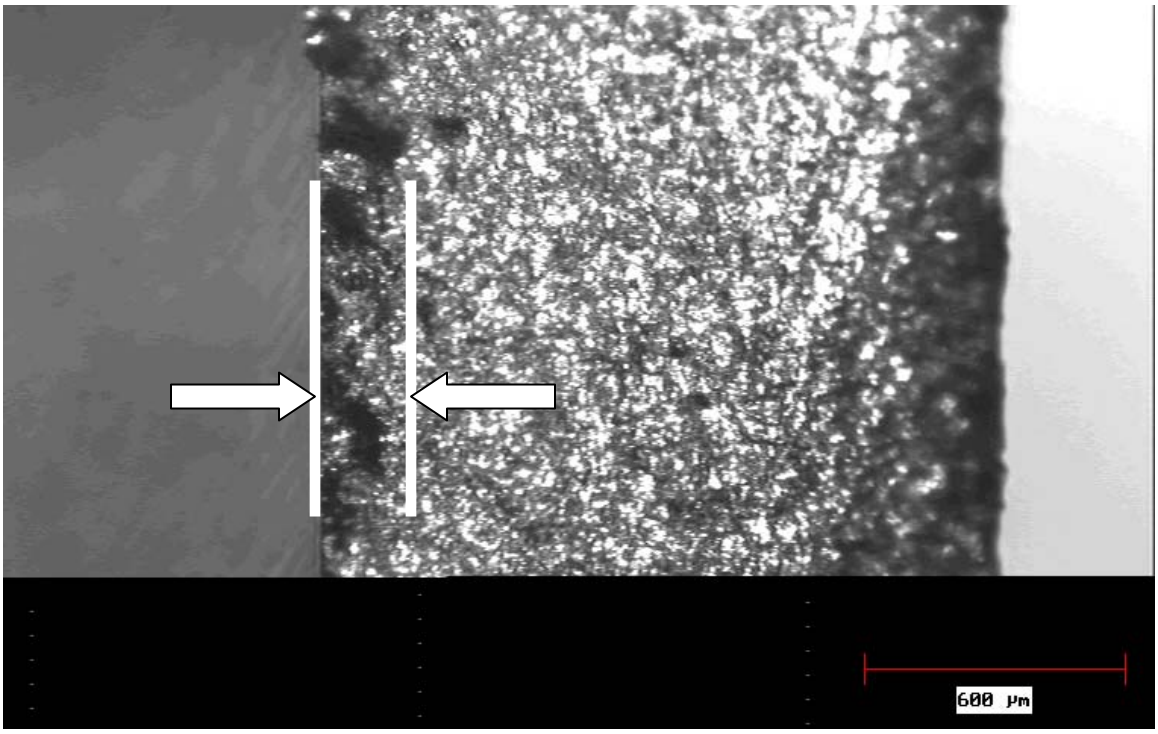

Figure 108 – Specimen LPH-5, 2024-T3 laser cut pre-corroded 5 minutes in a 30/1 ratio of 3.5% NaCl solution to H_2O_2 hydrogen peroxide at 14 mm deflection, Nf = 114,900. Close-up (50x) of several ratchet marks seen in Figure x above - ratchet marks can be seen originating at the left-hand (tension) surface; each indicating multiple fatigue crack initiations. Ratchet marks are relatively shallow and penetrate, as seen here, vertically into the surface only about 10% of the thickness. (photo # LPHS-014)

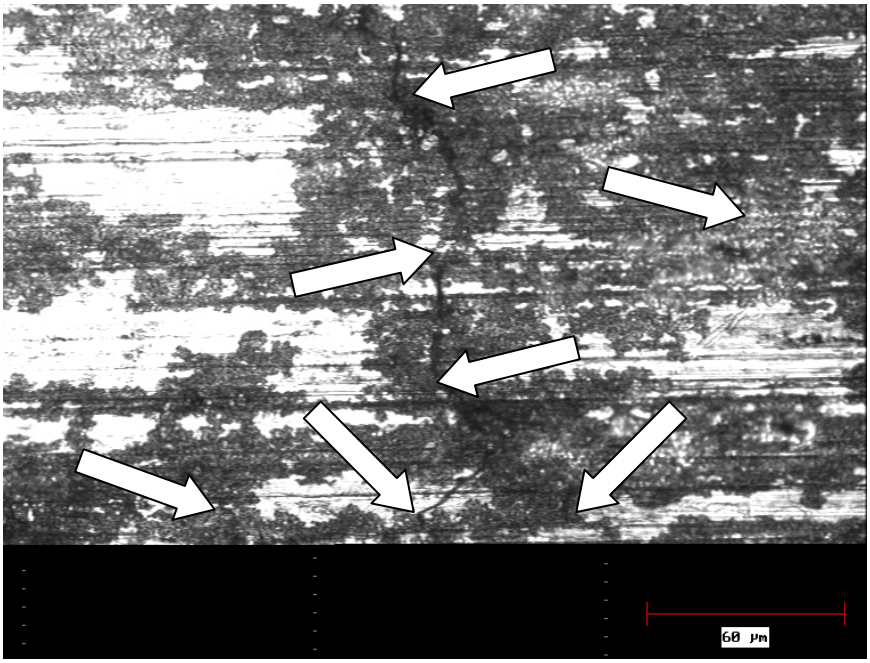

Figure 109 – Specimen LPH-5, 2024-T3 laser cut pre-corroded 5 minutes in a 30/1 ratio of 3.5% NaCl solution to H_2O_2 hydrogen peroxide at 14 mm deflection, Nf = 114,900. Close-up (500x) of several cracks originating from pits away from the primary fracture surface. (photo # LPHS-013)

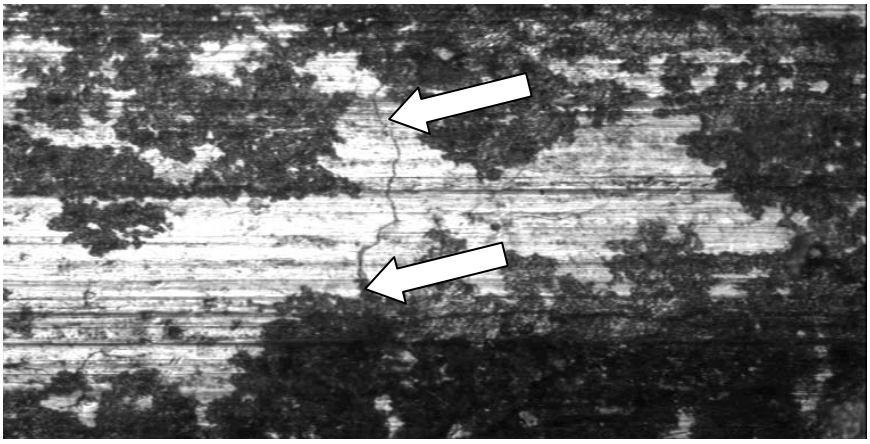

Figure 110 – Specimen LPH-5, 2024-T3 laser cut pre-corroded 5 minutes in a 30/1 ratio of 3.5% NaCl solution to H_2O_2 hydrogen peroxide at 14 mm deflection, Nf = 114,900. Close-up (500x) of another crack originating from pit fields away from the primary fracture surface; average pit depth this photo approximately 2 µm. (photo # PH-035)

4.13 – Pit Depth Determination

The specimens were microscopically inspected, post failure, and measured for pit depth. The depth measurements were obtained with the metallurgical microscope using the focal difference technique from ASTM G-46. Pit depths were randomly measured in about 5-10 locations throughout the corroded zone then averaged. The maximum depth corresponds to the deepest pit noted during the microscopic survey. Table 14 displays the measured pitting depth values recorded. The deeper pits appeared to be in and/or around material inclusions.

Table 14 – Measured Pit Depths of Failed Specimens

Spec. No.	Pit Range, µm	Ave Pit Depth, µm	Rounded Ave Pit Depth, µm	Max Pit Depth, µm
2PH-1	2-3	2.5	3	8
7PH-1	3-6	4.5	5	14
7PH-2	2-5	3.5	4	7
7PH-3	2-4	3	3	7
7PH-4	2-5	3.5	4	7
7PH-5	2-3	2.5	3	9
7PH-6	1-2	1.5	2	4
7PH-7	1-2	1.5	2	7
6PH-1	2-4	3	3	4
6PH-2	2-4	3	3	6
6PH-3	2-3	1.5	2	8
6PH-4	1-2	1.5	2	3
LPH-1	1-2	1.5	2	5
LPH-2	2-5	3.5	4	12
LPH-3	2-4	3	3	4
LPH-4	2-5	3.5	4	6
LPH-5	1-3	2	2	3

CHAPTER 5

DISCUSSION

5.1 – Corrosion

The fatigue loading in this study was accomplished in on-way bending which is judged to be more indicative of actual aircraft loading which is mostly flexing and bending vice a straight tensile type pulling load. The corrosive damage inflicted on test specimens was designed to be similar in nature to that actually achieved in a natural operational environment seen by an average aircraft; whether exposed to the routine humidity and rain of inland locations or the harsh ocean side proximities. The corrosion test coupons corresponded very well to the degrees of expected “natural” corrosion as can

be seen in Figure 111 showing an actual corroded 2024-T3 aircraft component compared to a test coupon done in this study. The pitting pattern is similar in appearance although the time to achieve the damage was 25-30 years for the typical operational exposure seen by JSTARS and only 30 minutes for the test coupon using the hydrogen peroxide accelerant. Even though the methods and times for the corrosion to occur differ greatly the end result of degree of pitting is roughly equivalent and is judged to be a suitable method to inflect corrosion damage for concise fatigue studies such as this.

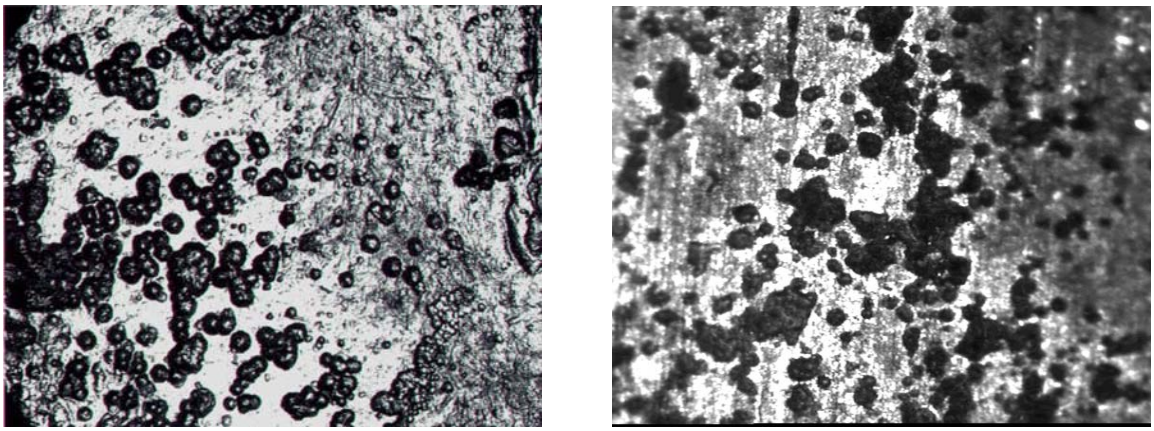

(a) E-8C JSTARS fuselage panel (b) Test coupon from this study

Figure 111 – Comparison of actual pitting with test coupons; (a) pits around a rivet hole in a 2024-T3 fuselage panel from a JSTARS aircraft, pit depth range 5-20 μm (0.0002 - 0.00078 inches) [46]; (b) 2024-T3 test coupon from this study, 50/1 ratio of NaCl solution to H_2O_2 for 30 min; pit depths about 2-4 μm (0.00008 - 0.00016 inches).

The corrosion produced by using H_2O_2 in conjunction with the 3.5% NaCl solution was much more effective in producing pits of a visually definable magnitude, that were readily distinguishable using only the metallurgical microscope. The pre-corrosion method using a 30/1 ratio of 3.5% NaCl to H_2O_2 proved to be adequate in

producing light to moderate pitting quickly, if exposure time was closely monitored to prevent excessive corrosion.

Table 1 listed the values of alloy compositions; of note are the ranges of the non-primary elements such as Si and Fe, found in 2024 and 7075. These values have a spread ranging from 0.0% to about 0.5% maximum. The strength properties of alloys can be dependent on these "debris" elements. As can be seen in Figure 112, for example, the spread of the fatigue life of 7075-T6 can be as much as 10^2. A major contributor of this spread is possibly dependent on the stated allowable ranges of these elements. For instance, Si and Fe have been shown to reduce the fracture toughness in Al alloys. The hardening components of the alloys are submicron size; however the constituents, previously mentioned in Chapter 2.1 (i.e.: Mg_2Si, Al_7Cu_2Fe), can be relatively large (2-50 μm) and provide no appreciable strengthening benefits; only probable sites for premature crack formation [32].

The mechanism of corrosion pitting is a combination of breakdown of the protective oxide layer on the surface of aluminum alloys by chlorides [20] but is more specifically the result of the dissimilarity of the constituents and the aluminum matrix. When exposing this situation to an electrolyte such as NaCl, galvanic corrosive attack results and corrosion pits are formed. There is variation within the literature in the exact composition of the constituents, for example Mg_2Si, Al_2CuMg, $Al_{23}CuFe_4$, but the theme is the same; dissimilar materials resulting in galvanic attack in the presence of an electrolytic corrosive solution such as NaCl. As seen in this study and by others [31, 62] these pits tend to coalesce along the rolled direction in aluminum sheet stock and that

when pits were present, fatigue cracks always initiated at the pits but in the absence of pits, cracks would initiate at large inclusions.

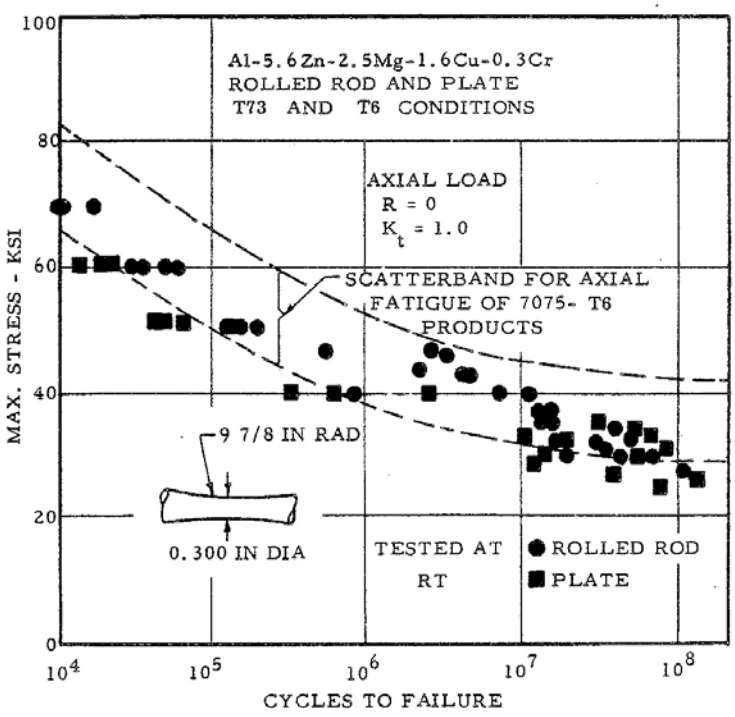

Figure 112 – 7075 Cycles to Failure [39]. Note wide band of N_f values; spread range is 10^1 to 10^2

Another observation noted in corroding the specimens was that the often corrosion magnitude varied significantly from the top surfaces to the bottom, likely due to the quantities of these constituents present. This represents an interesting concept of the possibility of performance properties of sheet alloys being orientation dependent; that is since fatigue life is strongly influenced by pitting (as well as larger inclusions) it serves to reason that higher concentrations of constituents on a tension surface may ultimately result in a fatigue life shorter than it would be if the installation of the structural member

was inverted (in compression). Additional experiments would need to be run to explore this possibility further.

5.2 – Depth of Pitting

The pit depth equation, $\mathbf{d = kt^{1/3}}$ where d is the depth (μm), t is time (minutes) and **k** (μm/min$^{1/3}$) is based on the material properties and corrosive environment [31, 48]. The values of **k** are calculated for the alloys in this study and are shown in Table 15. The calculation was based on pit depth and exposure time data from the pre-corrosion specimens, corroded at the ratio of 30/1 of 3.5% NaCl solution to H_2O_2. Some error

Table 15 – Pit Depth Equation **k** Values using a 30/1 ratio of 3.5% NaCl to H_2O_2

Alloy	k (ave)
2024-T3	1.46
2024-T3 Laser Cut	1.02
6061-T6	0.67
7075-T6	1.28

could be introduced in these numbers due the aforementioned fact that the hydrogen peroxide solution will go "stale" after a time [66]; for example, there should not be an appreciable difference in 2024-T3 and 2024-T3 LC since they are the same basic material except for method of fabrication. It was not recorded exactly when batches were mixed since the goal was to produce pits of suitable depth, generally irrelevant to the exposure time required. If calculated constants in the pitting depth equation are to be done accurately, fresh solution should be made up before each test session. However, the

lower k-value of 6061-T6 is somewhat anticipated since this alloy has excellent corrosion resistance in general, as compared to 2xxx and 7xxx series aluminums, especially relating to pitting in seawater [31, 39].

All the alloys tested exhibited a difference in corrosion rate from the top surface of the sheet to the bottom. The most pronounced difference was from 6061-T6 but followed closely in contrast was 7075-T6. the lesser of the 3-alloys tested was 2024-T3 which did display a difference in corrosion rate from one side to the other but in the accelerated corrosion rate testing using hydrogen peroxide in conjunction with the 3.5% salt solution, the subjective net difference was very minor.

An explanation of a slower pitting rate of 6061-T6 proposed by Minoda and Yoshida [52] and resides in the microstructural differences the noted from the specimen surface to the interior. They noted an equal distribution of Al matrix and Mg_2Si particles throughout the specimen; however, there were precipitant free zones (PFZ) at the surface but not within the material's interior. The PFZ's are less noble than either the Al matrix or Mg_2Si particles, resulting in an initial rapid galvanic pitting but then slowing greatly after penetrating beyond the PFZ influence. It would seem this lowering of the corrosion pitting rate could also be a function of constituent size; which typically ranges from 2-50 μm in diameter [31]. If there happens to be a higher quantity of constituents on the surface as compared to the interior of the material and the sizes of the constituents are near the lower values of the typical size range; then assuming they are anodic, once they have been dissolved away by galvanic reaction the net reaction would slow due to the depletion of the anode. This could explain the initial fast pitting to just a few

micrometers, then slowing considerably thereafter. This is an interesting phenomenon and should be studied further.

5.3 – Fatigue Data

As noted in overwhelming numbers throughout the literature reviewed, the presence of corrosion shortens the fatigue life significantly over that of un-corroded specimens. The degrees of life reduction varied from study to study but the preponderance of evidence reveals the negative influence corrosion inflicts on overall fatigue life and the associated structural integrity.

A recurring characteristic, in the fatigue specimens with pitting, was the presence of ratchet marks on the fracture surface. These marks coincide with the numerous fatigue crack initiation sites on the pitted specimens. The fracture surfaces of the un-corroded specimens were generally flat and smooth and had an obvious omission of these marks. Thus, ratchet marks are a direct indication that multiple cracks have nucleated and serve as a quick visual reference to substantiate the fact for the investigator.

5.3.1 – With only 3.5% NaCl

The appearance of corrosion is a distinct, singular concern in the general fatigue life; however, just operating in a moist, humid, salt laden environment has been shown by researchers to reduce the fatigue life compared to service in dry surroundings [42]. The data from testing performed without hydrogen peroxide generally support this observation as in Figures 113 - 115; in which this negative influence on 2024-T3, 6061-T6 and 7075-T6 can be clearly seen. The amount of corrosion present was negligible

without the H_2O_2 accelerant but the trend shows an obvious decrease in fatigue life of specimens exposed to the 3.5% NaCl solution while in a corroded-during status. Of notice are the 7075-T6 pre-corroded specimens of Figure 115, showing a trend of increased fatigue life over that of pristine. Examination of these pre-corroded specimens revealed essentially no corrosion and in general they appeared to be in pristine condition. No ratchet marks were noted on both the corroded-during or pre-corroded specimens and only one crack producing corrosion pit was noted in all the 2024-T3 and 7075-T6 specimens tested in this non-H_2O_2 regime. As mentioned, the normal spread of fatigue data is fairly wide and thus many more tests would need to be run in order to converge toward a meaningful value; plus without the added component of cyclic stress, the corrosion rate was nonexistent compared to the corroded-during.

Of greater interest though is the observation of 6061-T6 in only the NaCl solution. Higher deflection levels produced secondary/multiple fatigue crack initiation sites in all scenarios: pristine, corrode-during and pre-corroded. This behavior is distinctly different than the other alloys tested. Secondary cracks were noted on the pristine specimen at the 17 mm deflection point and at 16 mm deflection of the corroded-during and pre-corroded specimens. The material breakdown of Table 1 gives possibly some insight as to why the alloy showed multiple crack initiation and the other two alloys did not. The content of Fe (and possibly Si though it is listed as a primary alloying ingredient) are much higher than the other alloys and could result in earlier formation of fatigue cracks due to debris or tramp elements [32].

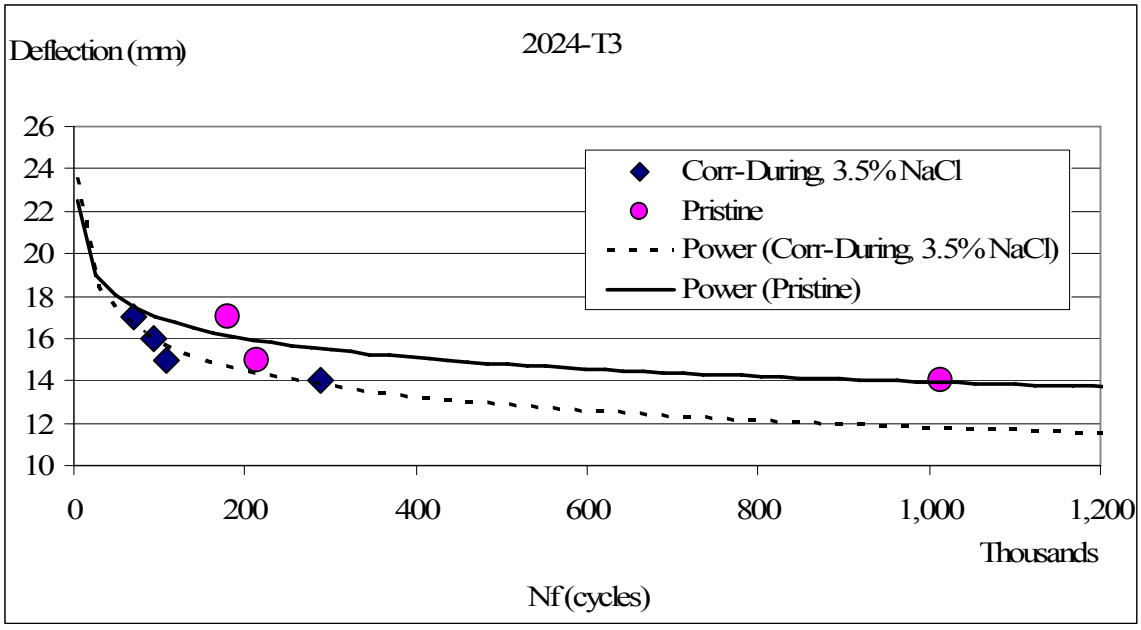

Figure 113 – Fatigue data for 2024-T3 comparing Pristine to Corroded During Cyclic Loading

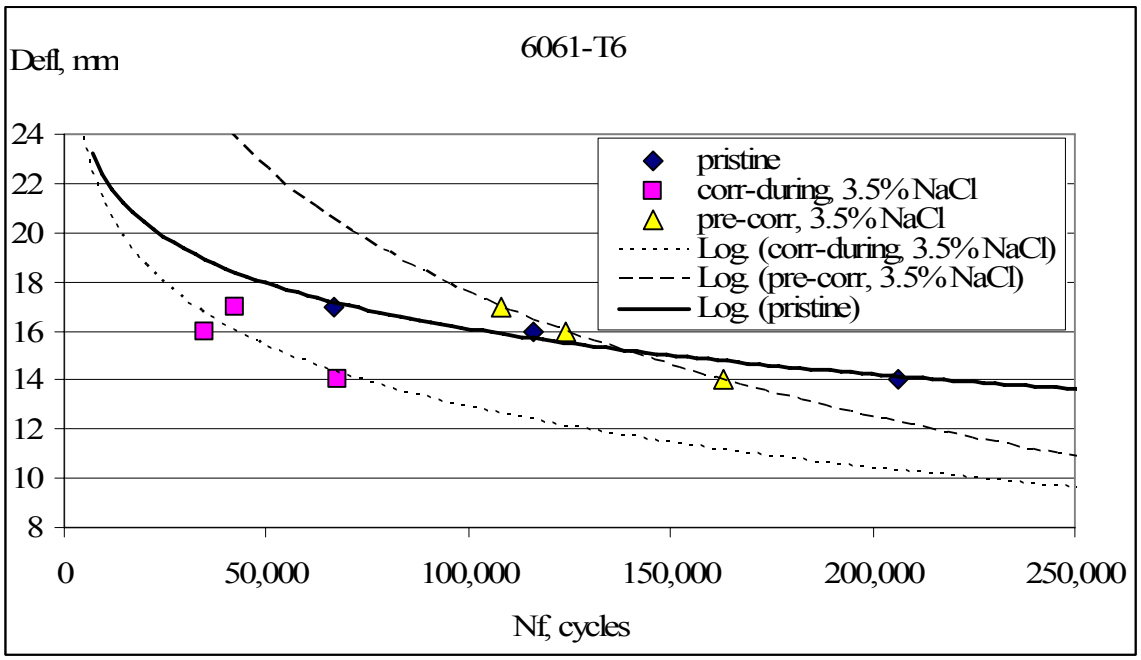

Figure 114 – Fatigue data for 6061-T6 comparing, pristine, corrode-during and pre-corroded

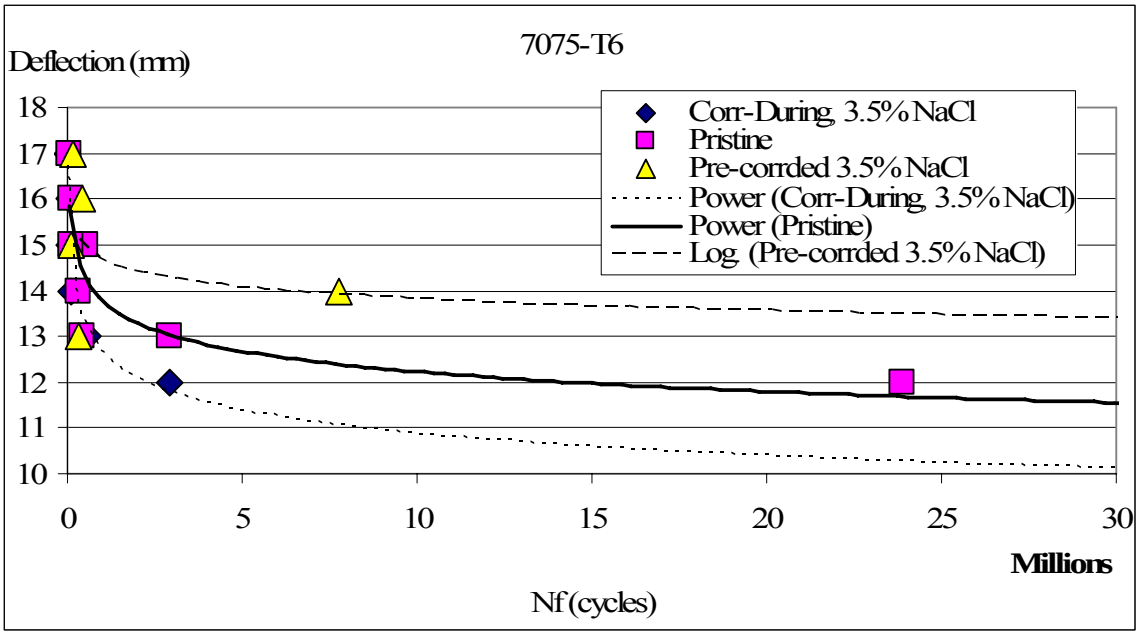

Figure 115 – Fatigue data for 7075-T6 comparing pristine, corrode-during and pre-corroded

5.3.2 – Pitting with 3.5% NaCl and H_2O_2

The overriding theme of this study was the significant reduction in fatigue life of specimens exhibiting even the slightest corrosion. Generally if pitting "penetrated" the surface, fatigue cracks nucleated and premature failures resulted. The pre-corroded specimens were pitted using a 3.5% NaCl solution with a 30/1 ratio of H_2O_2. Figure 116 shows the relationship of lives of specimens, with pre-corrosion pitting, under a 14 mm cyclic loading. The bar graph in Figure 117 illustrates the relative relationship of average pitting depths and the maximum pit depth noted for all alloys tested. The clustering of the average pitting depth values resides around the 2-4 μm range.

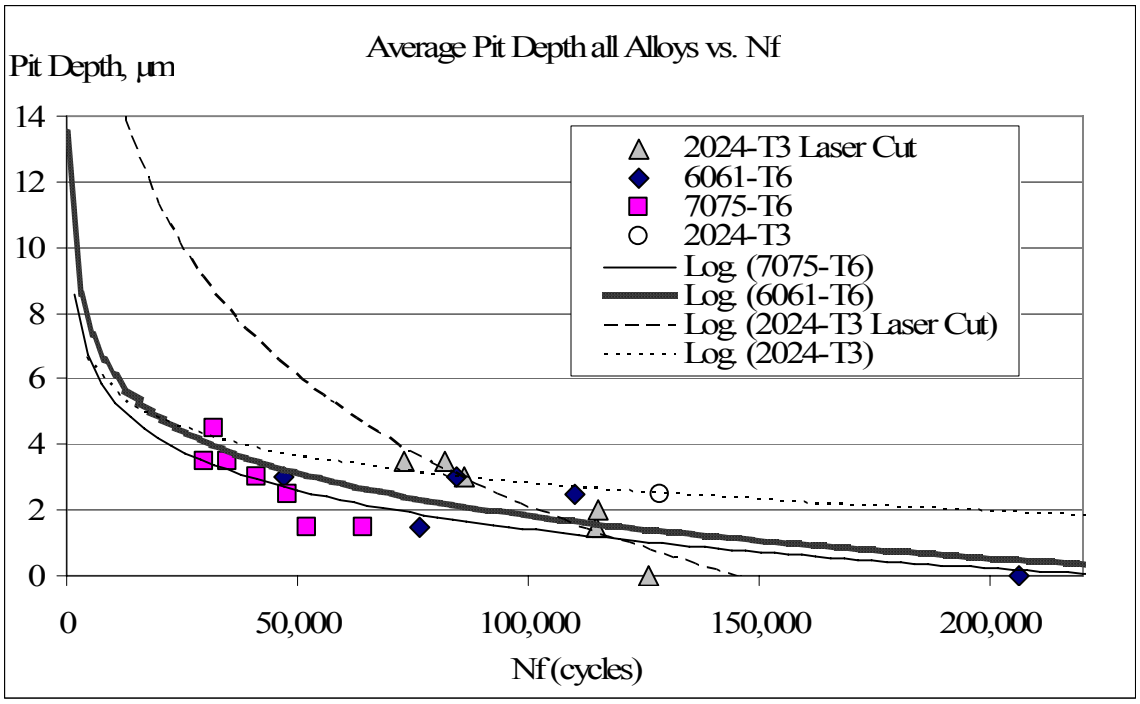

Figure 116 – Average Pit Depth for All Alloys Tested at 14 mm deflection and pre-corroded using 3.5% NaCl with a 30/1 ratio of H_2O_2.

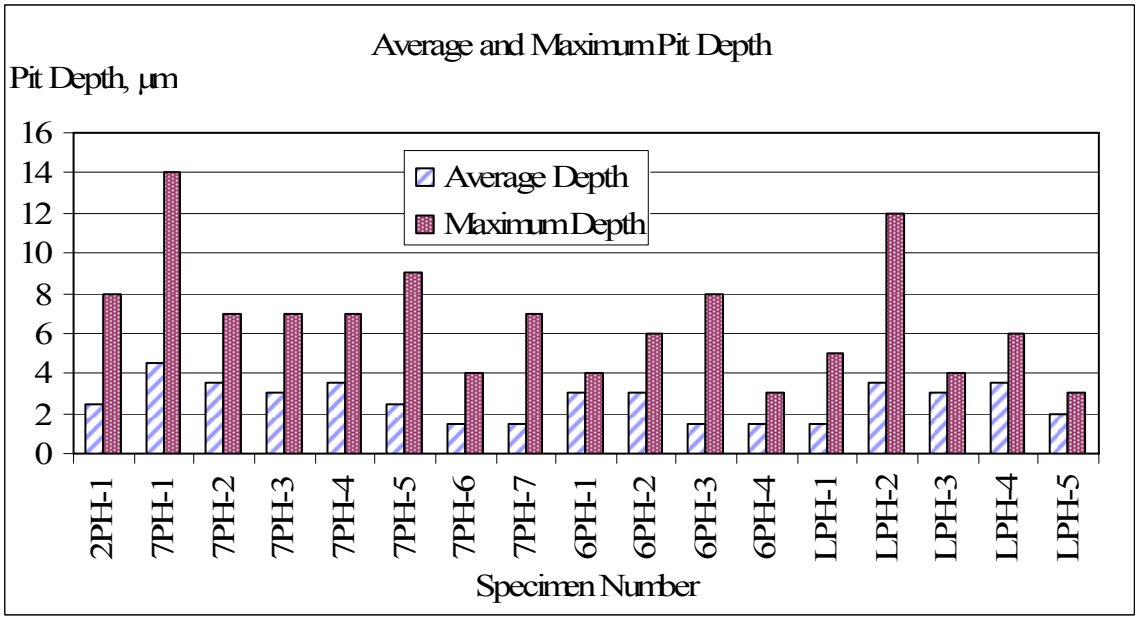

Figure 117 – Average and Maximum Pit Depth. The pit depths were measured for each specimen using the described microscopic methods from ASTM G-46. Pre-corroded using 3.5% NaCl with a 30/1 ratio of H_2O_2. The average depths for pits to cause a significant reduction in fatigue life were in the 2-4 µm range.

A few facts are noted in the preliminary test data of Table 8. Specimens T-1 and T-8 are 2024-T3 corroded-during specimens that are exposed to the same deflection stress but to differing concentration ratios; 15/1 and 40/1 respectively. The concentration is notably lower but the failure cycles are essentially the same indicating once a minimum pitting threshold has been reached the heavier corrosion may not correspond linearly. Tugle {57] noted a similar fact in his study on pre-corroded 7075-T6 sheet; that specimens generally had the same fatigue life regardless of environmental exposure time.

5.4 – Pitting Life Reduction Factor

The modeling of corrosion pitting using a 3.5% NaCl solution with H_2O_2 has been shown to have detrimental affects on the fatigue life of the alloys tested. A typical convention for relaying the loss in fatigue life over that of pristine specimens through a life reduction factor; that is the N_f of the corroded specimens is reduced by a multiple as compared to the pristine N_f. Figure 118 compares all alloys tested, relating average pit depth and the N_f reduction factor (over pristine specimens). An interesting observation is the average pit depths are essentially the same but the reduction in life factors are largely different. The 7075-T6 and 2024-T3 machine cut alloys are about the same; 7.4 and 7.9 respectively. The 2024-T3 laser cut and 6061-T6 machine cut are paired off fairly closely as well; 1.4 and 2.9 respectively.

However the largest contrast of note is between the 2024-T3 machine cut and the 2024-T3 laser cut specimens; the same alloy pitted to about the same depth but varying significantly in the degree of fatigue life reduction. This primary difference in the two is the method of manufacture; machine vs. laser cut. As mentioned previously, it is a fact

that laser cutting results in a significant decrease in fatigue life of these aluminum alloys [24 - 27]. On the other hand, corrosion pitting on its own account is not necessarily significantly detrimental to the fatigue life of the laser cut specimens. The range in test lives of the laser cut 2024-T3 specimens were lessened slightly with increasing exposure time and depth, signifying that slight amounts of corrosion will transition crack initiation away from the edge, to pits.

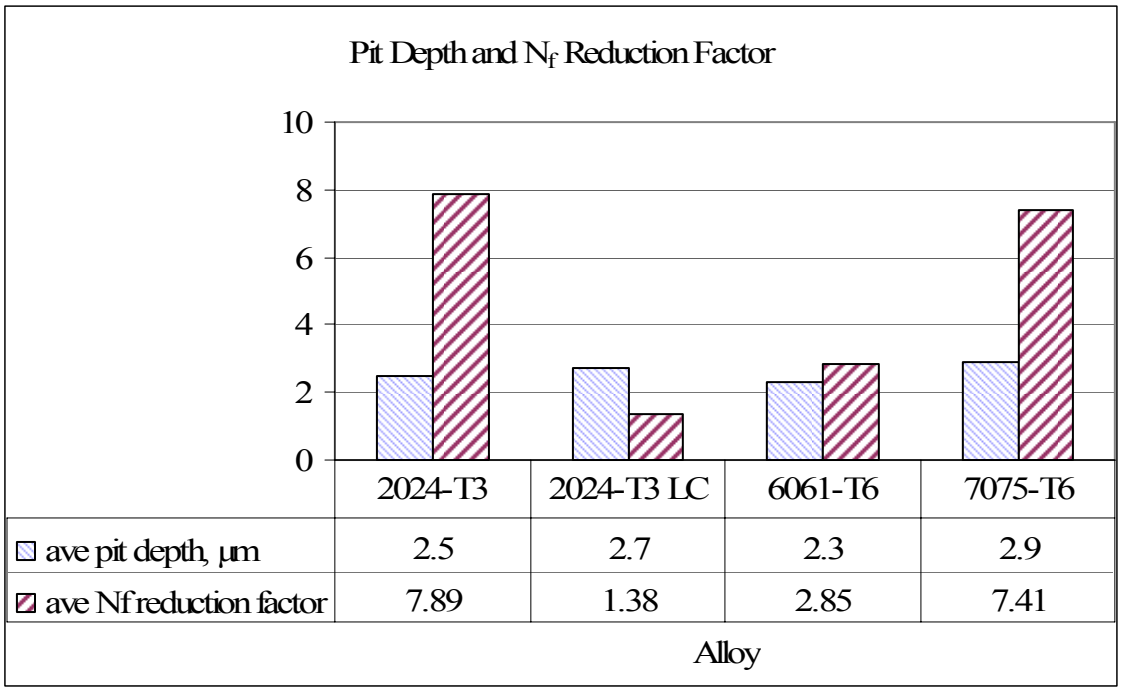

Figure 118 – Average Pit Depth and Fatigue Life Reduction Factors for Pre-Corroded Alloys in 3.5% NaCl and H_2O_2

5.5 – Critical Pit Depth

The pitting depth varied greatly in what most of the literature considered the "critical pit depth". The general definition is the minimum depth that results in the origination of a fatigue crack and subsequent propagation. All prior in-house studies resulted in fatigue cracks originating at the edge of the specimens. Studies like Jones and Hoeppner [28,29] were done using pit depths significantly deeper than those created in this study as did most other researches in the reviewed literature, with numbers generally at least a factor of 10 greater. Jones [30], in another paper, reported the critical pit depth for 7075-T6 to be 20 μm in 1.6 mm thick sheet. Using methods beyond the scope of this study, Nakai et al [54] was able to map out the progression of pit growth, to crack initiation, to crack propagation using atomic force microscopy; their observations were much more in line with the 2-4 μm found in this study. Figure 119 shows a plot of pit-crack growth in 7075-T651 and distinctly reveals a transition from pit growth to crack initiation at about the 2 μm mark. . Also noted was that fatigue cracks did not always initiate at the deepest point in a pit but at a grain boundary within the pit.

The grain sizes revealed by the microstructure photographs of Section 4.x indicated a thickness range of about 5-25 μm for 2024-T3 and 7075-T6 (6061-T6 grain thickness was not determined due to difficulty etching in the T6 temper but it is assumed to be of similar dimensions of the other two alloys). Many of the grains near the surface appeared slightly thinner than the bulk material toward the inner thickness; possibly < 5 μm. The 2-4 μm pit depth dimension is near the thickness value of many of these grains near the surface, thus leading one to the possibility of a direct relationship between the critical pit depth and grain size of the alloy. Based on measurements with the

metallurgical microscopic, the average pit conservatively penetrates the surface of the alloy greater than 50% of the thickness of numerous surface grains. This penetration must assuredly be located within or very near the grain boundary, thus resulting in crack initiation within the grain boundary; this assumption supports the mechanism of crack initiation via intergranular propagation before transitioning to transgranular [43].

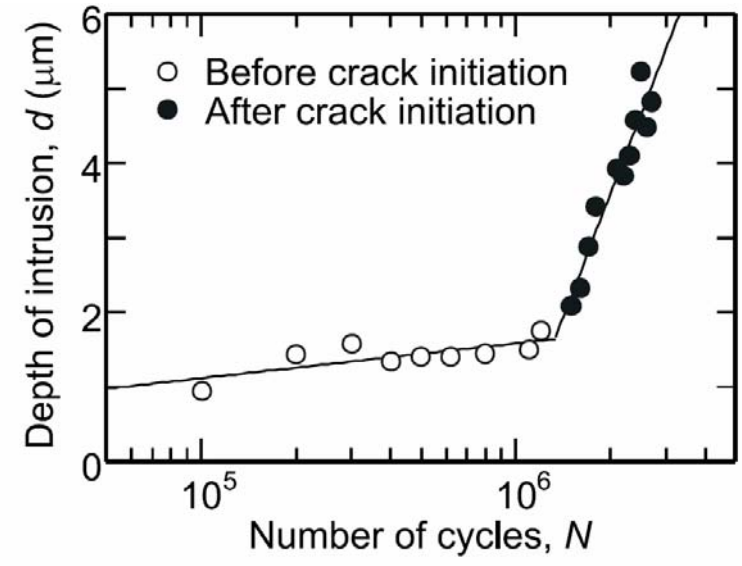

Figure 119 – Depth of corrosion/crack intrusion into the surface of 7075-T651 vs. loading cycles [54]

CHAPTER 6

CONCLUSION

Fatigue testing in an environment mimicking seawater salt concentrations, combined with hydrogen peroxide to accelerate the process, appears to present a reasonable corrosion model for a simulated service environment for aging aircraft. The presence of corrosion pitting, created in this study, significantly reduces the fatigue life over that of pristine un-corroded specimens in the 1.6 mm (0.063 inch) thickness aluminum sheet alloys tested. In the tests performed using the 3.5% salt solution without the hydrogen peroxide accelerant, a general reduction in fatigue life was noted; however, signs of corrosion pitting were non-existent using ordinary visual and microscopic inspection. Several key observations of this study follow:

The critical pit depth required for fatigue crack initiation was 2-4 μm (0.00008 - 0.00016 inches).

The first grain boundary can be only a few micrometers deep and cracks tended to initiate once the pit had penetrated about 50% of the surface grain thickness.

Very useful indicators of fatigue crack initiation are the presence of ratchet marks, which indicate multiple fatigue crack origination sites.

Corrosion pitting reduced the fatigue life of all specimens tested by an average factor of 4.6, as compared to pristine.

The effect on fatigue life by corrosion pits is much less in laser-cut 2024-T3 compared to machine-cut 2024-T3.

The corrosion magnitude often varied significantly from the top surface to the bottom in the aluminum sheet alloys tested; this likely due to the differences in surface chemistry makeup, such as quantities of constituents or inclusions present.

Cyclic loading in the presence of a salt solution environment notably reduces the fatigue life over specimens cycled in dry air, even with no obvious pitting present.

REFERENCES

[1] Gruenberg, K.M., Craig, B.A., Hillbery, B.M., Bucci, R.J., Hinkle, A.J., *Predicting Fatigue Life of Pre-Corroded 2024-T3 Aluminum*, International Journal of Fatigue, 26 (2004), pp 629–640

[2] DuQuesnay, D.L., Underhill, P.R. and Britt, H.J., *Fatigue Crack growth from corrosion damage in 7075-T6511 Aluminum Ally Under Aircraft Loading*, International Journal of Fatigue, Vol 25, (2003), pp 371-377

[3] Aloha Flight 243, Maui HI, National Transportation Safety Board ID: AAR/89-03 (1988)

[4] Firefighting C-130 Wing Separation, National Transportation Safety Board ID: LAX02GA201, (2002)

[5] Miami Flying Boat Accident, National Transportation Safety Board ID: DCA06MA010, (2005)

[6] Seher, C. and Smith, C., *Managing the Aging Aircraft Problem*, The AVT Symposium on Aging Mechanisms and Control, Manchester, England, (2001)

[7] Walker, CA, T-130 Firefighter Aircraft crash, photo, (2002) http://www.wildlandfire.com/pics/air4/air4.htm

[8] Newman, J.A., Piascik, R.S. and Lindenberg R.A. *Failure Analysis of a Helicopter External Fuel-Tank Pylon*, Joint investigation report by Army Research Laboratory, NASA Langley and U.S. Coast Guard, (2002)

[9] KC-135 Corrosion and Service Life Report, KC-135 Program Office, Oklahoma City Air Logistics Center, (2003)

[10] Fry, T.A., Bowman, D.R., Jones, R.C., McGuire, R.J., *The Development and Application of an Aging Mechanical Systems Methodology for Commercial Aircraft Systems*, 9th Joint FAA/DoD/NASA Conference on Aging Aircraft (2006)

[11] Aloha Flight 243, photo, (1988), http://www.disastercity.info/flt243/index.htm

[12] Cooper, T.D., and Kelto, C.A., Fatigue in Machines and Structures – Aircraft, USAF Materials Laboratory Wright Paterson AFB, OH, presented at ASM Science Seminar (1978)

[13] Report to Congressional Committees, *Opportunities to Reduce Corrosion Costs and Increase Readiness*, Report GAO-03-753, United States General Accounting Office, July (2003)

[14] Agarwala, V.S. and Ahmed, S., *Corrosion Detection and Monitoring – A Review*, Paper 00271, National Association of Corrosion Engineers, Corrosion, (2000)

[15] Agarwala, V.S., *Naval Research Reviews*, US Office of Naval Research, Vol. 50 (No. 4), 1998, p 14-24

[16] Kinzie, *Cost of Corrosion*, presented at the Joint FAA/DoD/NASA Aging Aircraft Conference, 2002

[17] Macdonald, D.D. and Engelhardt, G.R., *Unification of the Deterministic and Statistical Approaches for Predicting Localized Corrosion Damage in Aircraft Aluminum Alloys*, 9th FAA/DoD/NASA Joint Aging Aircraft Conference, (2006)

[18] Lincoln, J.W., *Fatigue in the Presence of Corrosion, Technical Evaluation Report*, RTO-MP-18, North Atlantic Treaty Organization, Corfu, Greece, (1998)

[19] FAA/DoD/NASA Joint Aging Aircraft Conference, 10th annual to be held Apr 2007, http://www.agingaircraft.utcdayton.com/

[20] Jones, D.A., *Principles and Prevention of Corrosion*, 2nd Ed., Prentice Hall, Inc., (1996)

[21] Wanhill, R.J.H., *Aircraft Corrosion and Fatigue Damage Assessment*, Proceedings, *U.S. Air Force ASIP Conference*, 1995, p. 983-1027

[22] American Society of Metals Handbook, Vol 13b, *Corrosion: Fundamentals, Testing and Protection*, (2003)

[23] Kaplan, M.P. and Wolff, T.A., Life Extension and Damage Tolerance of Aircraft, http://www.aviationtoday.com/reports/extension.htm

[24] Dashputra, Y.P., *Effects of Laser Cutting on the Fatigue Properties of 0.063 inch Aluminum 7075-T6 Sheet*, Department of Mechanical and Aerospace Engineering, Oklahoma State University, Masters Report (2005)

[25] Jagathrakshakan, K., *Effects of Laser Cutting on the Edge Quality and Fatigue Properties of Aluminum Alloy 6061-T6*, Department of Mechanical and Aerospace Engineering, Oklahoma State University, Masters Report (2005)

[26] Jakkamreddy, S., *Study on the Effect of Edge Conditions on the Fatigue Properties of 2024-T3 Aluminum Sheet*, Department of Mechanical and Aerospace Engineering, Oklahoma State University, Masters Report (2005)

[27] Tyagi, P., *Fatigue Studies on Laser Cut and Deburred Aluminum 2024-T3*, Department of Mechanical and Aerospace Engineering, Oklahoma State University, Masters Report (2003)

[28] Jones K, Hoeppner DW, *Pit-To-Crack Transition in Pre-Corroded 7075-T6 Aluminum Alloy Under Cyclic Loading*, Corrosion Science 47 (2005) 2185–2198

[29] Jones K, Hoeppner DW, *Prior Corrosion and Fatigue of 2024-T3 Aluminum Alloy*, Corrosion Science xxx (2005) xxx–xxx (Article in Press)

[30] Jones K, *Effect of Microstructure on Pit-to-Crack transition of 7075-T6 Aluminum Alloy*, (Dec 2004), PhD Dissertation, University of Utah

[31] Hatch, J.E., *Aluminum: Properties and Physical Metallurgy*, American Society of Metals Handbook (1984)

[32] Hertzberg, R.W., *Deformation and Fracture Mechanics of Engineering Materials*, 4th Ed., Wiley & Sons, Inc. (1996), pp 418-435

[33] Santer, J.S. and Eylon, D., *Fatigue Behavior and Failure Mechanisms of 7075 Aluminum Alloys*, Metalurgical Transactions, Vol 10A, (1979), pp 841-848

[34] VanOrden, J.M., Krupp, W.E., Ryder, J.T., *Effects of Purity on Fatigue and Fracture of 7xxx-T6511 Aluminum Extrusion*, Journal of Aircraft, Vol 16 (1979), pp 327-335

[35] Wright, T.E., Godard, H.P. and Jenks, I.H., Corrosion, Vol 13 (1957), p 481

[36] Person, N.L, *Fatigue Properties of Prior-Corroded Aluminum Sheet Alloys*, Materials Performance, Vol 14, (1975), p 22

[37] N.A.Miller, *Some Factors Influencing the Corrosion Fatigue Behavior of a High-Strength Aluminum Alloys*, New Zeland Journal of Science, Vol 12, (1969), p 346

[38] Ito, M. and Takeuchi, K., *The Effects of Atmospheric Humidity and Duration of Proir-Corrosion in Atmosphere on the Fatigue Strength of Some Aluminum Alloys*, Sumitomo Light Metals Technology Reports, Vol 16, (1975), p 17

[39] Brown, W.F., Mindlin, H., Ho, C.Y., *Aerospace Structural Metals Handbook*, CINDAS/USAF CRDA Handbooks, Purdue University, (1994)

[40] Matweb, material properties database, http://www.matweb.com

[41] Leybold, HA, *et al*, *An Investigation of the Effects of Atmospheric Corrosion on the Fatigue Life of Aluminum Alloys*, (Sep 1958), Technical Note 4331, National Advisory Committee for Aeronautics

[42] Hahn, C.T. and Simon, R., *A Review of Fatigue Crack Growth in High Strength Aluminum Alloys and the Relevant Metallurgical Factors*, Engineering Fracture Mechanics, Vol 5 (1973), pp 523-540

[43] Krzysztof, K, *Mechanism of Corrosion and Corrosion Fatigue of 2024-T3 Aluminum Alloy in Hydrochloric Acid Solutions*, PhD Dissertation, University of Pennsylvania, (1996)

[44] Chen G.S., Wan, K.C., Gao, M., Wei, R.P., Flournoy, T.H., *Transition from Pitting to Fatigue Crack Growth - Modeling of Corrosion Fatigue Crack Nucleation in a 2024-T3 Aluminum Alloy*, Materials Science and Engineering, A219 (1996), pp 126-132

[45] Bray, G.H., Bucci, R.J., Colvin, E.L., Kulak, M., *Effects of prior corrosion on the S:N Fatigue Performance of Aluminum Alloys 2024-T3 and 2524-T3*, in: Effects of Environment on the Initiation of Crack Growth ASTM STP 1298, ASTM, Philadelphia, (1997), p. 89.

[46] Chandrasekaran V, Taylor MS, Hoeppner DW, *A Preliminary Study to Correlate Pit Depth to "Short" Fatigue Crack Growth Rates Of 2024-T3 Aluminum Alloy Specimens,* prepared under Subcontract Number NCI USAF 9138-003 by FASIDE International, Inc., Salt Lake City, UT, (1999)

[47] Frantziskonis, G.N., Simon, L.B., Woo, J. and Matikas, T.E., *Multiscale characterization of Pitting Corrosion and Application to an Aluminum Alloy*, European Journal of Mechanics A/Solids 19 (2000), pp 309-318

[48] Wang, Q.Y., Kawagoishi, N., Chen, Q., *Effect of Pitting Corrosion on Very High Cycle Fatigue Behavior*, Scripta Materialia, Vol 49, (2003), pp 711-716

[49] Van der Walde, K., Brockenbrough, J.R., Craig, B.A., Hillberry, B.M., *Multiple Fatigue Crack Growth in Pre-corroded 2024-T3 Aluminum*, International Journal of Fatigue, Vol 27 (2005), pp 1509-1518

[50] Kermanidis, A.T., Petroyiannis, P.V. and Pantelakis, S.G., *Fatigue and Damage Tolerance Behavior of Corroded 2024-T351 Aircraft Aluminum Alloy*, Theoretical and Applied Fracture Mechanics, Vol 43 (2005), pp 121-132

[51] Ishihara, S., Saka, S., Nan, Z.y., Goshima, T., Sunada, S., *Predication of Corrosion Fatigue Lives of Aluminum Alloy on The Basis of Corrosion Pit Growth Law*, Fatigue and Fracture of Engineering Materials and Structures, Vol 20 (2006), pp 472-480

[52] Minoda, T. and Yoshida, H., *Effect of Grain Boundary Characteristics on Intergranular Corrosion Resistance of 6061 Aluminum Alloy Extrusion*, Metallurgical and Materials Transactions, Vol 33A, (2002), pp 2891-2898

[53] Holroyd, N J H and Hardie, D*, Factors Controlling Crack Velocity in 7000 Series Aluminum Alloys During Fatigue in an Aggressive Environment*, (1983) Corrosion Science, Vol. 23, No. 6, pp. 527-546

[54] Nakai, Y, et al, *Atomic-Force Microscopy of Corrosion Pits and Crack Initiation in Fatigue of Metals*, Proceedings from 10th International Conference on Fracture, (2001)

[55] Sankaran K.K., Perez, R., Jata, K.V., *Effects of Pitting Corrosion on the Fatigue Behavior of Aluminum Alloy 7075-T6: Modeling and Experimental Studies*, Materials Science and Engineering A297 (2001) 223–229

[56] Huang, T.S. and Frankel, G.S., *Localized Corrosion Growth Kinetics in AL Alloys*, 6th Joint FAA/DoD/NASA Aging Aircraft Conference (2002)

[57] Tuegel EJ, Mills TB, *Correlation of Holistic Structural Assessment Method with Corrosion-Fatigue Experiments*, presented at Aging Aircraft Symposium (2002)

[58] Gallagher, J.P., Giessler, F.J., Berens, A.P. and Engle, R.M., USAF Damage Tolerant Design Handbook, Pub No.: AFWAL-TR-82-3073, (1984), pp 3.4.1-3.4.11

[59] Wang, Q.Y., Pidaparti, R.M., Palakal, M.J., *Comparative Study of Corrosion-Fatigue in Aircraft Metals*, AIAA Journal, Vol 39, No 2, Feb, (2001)

[60] Shafiq, B. and Argarwala, V.S., *Corrosion Fatigue in 7075-T6 Aluminum: Life Prediction Issues for Carrier Based Operations*, Journal of Aircraft, Vol 41, (2004), pp 393-398

[61] Quispitupa, A., Shafiq, B., Suarez, O.M., Uwakweh, O. and Duque, N.B., *Corrosion Fatigue of High-Strength Aircraft Structural Alloys*, Journal of Aircraft, Vol 43, 2006, pp 787-792

[62] Pao P.S., Gill S.J., Feng C.R., *On Fatigue Crack Initiation from Corrosion Pits in 7075-T7351 Aluminum Alloy*, Scripta Materialia. Vol 43 (2000) 391–396

[63] Pao P.S., Feng C.R., and Gill S.J., *Corrosion Fatigue Crack Initiation in Aluminum Alloys 7075 and 7050*, Corrosion, Oct (2000), p 1022

[64] Birbilis, N., Cavanaugh, M.K., Buchheit, R.G., Harlow, D.G., and Wei, R.P., *Understanding Damage Accumulation upon AA7075-T651 used in Airframes from a Microstructural Point of View,* Ohio State University Dept. of Materials Science and Engineering, and Lehigh University Dept. of Mechanical Engineering and Mechanics, (2005)

[65] Lide, D.R., *Handbook of Chemistry and Physics*, CRC, Ed 86, (2006), p 14-15

[66] American Society of Testing Materials (ASTM), *Standard Practice for Evaluating Intergranular Corrosion Resistance of Heat Treatable Aluminum Alloys by Immersion in Sodium Chloride + Hydrogen Peroxide Solution*, G110-92

[67] American Society of Testing Materials (ASTM), *Standard Guide for Examination and Evaluation of Pitting Corrosion*, G46-94

VITA

William Garlon King, Jr.

Candidate for the Degree of

Master of Science

Thesis: CRITICAL CORROSION PIT DEPTH FOR FATIGUE CRACK INITIATION IN 2024-T3, 6061-T6 AND 7075-T6 ALUMINUM ALLOYS

Major Field: Mechanical Engineering

Biographical:

Personal Data: Born in Atmore, AL, 29 Oct 1956. Son of Dr. W.G. King and Jean H. King of Walnut Hill, FL. Married to Charlotte W. King; three children: Bryan, Shannon and David King; one daughter-in-law Tracey King, and one grandson Brody King.

Education: Finished High school at Escambia County High School, Atmore, Al in 1975; Batchelor of Science in Mechanical Engineering, Auburn University, Auburn, AL in Mar 1983; Master of Science in Mechanical Engineering, Oklahoma State University, Stillwater, OK in Dec 2006

Experience: Employed as a civilian Aerospace and Mechanical Engineer for the U.S. Department of Defense for over 20 years (for the Navy and Air Force). Employed at five installations in five different states; Florida, Georgia, Alabama, Alaska and Oklahoma.

Professional Memberships:

Registered Professional Engineer, State of Alaska, # 11044

Name: William Garlon King, Jr. Date of Degree: December, Year 2006

Institution: Oklahoma State University Location: Stillwater, Oklahoma

Title of Study: CRITICAL CORROSION PIT DEPTH FOR FATIGUE CRACK INITIATION IN 2024-T3, 6061-T6 AND 7075-T6 ALUMINUM ALLOYS

Pages in Study: 147 Candidate for the Degree of Master of Science

Major Field: Mechanical Engineering

Scope and Method of Study: Study the effects of corrosion pitting of 2024-T3, 6061-T6 and 7075-T6 aluminum alloys in 1.6 mm (0.063 inch) sheet thickness and determine the critical pit depth required for a fatigue crack to initiate. The corrosion pitting was accomplished using a 3.5% NaCl solution with hydrogen peroxide added as an accelerant. The pitting specimens were fatigue cycled in one-way bending until failure and the cycles to failure recorded. The specimens were examined with a metallurgical microscope, using the focus method of ASTM G46 to determine pitting depth.

Findings and Conclusions: The presence of corrosion significantly reduces the fatigue life of the alloys tested as compared to the fatigue life of pristine (un-corroded) specimens. The average pitting depth required to initiate fatigue cracks was determined to be 2-4 μm (0.00008 – 0.00016 inches). This pitting depth corresponded with typical grain sizes at the surface and cracks began to initiate once pitting had penetrated about 50% of the grain thickness. Ratchet marks were noted on the fracture surface of the failed specimens, indicating multiple fatigue initiation sites; making it a useful indicator of fatigue crack nucleation. The effects of laser cutting aluminum sheet is detrimental to the fatigue life as compared to specimens manufactured using standard machining; however, the effects of corrosion pitting reduced the life of the laser cut 2024-T3 specimen to a much lesser degree that the machine cut 2024-T3 specimens, indicating that laser cutting is not necessarily bad.

ADVISER'S APPROVAL: Dr. C.E. Price